NTNU – Trondheim
Norwegian University of
Science and Technology

Maintaining Voltage Stability

An Analysis of Voltage Stability Indicators and
Mitigating Actions

Vegar Storvann

Master of Science in Electric Power Engineering
Submission date: June 2012
Supervisor: Kjetil Uhlen, ELKRAFT
Co-supervisor: Emil Hillberg, ELKRAFT

Norwegian University of Science and Technology
Department of Electric Power Engineering

Problem Description

Modern power systems are characterised by a growing load demand and increasing power transfers over longer geographical distances, often combined with environmental challenges related to construction of new transmission lines. Combined with the society's increasing dependency of a reliable power supply, the importance of preventing large disturbances and properly identifying the distance to the stability limits of the system is growing.

The purpose of this thesis is to develop a system integrity protection scheme (SIPS) for voltage instability based on voltage stability indicators and signals from overexcitation limiters (OELs).

First, a literature study will be carried out to identify and examine existing voltage stability indicators. The performance of a few selected indices is then to be examined based on simulations in a model of the IEEE Reliability Test System. The feasibility of using the indicators in a SIPS will be emphasised, and the usefulness of signals from OELs is also to be studied. Finally, the proposed SIPS is to be tested in the Hammerfest/Skaidi-region in a model of the Norwegian power system.

Preface

This thesis constitutes the final work of the last semester of the M.Sc. programme Electric Power Engineering at the department of Electrical Power Engineering at the Norwegian University of Science and Technology.

Many thanks are due to my supervisors Ph.D.-candidate Emil Hillberg and Professor Kjetil Uhlen for excellent guidance and helpful discussions throughout the work with this thesis, and for allowing me to work on such an interesting subject. I would also like to thank research scientist Trond Toftevaag at SINTEF Energi for his advices on even the most obscure subjects.

Trondheim, 21.06.2012

Vegar Storvann

Abstract

The society's dependency of a reliable power supply is increasing, and properly identifying the distance to the stability limits of the power system and avoiding blackouts is thus becoming increasingly important. In this thesis, a system integrity protection scheme (SIPS) for voltage instability is proposed. First, six voltage stability indicators are studied and compared, and their performance is tested in several power system models. They are first tested in a two-bus system where the load impedance is gradually increased until the load-side voltage reaches zero. The performance of the indicators is then tested under circuit contingencies in models of the IEEE Reliability Test System and of the Norwegian power system. From the results, the most reliable indicators seem to be the ones that are based on local measurements (SDI, ISI and VSI_{SCC}).

Several actions to mitigate voltage instability are described and tested in the power system models, including load shedding, switching of reactive compensation equipment, increasing AVR set points and increasing the active power generation. Of the unconventional actions, increasing AVR set points appears to be the most effective mitigation action.

A SIPS is proposed based on the above mitigation actions, voltage stability indicators and signals from activation of OELs. The principle behind the scheme is to avoid load shedding as far as possible by using indicator values and OEL activation signals to initiate preventive mitigation actions to relieve the situation when the system is approaching instability. This also reduces the necessary amount of load to shed to stabilise the system.

Simulations show that the proposed SIPS works as long as it has an adequate amount of mitigation actions available. In the simulations in the model of the Hammerfest/Skaidi region in Northern Norway, there was a general lack of possible mitigation actions, providing no alternative other than shedding large amounts of load to prevent voltage collapse after critical contingencies.

Sammendrag

På grunn av samfunnets økende avhengighet av en pålitelig elektrisitetsforsyning blir det stadig viktigere å unngå mørklegging av nettområder, og å være i stand til å nøyaktig beregne stabilitetsmarginene i kraftsystemet. I denne rapporten beskrives et forslag til et systemvern mot spenningsustabilitet basert på spenningsstabilitetsindikatorer og signaler fra feltstrømbegrensere i systemet. Seks utvalgte indikatorer har blitt studert og sammenlignet med hverandre, og ytelsen til disse har blitt testet i flere kraftsystemmodeller. Først har de blitt testet i en to-nodemodell hvor lastadmittansen ble økt gradvis under ulike ideelle forhold. Ytelsen til indikatorene ble deretter undersøkt under utfall av linjer i modeller av IEEE Reliability Test System og Statnett sin Norgesmodell. Resultatene viser at indikatorer basert på lokale målinger (SDI, ISI og VSI_{SCC}) er mest pålitelige.

Flere tiltak for å motvirke og forebygge spenningsustabilitet er beskrevet og testet i kraftsystemmodellene, inkludert belastningsfrakobling, inn- og utkobling av fasekompenseringsutstyr, økning av spenningssettpunkt på spenningsregulatorer og økning av aktiv effektproduksjon. Økning av spenningssettpunkt viste seg å være det mest effektive av de ukonvensjonelle tiltakene.

Det foreslåtte systemvernet skal forsøke å holde spenningsstabilitetsmarginen innenfor forhåndsdefinerte grenser og unngå belastningsfrakobling så langt det er mulig. For å oppnå dette må vernet iverksette alternative tiltak for å øke marginen. Dette vil også redusere mengden last som eventuelt må kobles ut dersom systemet blir ustabilt. Simuleringer viser at systemvernet vil fungere så lenge tilstrekkelige mottiltak er tilgjengelige. I simuleringene som ble gjort i Skaidi/Hammerfest-området i Norgesmodellen var svært få mottiltak tilgjengelige, og belastningsfrakobling var dermed eneste utvei.

Contents

List of Figures

List of Tables

List of Appendices

Glossary

AVR	Automatic voltage regulator
FVSI	Fast Voltage Stability Index, see Section 3.2
Instability point	Here: Point (power/voltage) at which the system becomes voltage unstable, often assumed to correspond with the maximum loadability point.
ISI	Impedance Stability Index, see Section 3.6
L_{mn}	Line Stability Index, see Section 3.3
Maximum loadability point	Point of maximum power transfer level, i.e. the tip of the nose curve
OEL	Overexcitation limiter, part of the excitation system that limits the field current to protect the field winding from overheating
OLTC	On-load tap changer
PMU	Phasor measurement unit – device that measures voltage and current phasors, using a common time source for synchronisation
SDI	S-difference indicator, see Section 3.5
SIPS	System Integrity Protection Scheme
SVC	Static Var Compensator – A shunt-connected static var generator or absorber whose output is adjusted to exchange capacitive or inductive current to maintain or control specific parameters of the electrical power system [1].

TPSI	Transmission Path Stability Index, see Section 3.4
UEL	Underexcitation limiter, part of the excitation system that maintains the field current above a predefined level to prevent machine instability and stator core end-region heating.
VIP	Voltage Instability Predictor, see Section 3.6
VSI_{SCC}	A voltage stability index based on short-circuit capacity, see Section 3.7

Nomenclature

δ	Voltage angle or voltage angle difference
ϕ	Power factor angle
θ	Angle of, or angle difference between, arbitrary non-voltage phasors
E	Sending-end voltage, equivalent voltage or electromotive force (emf)
I	Current
P	Active power
Q	Reactive power
R	Resistance
S	Apparent power
SCC	Short-circuit capacity
U	Voltage
X	Reactance
Z	Impedance

Phasors are indicated by an arrow above the symbol, e.g. $\vec{U}$

Conjugates of complex numbers are indicated by an asterisk, e.g. $\vec{I}^*$

1 Introduction

1.1 Background and Objective

Modern power systems are characterised by a growing load demand and increasing power transfers over longer geographical distances, often combined with environmental challenges related to construction of new transmission lines. Combined with the society's increasing dependency of a reliable power supply, the importance of preventing large disturbances and properly identifying the distance to the stability limits of the system is growing.

Voltage instability has been the cause of several major blackouts in the last few decades [2], and the purpose of this thesis is to develop a system integrity protection scheme (SIPS) for voltage instability based on voltage stability indicators and signals from overexcitation limiters (OELs).

1.2 Scope of Work

In the work with this thesis, voltage stability indicators suitable for use in online applications is to be identified and examined, together with possible actions to mitigate voltage instability. Based on this information, a SIPS for voltage instability will be developed. The proposed SIPS is then to be tested, along with the voltage stability indicators, in models of the IEEE Reliability Test System (IEEE RTS) and of the Hammerfest/Skaidi region in the Norwegian power system.

The simulations are done in PSS/E version 32.1.0, a power system simulation program developed by Siemens PTI. This program was chosen mainly because models of both the IEEE RTS and the Norwegian power system are available for PSS/E.

Even though power system stability is a multifaceted phenomena, the scope of this thesis is limited to the study of voltage stability.

1.3 Outline of Thesis

In Chapter 2 the background theory of voltage stability is presented, followed by Chapter 3 with descriptions and theory behind six selected voltage stability indicators. Chapter 4 presents conventional and unconventional mitigating actions to prevent voltage instability, and in Chapter 5 a SIPS and an algorithm for applying mitigation actions is described. Chapters 6, 7 and 8 present and discuss simulation results from case studies in a simple two-bus system, a model of the IEEE RTS and a model of the Norwegian power system. A summarising discussion and conclusions are provided in chapters 9 and 10.

2 Voltage Stability

This chapter will elaborate on the concept of voltage stability and causes of voltage instability.

Voltage stability is a subset of power system stability, as shown in Figure 2.1. Lack of voltage stability in a power system leads to an uncontrollable drop (or rise) in system voltages following a disturbance. It is initially a local phenomena, but the consequences can spread to a wider area due to cascading effects, referred to as a *voltage collapse*.

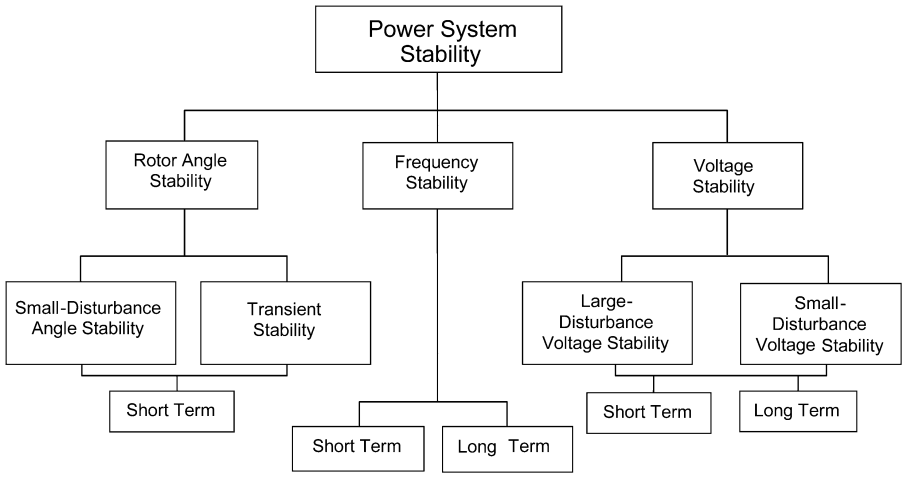

Figure 2.1: Classification of power system stability, from [3].

2.1 Definitions

There are several definitions of voltage stability in the literature. Two proposed definitions, one from a book on the subject by van Cutsem and Vournas [4], and one from a joint IEEE/CIGRE report [3], are presented here.

Van Cutsem and Vournas [4] define the opposite of voltage stability, voltage *instability*, as:

> Voltage instability stems from the attempt of load dynamics to restore power consumption beyond the capability of the combined transmission and generation system.

This is a very clear and concise definition of voltage instability by its cause. Another definition of voltage stability is given by the *IEEE/CIGRE Joint Task Force on Stability Terms and Definitions* in the report "Definition and Classification of Power System Stability" [3]:

> Voltage stability refers to the ability of a power system to maintain steady voltages at all buses in the system after being subjected to a disturbance from a given initial operating condition.

This is a more general definition than the previous one, in that it does not specify any causes of voltage instability. In addition to these definitions, it is useful to consider different classifications of voltage stability, so a summary of the classifications from the IEEE/CIGRE report is given below.

Voltage stability is classified into two subcategories; *large-disturbance voltage stability* and *small-disturbance voltage stability*. This is also shown in Figure 2.1.

Large disturbance voltage stability refers to the voltage stability of the system after being subjected to a large disturbance, such as system faults, loss of generation or circuit contingencies (loss of lines or cables).

Small-disturbance voltage stability refers to the voltage stability when subjected to small perturbations such as incremental changes in system load.

Additionally, voltage stability can be either a long-term or a short-term phenomenon, depending on the dynamics involved. In the case of short-term voltage stability, fast acting load components are involved, and the time period is in the order of several seconds.

Long-term voltage stability involves slow acting components like tap-changing transformers, thermostat controlled loads and generator excitation limiters. In this case, the time period is in the order of (several) minutes.

2.2 System Loadability Limit

Voltage instability is generally a result of a load response to a disturbance that will cause the maximum power transfer level of the system to be exceeded. The maximum power transfer level is determined by several factors, and can be illustrated by considering a simple network consisting of a transmission line with a generator in one end supplying a load in the other end, as shown in Figure 2.2. The load is assumed to be constant and independent of voltage. The resistances of the generator and the transmission line are ignored, and it is assumed that the generator's AVR is active so that the voltage on the generator bus, E, is constant. The validity of the latter assumption will be discussed in Section 2.4.

The active and reactive power consumed by the load is determined by the power flow equations of the system, Equation (2.1):

$$P_L = \frac{EU}{X} \sin \delta \tag{2.1a}$$

$$Q_L = \frac{EU}{X} \cos \delta - \frac{U^2}{X} \tag{2.1b}$$

E and U are the voltages at the generator and load buses, respectively, X is the reactance of the transmission line and δ is the voltage angle difference between E and U.

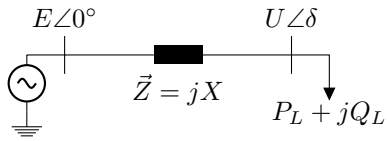

Figure 2.2: Equivalent circuit of a simple two-bus system.

By using the identity $\sin^2\delta + \cos^2\delta = 1$, δ can be eliminated from Equation (2.1):

$$\left(\frac{EU}{X}\right)^2 = P_L^2 + \left(Q_L + \frac{U^2}{X}\right)^2 \tag{2.2}$$

Rewriting as a quadratic equation with respect to U^2 gives:

$$\left(U^2\right)^2 + (2XQ_L - E^2)U^2 + X^2(P_L^2 + Q_L^2) = 0 \tag{2.3}$$

Solving the equation and expressing the relationship between P_L and Q_L by the power factor, $Q_L = P_L \tan\phi$, the load voltage can be expressed as a function of load power and the power factor of the load [4]:

$$U = \sqrt{\frac{E^2}{2} - XP_L\tan\phi \pm \sqrt{\frac{E^4}{4} - X^2P_L^2 - XE^2P_L\tan\phi}} \tag{2.4}$$

This equation can be simplified by expressing the load voltage and load power in per unit as $u = \frac{U}{E}$ and $p = P_L/\frac{E^2}{X}$:

$$u = \sqrt{\frac{1}{2} - p\tan\phi \pm \sqrt{\frac{1}{4} - p^2 - p\tan\phi}} \tag{2.5}$$

Equations (2.4) and (2.5) are often represented as a *PV curve* for the system, and Figure 2.3 shows examples of PV curves for three values of the load power factor, $\cos\phi$. Due to the characteristic shape of the curves, they are also called *nose curves*, and the tip of the curve represents the maximum power transfer level of the system for a given load.

From basic circuit theory it is known that the maximum power transfer level is reached when the magnitude of the load impedance becomes equal to the magnitude of the source impedance (here represented by the line impedance), $|Z_{\text{Source}}| = |Z_{\text{Load}}|$ [4, ch.2]. For all other transfer levels on the curve, there are two solutions, one at a high voltage and one at a lower voltage. The higher voltage solution is the normal mode of operation.

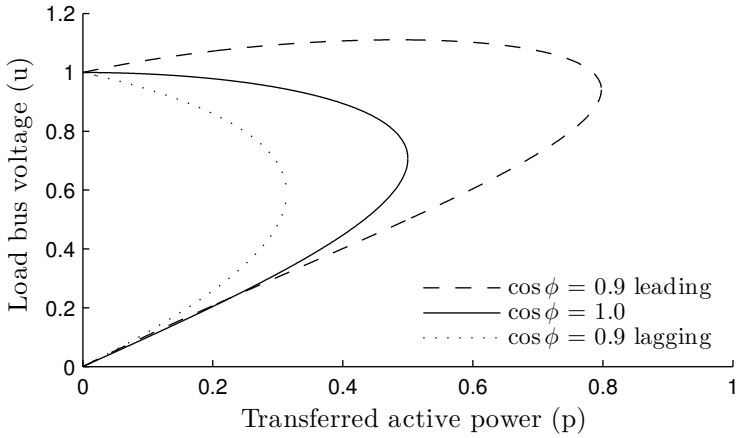

Figure 2.3: PV curves for the simple two-bus system for different values of ϕ.

At the maximum power transfer level, there is only one solution to Equation (2.4), which is when the value of the inner root becomes zero, or, with $P_L = P_{L\,max}$:

$$X^2 P_{L\,max}^2 + X E^2 P_L \tan\phi - \frac{E^4}{4} = 0 \tag{2.6}$$

This is a quadratic equation with respect to P_L, and one solution is:

$$P_{L\,max} = \frac{E^2}{2X}\left(-\tan\phi + \sqrt{1+\tan^2\phi}\right) \tag{2.7}$$

Simplifying further gives

$$P_{L\,max} = \frac{E^2}{2X}\left(\frac{1-\sin\phi}{\cos\phi}\right) \tag{2.8}$$

which is the maximum power transfer level of the system for a given load power factor.

The lower part of the PV curve is initially stable, but when considering load dynamics such as load restoration mechanisms that try to achieve a higher load level due to a reduction in the voltage, it becomes unstable. A slight increase in

the load admittance would result in an increased current, and thus a decreased load voltage and a decreased power transfer level.

It should be noted that the system does not collapse until the P/V characteristic of the load no longer intersects the PV curve of the system. For constant power loads, this coincides with the tip of the nose curve, but for loads with other characteristics, this is normally somewhere on the lower half of the nose curve. Figure 2.4 illustrates these intersection points for a constant power load and a ZIP-type load.

2.3 Causes of Voltage Instability

2.3.1 Load Restoration

The power consumed by loads depends on the voltage characteristics of each load. Often loads can be said to have two voltage characteristics, one transient and one long-term, or steady-state, characteristic. When subjected to a disturbance, the transient characteristic is prevailing and the consumed power varies accordingly. The voltage characteristic of the load will then gradually return to the steady-state characteristic due to the dynamics of the load components.

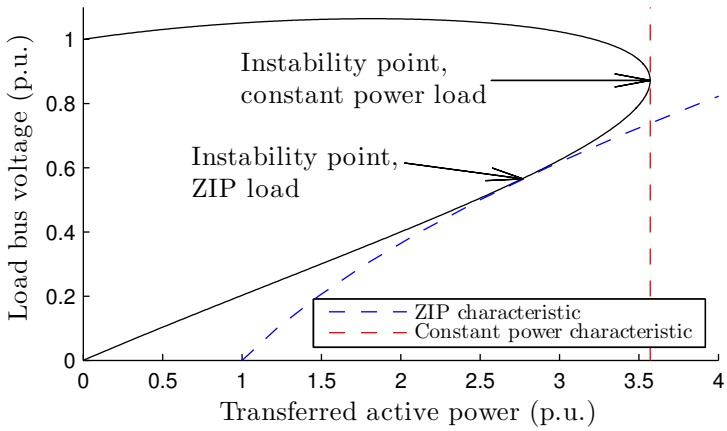

Figure 2.4: Instability points for two load characteristics.

The steady-state load characteristic is normally constant (i.e. independent of voltage) [1], so that if the voltage on the load bus drops, loads attempt to *restore* the consumed power to the pre-disturbance level. This causes further depression of the load bus voltage due to an increase in the load current, which in some cases can cause the system to exceed its maximum power transfer limit.

Load restoration mechanisms can be divided into two main categories, fast-acting and slow-acting mechanisms. Slow-acting restoration mechanisms typically include onload tap changers (OLTCs) on transformers and thermostat controlled loads. Fast-acting loads include induction motors and electronically controlled loads.

Residential loads are typically voltage dependent [1], but due to OLTCs, the load-side voltage (and thus the power) will remain constant until the tap changer reaches the end of the tap range.

Industrial loads normally include a large share of induction motors and/or electronically controlled loads with fast-acting restoration mechanisms.

2.3.2 Increase in Load Demand

Another way for the system to become unstable is due to a general increase in load demand (for example during morning hours), where the load slowly but gradually increases past the maximum loadability limit and/or reactive power reserves reach their limit. If the system initially is in a poor condition, the load increase could be enough to push the system past the maximum power transfer limit.

2.4 Synchronous Generator Reactive Power Capability

The assumption in Section 2.2 of E being constant is only valid as long as none of the reactive power limits of the generator are reached. If one of these limits are encountered, E is no longer constant, but varies with the load power. The generator can then be represented as a constant voltage behind a reactance (the classical generator model). In the example in Section 2.2, this can

be represented as an increase in both the reactance X and the voltage E in Figure 2.2.

From Equation (2.8) it is evident that an increase in the reactance gives a reduced power transfer capability. It is therefore important to include the reactive limits of generators in voltage stability studies.

A complete description of the reactive power limits of synchronous generators can be found in Appendix A.

2.5 Reactive Compensation

Reactive compensation can be used to increase the voltage at a load bus. There are two ways to do this, either by shunt compensation at the load bus or by series compensation.

2.5.1 Shunt Compensation

Shunt compensation can be achieved by installing for example a capacitor bank, an SVC or a STATCOM at the load bus. The advantage of shunt compensation is that it supplies reactive power close to where it is needed (at the load bus).

From a voltage stability perspective, the disadvantage of shunt compensation is that at large load levels with heavy compensation, the maximum loadability point occurs at voltage levels that are close to nominal values. Thus, the voltage will give no indication of the proximity to voltage collapse, and protection schemes such as undervoltage load-shedding relays may respond too late.

The dashed curve in Figure 2.3 illustrates such a case (as indicated by the leading power factor). Also note that compared to the case with unity power factor, the maximum power transfer level is nearly doubled.

2.5.2 Series Compensation

Series compensation is achieved by including a capacitive element in series with the transmission line. The capacitor will reduce the net reactance of the line,

and thus increase the maximum loadability limit (as seen from Equation (2.8) when X is reduced). The effect of both compensation types on a purely resistive load is shown in Figure 2.5.

2.6 Analysing Voltage Stability

The voltage stability of a system can be analysed in many ways, and the maximum loadability of the system is usually examined with regard to circuit contingencies or loss of generation. Two categories of analysis methods are presented here, power flow simulations and dynamic time-domain simulations, although they only represent a subset of the available methods.

2.6.1 Static Power Flow Analysis

Regular power flow simulations can be applied to determine the PV curve or the maximum power transfer levels of a system by gradually increasing the load until a solution no longer exists. The simulation will have problems converging close to the point of collapse because the Jacobian matrix of the system becomes singular.

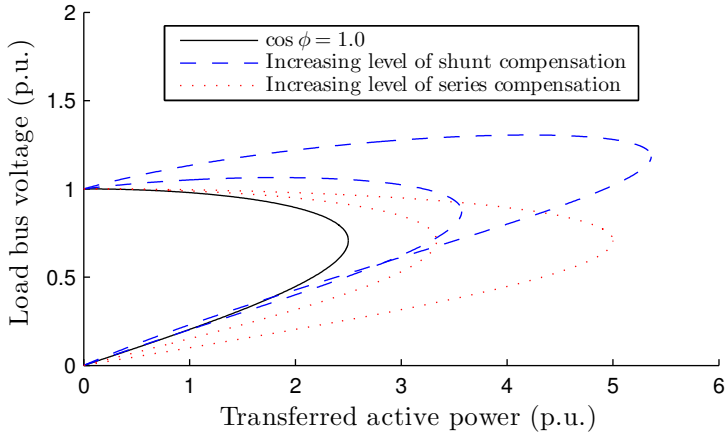

Figure 2.5: PV curves for the simple system for various levels of shunt and series compensation.

Another way to determine the PV curve for the system is the *continuation power flow* algorithm. Continuation power flow is an iterative method that finds a series of power flow solutions at different load levels by employing a predictor-corrector scheme. The advantage of this method is that the power flow equations are reformulated so that they are well-conditioned at all possible loading conditions. This allows determining the maximum power transfer level of the system, and it also allows finding the lower half of the PV curve.

Based on a known base-case power flow solution, the continuation power flow method estimates (predicts) a new solution for the system at an increased load level, and then corrects the prediction by solving the power flow equations. For further details, see [5].

2.6.2 Time-domain Simulations

As an alternative or complementary method to the power flow approach, dynamic time-domain simulations can be used. Time-domain simulations will give a more detailed and accurate system response, assuming that good models are used.

The disadvantage of dynamic time-domain simulations is that they are computationally heavy, and, in the case of voltage stability, long time constants are involved, requiring long-term simulations to fully include all the dynamics involved. For large systems, full model long-term simulations might not be feasible, therefore simulation tools such as PSS/E have special simulation modes that are optimised for long-term dynamic simulations.

When considering a generator's reactive power capability, static power flow methods will normally use the generator's reactive limits as they are defined at the nominal power level. At lower power levels, the reactive power capability of a generator is higher, as can be seen in Figure 2.6, where the error can be up to 25 Mvar, implying that results from a static power flow analysis can be conservative. If proper models are used, dynamic simulations provide more realistic utilisation of the generator reactive power capabilities, and can also reveal how the temporary overload capabilities of the generators come into play.

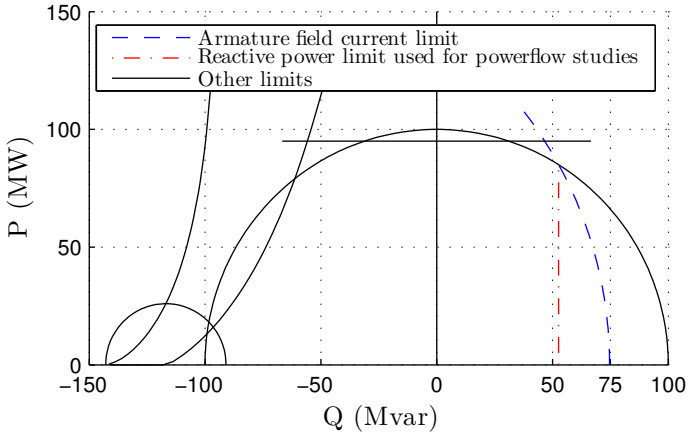

Figure 2.6: Example capability diagram for a salient-pole synchronous machine.

2.7 Effect of Excitation Limiters on Voltage Stability

Excitation limiters restrict the available reactive capability of generators. In this section, the effect they have on the voltage stability of a system is discussed.

2.7.1 System Loadability

When considering the maximum power transfer level of a system, the over-excitation limiter plays an important role. In Section 2.2, the PV curve for a simple system is derived. Considering the same system, where the voltage source (E) is a generator with a maximum reactive power limit, the PV curve will be different than described earlier.

When the generator reaches its field current limit, it can no longer be represented as an ideal, constant voltage source at the generator bus. Instead, it can be represented as a constant equivalent voltage behind the synchronous reactance of the generator. The result of this is that in Equation (2.4), the equation for the PV curve, both E and X increase, as was explained in Section 2.4. Figure 2.7 illustrates this condition for a 132 kV system, where the dashed line represents the effect of the field current limit.

In the case shown in the figure, the line reactance is high, 0.3 p.u. (referred

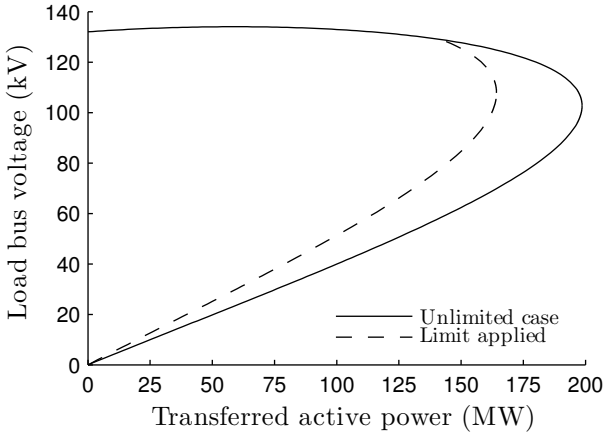

Figure 2.7: The effect of generator limitations on voltage stability.

to 100 MVA and 132 kV), corresponding to a line length of approximately 150 km (duplex FeAl 329 "Curlew"). The transfer limit is 200 MW in the unlimited case, and is reduced by approximately 35 MW when the excitation limit is considered.

The time delay of the OEL allows operating the system at a higher voltage and power level than the dashed line represents, but only for a limited amount of time. The higher the reactive power demand, the sooner the OEL will be activated due to the larger field current.

Although the example considered here is very simple, the same principles can be applied on any power system, since any system can be reduced to a similar Thévenin equivalent.

3 Voltage Stability Indicators

In this chapter, voltage stability indicators are first discussed in general, followed by a presentation and comparison of a few selected indicators. In the following derivations, i is always the sending-end bus (of a line) and j is the receiving-end bus.

3.1 Background

Many voltage stability indicators have been proposed in the literature, see e.g. references [4, 6, 7] for several examples. Reference [7] gives a comparison of a large set of indicators, where the indicators are classified as either *given state based indicators* or *large deviation based indicators*.

Given state based indicators are defined as indicators that exclusively consider the given, i.e. studied, state of the system. The indices calculate a characteristic that, at the point of voltage collapse, takes a theoretical critical value. This implies that the indices do not attempt to predict the further evolution of the state of the system [7].

Large deviation based indicators track the system's behaviour for increase in loads or transfer from a given system state, following a predefined pattern, until the system reaches voltage instability. In this way, these indicators provide the MW/Mvar distance to voltage collapse [7].

The indicators described in this report were selected based on the following criteria:

1. The indicators must be suitable for online application in a system integrity protection scheme (SIPS). This implies:
   a) Indicators must be able to continuously assess the current situation.
   b) Changes in network topology should not result in a delayed indicator response due to e.g. heavy computations.

2. The indicators should be based upon as few assumptions as possible (ref. Ockham's razor [8]), such as e.g. load increase patterns or sets of predefined contingencies.
3. The indicators must be reasonably straight forward to implement within the timeframe of the study.

The above criteria eliminates all large deviation based indicators, as they, per definition, are based on an assumed behaviour of the system. This class of indicators is therefore unsuitable to use in a SIPS, since a SIPS ideally should be able to respond to any contingencies and circumstances in the system, including those that may not have been planned for.

The final set of indicators selected for further studies are listed in Table 3.1.

3.2 Fast Voltage Stability Index – FVSI

The *fast voltage stability index* (FVSI) [9] is an indicator based on measurements of voltages and reactive power. The line model used to derive the indicator is shown in Figure 3.1. In the following derivation, bus i is used as the reference bus, with the voltage angle set to 0°.

FVSI is a line indicator, and the derivation of the index begins with the general equation for the current in a line between two buses, bus i and j:

$$\vec{I}_{ij} = \frac{\vec{U}_i - \vec{U}_j}{\vec{Z}_{ij}} \tag{3.1}$$

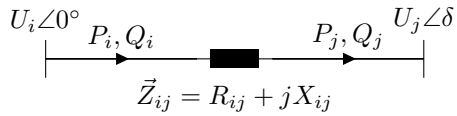

Figure 3.1: Line model for derivation of the fast voltage stability index.

Table 3.1: Selected set of voltage stability indicators.

Abbr.	Name	Basic equation	Stab.lim.	Ref.
FVSI	Fast Voltage Stability Index	$\frac{4Z_{ij}^2 Q_j}{U_i^2 X_{ij}}$	≤ 1.0	[9]
L_{mn}	Line Stability index	$\frac{4X_{ij}Q_j}{\left(\lvert U_i\rvert \sin(\theta-\delta)\right)^2}$	≤ 1.0	[10]
TPSI	Transmission Path Stability Index	$0.5U_g - \Delta U_d'$	≥ 0.0	[11]
SDI	S-difference Indicator	$1 + \frac{\left\lvert \vec{I}_{ji}^{(t)} \Delta \vec{U}_j^{(t+1)} \right\rvert}{\left\lvert \vec{U}_j^{(t)} \Delta \vec{I}_{ji}^{(t+1)} \right\rvert} \cos\theta$	≥ 0.0	[12, 13]
ISI	Impedance Stability Index	$\frac{Z_{sys}}{Z_{load}}$	≤ 1.0	[14, 15]
VSI_{SCC}		$\frac{2S_L X_{th}(1+\sin\phi)}{E_{th}^2}$	< 1.0	[16]

The apparent power received at bus j is found by multiplying Equation (3.1) with the voltage at bus j:

$$P_j + jQ_j = \vec{I}_{ij}\vec{U}_j = \vec{U}_j \frac{\vec{U}_i - \vec{U}_j}{\vec{Z}_{ij}} \tag{3.2}$$

The imaginary part of Equation (3.2) is the reactive power received at bus j, which can be described as:

$$Q_j = \frac{U_i U_j \left(R_{ij} \sin\delta + X_{ij} \cos\delta\right) - X_{ij} U_j^2}{R_{ij}^2 + X_{ij}^2} \tag{3.3}$$

and rewritten as a second-order equation for U_j:

$$U_j^2 - U_j U_i \left(\frac{R_{ij}}{X_{ij}} \sin\delta + \cos\delta\right) + \left(X_{ij} + \frac{R_{ij}^2}{X_{ij}}\right) Q_j = 0 \tag{3.4}$$

FVSI is based on the principle that the system is stable as long as there are only real solutions to Equation (3.4). In other words, the system is stable as long as the discriminant[1] of Equation (3.4) is not negative:

$$\left[\left(\frac{R_{ij}}{X_{ij}} \sin\delta + \cos\delta\right) U_i\right]^2 - 4\left(X_{ij} + \frac{R_{ij}^2}{X_{ij}}\right) Q_j \geq 0 \tag{3.5}$$

Simplifying the expression, and assuming that the angle difference, δ, is normally very small ($\delta \approx 0, R_{ij} \sin\delta \approx 0$ and $X_{ij} \cos\delta \approx X_{ij}$) gives:

$$(X_{ij} U_i)^2 \geq 4 X_{ij} (X_{ij}^2 + R_{ij}^2) Q_j \tag{3.6}$$

FVSI is thus defined as the ratio between the two terms [9]:

$$\frac{4 Z_{ij}^2 Q_j}{U_i^2 X_{ij}} = \mathrm{FVSI}_{ij} \leq 1 \tag{3.7}$$

As shown by Equation (3.7), the power transmission through the line i-j is stable as long as FVSI_{ij} is less than 1.

[1] The solutions to the quadratic equation $ax^2 + bx + c = 0$ are $x = \frac{-b \pm \sqrt{b^2 - 4ac}}{2a}$, where $b^2 - 4ac$ is defined as the discriminant of the equation.

3.3 Line Stability Index – L_{mn}

The *line stability index* (L_{mn}) [10] is, like FVSI, based on the power flow equations for a transmission line.

Continuing from Equation (3.3), replacing $R + jX$ by $Z\angle\theta$, gives an expression for the received reactive power at bus j:

$$Q_j = \frac{U_i U_j}{Z_{ij}} \sin(\theta - \delta) - \frac{U_j^2}{Z_{ij}} \sin\theta \tag{3.8}$$

Using the same technique as for FVSI, the receiving-end voltage can be expressed as a second-order equation:

$$U_j^2 \sin\theta - U_j U_i \sin(\theta - \delta) - Q_j Z_{ij} = 0 \tag{3.9}$$

Similarly, the system is stable as long as the discriminant of Equation (3.9) is not zero:

$$U_i^2 \sin^2(\theta - \delta) - 4 Q_j Z_{ij} \sin\theta \geq 0 \tag{3.10}$$

Rearranging the equation and using the fact that $Z_{ij} \sin\theta = X_{ij}$ gives the equation for the line stability index L_{mn}:

$$\frac{4 X_{ij} Q_j}{U_i^2 \sin^2(\theta - \delta)} = L_{mn} \leq 1.0 \tag{3.11}$$

As long as the value of the index stays below 1.0, the system is stable.

3.4 Transmission Path Stability Index – TPSI

The *transmission path stability index* (TPSI) [11] is based on measurements of voltage phasors throughout the system. The basic principle behind TPSI can be illustrated by considering a two-bus system as shown in Figure 3.2, with a generator supplying a load via a transmission line.

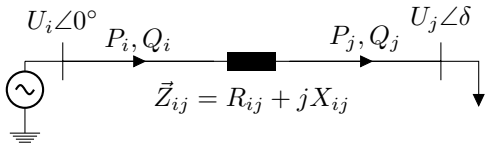

Figure 3.2: Two-bus system with source and load.

3.4.1 Two-bus System

The active and reactive power consumed by the load are given by the power flow equations of the system, (3.12a) and (3.12b), where line resistance is neglected:

$$P_j = \frac{U_i U_j}{X_{ij}} \sin\delta \tag{3.12a}$$

$$Q_j = \frac{U_i U_j}{X_{ij}} \cos\delta - \frac{U_j^2}{X_{ij}} \tag{3.12b}$$

Solving the equation set (3.12) for U_j (see Section 2.2 for a detailed derivation) gives:

$$U_j = \sqrt{\frac{U_i^2}{2} - X_{ij}Q_j \pm \sqrt{\frac{U_i^4}{4} - X_{ij}^2 P_j^2 - X_{ij}U_i^2 Q_j}} \tag{3.13}$$

Equation (3.13) describes the PV-curve of the system. As described in Chapter 2, the maximum power transfer level occurs when the equation has only one solution, which is when the value of the inner square root is zero. U_j at the maximum power transfer level thus becomes:

$$U_j\big|_{P_j\,max} = \sqrt{\frac{U_i^2}{2} - X_{ij}Q_j} \tag{3.14}$$

Inserting Equation (3.12b) for Q_j in (3.14) and rearranging provides the basic criterion that TPSI is based on:

$$0.5U_i - U_j\cos\delta = 0 \tag{3.15}$$

The voltage vectors at a distance from the maximum power transfer level are illustrated in Figure 3.3, which also shows the elements of Equation (3.15).

To rephrase Equation (3.15), the system is at the maximum power transfer level when the projection of the *receiving end* voltage, U_j, onto the sending end voltage, U_i, is equal to half the sending end voltage. Looking at it oppositely, the system is at the maximum power transfer level when the projection of the *voltage drop* between the two nodes onto the sending end voltage, denoted ΔU_d, is equal to half the sending end voltage.

TPSI is calculated from the latter view:

$$\Delta U_d = U_i - U_j \cos\delta \tag{3.16a}$$

$$\text{TPSI} = 0.5U_i - \Delta U_d \geq 0 \tag{3.16b}$$

Thus, the system is at the critical loading point when the value of TPSI is zero.

A physical interpretation of Equation (3.16) is that the voltage drop across the line impedance equals the load-side voltage. This implies that the line impedance equals the load impedance, and is the condition that corresponds to the tip of the PV curve (see Section 2.2).

3.4.2 Radial Network

Real power systems are rarely two-bus systems, and the basic TPSI principle can be extended to be applied to radial networks. An example of such a network is shown in Figure 3.4, where a generator supplies loads along a radial system consisting of four buses.

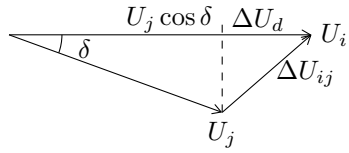

Figure 3.3: Vector diagram for a two-bus system.

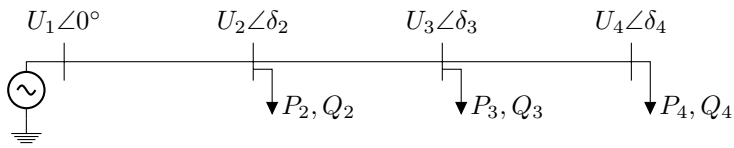

Figure 3.4: Single-line diagram for a four-bus radial power system.

If Equation (3.16) is used directly with e.g. buses $i = 1$ and $j = 4$, the result can become too conservative since the equation does not account for the effect of the loads at the intermediate buses (buses two and three in the figure). Reference [11] therefore suggests the following method:

1. Project each voltage phasor onto the voltage phasor of the preceding bus and calculate the projected voltage drop, ΔU_d, using Equation (3.16a).
2. Project the sum of all voltage drops (ΔU_d) onto the generator bus voltage phasor, giving an equivalent voltage drop for the radial system.

The projected voltage drop between nodes k the preceding node $k-1$ is thus given as

$$\Delta U_{d\ k-1} = U_{k-1} - U_k \cos\delta_{k,k-1} \tag{3.17}$$

where $\delta_{k,k-1}$ is the angle between the two voltage phasors. $\Delta U_{d\ k-1}$ is then further projected onto the generator bus voltage phasor:

$$\Delta U'_{d\ k-1} = \Delta U_{d\ k-1} \cos\delta_{k-1,1} \tag{3.18}$$

The total equivalent voltage drop is calculated as the sum of all $\Delta U'_{d\ k-1}$:

$$\Delta U'_d = \sum_{k=2}^{n} (U_{k-1} - U_k \cos\delta_{k,k-1}) \cos\delta_{k-1,1} \tag{3.19}$$

where n is the total number of buses in the system. The elements of the above three equations are illustrated in Figure 3.5, which also shows the difference between Equations (3.16a) (in blue) and (3.19) (in red).

The corrected TPSI equation now becomes

$$\text{TPSI} = 0.5U_1 - \Delta U'_d \tag{3.20}$$

where U_1 is the voltage on the generator bus.

3.4.3 Meshed Network

The TPSI algorithm was developed for use in meshed grids, but the above equations are only applicable to radial networks. Reference [11] therefore proposes an algorithm that identifies *transmission paths* in meshed networks. Two types of transmission paths are defined; active and reactive transmission paths.

An active transmission path is defined as a sequence of connected buses with monotonously decreasing voltage *angles*, starting at an *active generator bus*. Active generator buses are defined as buses whose voltage *angle* is larger than that of all adjacent buses.

Similarly, a reactive transmission path is defined as a sequence of connected buses with monotonously decreasing voltage *magnitudes*, starting at a *reactive* generator bus, where reactive generator buses are buses whose voltage *magnitude* is larger than that of all adjacent buses.

Equation (3.20) can then be applied to the transmission paths to determine the voltage stability of the paths.

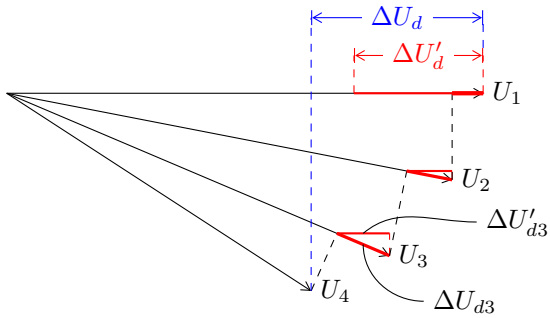

Figure 3.5: Vector diagram for the radial system, based on Fig. 2 in [11], showing the difference between the two-bus TPSI equation (in blue) and the radial TPSI equations (in red).

Due to the nature of meshed grids, several transmission paths can lead to the same load bus. In such cases, the bus is voltage stable as long as at least one of the transmission paths is stable. However, as soon as one of the paths becomes unstable, the losses increase drastically and transmission through the remaining paths increases to accommodate these losses, bringing them closer to instability. The weakest path therefore determines the voltage stability of the bus [11].

The authors of [11] acknowledge that there is no theoretical justification for using TPSI = 0 as a collapse criterion in meshed grids, but it corresponds well with the simulation results presented in the reference.

3.5 S-Difference Indicator – SDI

The *S-difference indicator* (SDI) [12], also referred to as SDC [13], is calculated using measurements of the apparent power flow at the receiving end of a transmission line. The indicator is based on the principle that when voltage instability is reached, the power losses in the line increase drastically. This causes an increase in apparent power at the sending end due to the increased transmission losses, while there is no increase in apparent power at the receiving end. Such a condition can be identified by consecutive measurements of the apparent power at the receiving end.

Two consecutive measurements of voltage and current phasors at the receiving end of the line are used: $\vec{U}j^{(t)}$, $\vec{U}j^{(t+1)}$, $\vec{I}_{ji}^{(t)}$, $\vec{I}_{ji}^{(t+1)}$. Indices t and $t+1$ indicate two consecutive measurements. The apparent power at the receiving end is given by:

$$\vec{S}_j^{(t)} = \vec{U}_j^{(t)} \cdot \vec{I}_{ji}^{(t)*} \tag{3.21}$$

By applying the difference between the two measurements, given by

$$\Delta\vec{U}_j^{(t+1)} = \vec{U}_j^{(t+1)} - \vec{U}_j^{(t)} \tag{3.22}$$

$$\Delta\vec{I}_{ji}^{(t+1)} = \vec{I}_{ji}^{(t+1)} - \vec{I}_{ji}^{(t)} \tag{3.23}$$

the apparent power at $t+1$ can be expressed as:

$$\begin{aligned}\vec{S}_j^{(t+1)} &= \left(\vec{U}_j^{(t)} + \Delta\vec{U}_j^{(t+1)}\right) \cdot \left(\vec{I}_{ji}^{(t)} + \Delta\vec{I}_{ji}^{(t+1)}\right)^* \\ &= \vec{U}_j^{(t)}\vec{I}_{ji}^{(t)*} + \vec{U}_j^{(t)}\Delta\vec{I}_{ji}^{(t+1)*} + \vec{I}_{ji}^{(t)*}\Delta\vec{U}_j^{(t+1)} + \Delta\vec{U}_j^{(t+1)}\Delta\vec{I}_{ji}^{(t+1)*} \quad (3.24)\end{aligned}$$

The rightmost term in the above equation can be ignored since the value is normally very small (two small delta values multiplied by each other), and an approximate expression for the change in active power, $\Delta\vec{S}_j^{(t+1)}$, can be found [12]:

$$\Delta\vec{S}_j^{(t+1)} \approx \vec{U}_j^{(t)}\Delta\vec{I}_{ji}^{(t+1)*} + \vec{I}_{ji}^{(t)*}\Delta\vec{U}_j^{(t+1)} \quad (3.25)$$

As described above, the lack of change of the receiving end power, i.e. $\Delta\vec{S}_j^{(t+1)} = 0$, may be an indication of voltage collapse. This can occur under two conditions, either when the two terms are equal and have opposite phase angles, or when both $\Delta\vec{I}_{ji}^{(t+1)}$ and $\Delta\vec{U}_j^{(t+1)}$ are zero. The latter condition describes the normal steady-state operating condition and should be disregarded.

Based on Equation (3.25), the SDI indicator is thus defined as

$$\text{SDI} = 1 + \frac{\left|\vec{I}_{ji}^{(t)*}\Delta\vec{U}_j^{(t+1)}\right|}{\left|\vec{U}_j^{(t)}\Delta\vec{I}_{ji}^{(t+1)*}\right|}\cos\theta \geq 0 \quad (3.26)$$

where θ is the angle between the two terms.

Voltage collapse occurs when SDI = 0, but for practical reasons, the critical threshold for taking action should be determined by detailed system analysis and is recommended to be less than 0.2 [12].

It should be noted that the indicator is only valid for lines that consume reactive power, i.e. it can not be applied on cables or lightly loaded overhead lines.

3.6 Impedance Stability Index – ISI

The *impedance stability index* (ISI) [14] is based on measurements of load and system impedances, and a similar principle has been proposed to be used in a relay for voltage instability prediction [17, 18].

According to Thévenin's theorem, any electrical system can be represented by a voltage source (E_{th}) and a series impedance (Z_{sys}). As mentioned in Section 2.2, the maximum power transfer level of the system is reached when the amplitude of the load impedance becomes equal to the amplitude of the system's Thévenin impedance (as seen from the load bus), $|\vec{Z}_{sys}| = |\vec{Z}_{load}|$. The ISI is defined as the ratio between the two impedances:

$$\text{ISI} = \frac{Z_{sys}}{Z_{load}} \leq 1 \tag{3.27}$$

Estimating the Thévenin equivalent

There are many ways to obtain the Thévenin equivalent of the power system, see e.g. references [19, 20, 21]. A relatively simple method described in [21, ch.2.3.2] is presented below.

The Thévenin equivalent of a power system as seen from a bus j is illustrated in Figure 3.6. From this, the following equation can be derived:

$$\vec{E}_{th}^{(t)} = \vec{U}_{j}^{(t)} + \vec{I}^{(t)}\vec{Z}_{sys}^{(t)} \tag{3.28}$$

$\vec{U}_j$ and $\vec{I}$ are measured at the load bus, but Equation (3.28) still has two unknown vectors, $\vec{E}_{th}$ and $\vec{Z}_{sys}$. There are infinitely many solutions to this

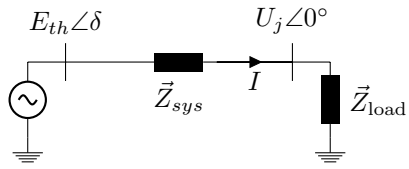

Figure 3.6: Thévenin equivalent of a power system at node j.

equation, and one way to work around this problem is to use two (or more) consecutive measurements of the load bus voltage and current and assume that the Thévenin voltage and impedance, $\vec{Z}_{sys}$ and $\vec{E}_{th}$, are constant between the measurements:

$$\left.\begin{array}{l}\vec{E}_{th}^{(t)} = E_{th}^{(t+1)} \\ \vec{Z}_{sys}^{(t)} = Z_{sys}^{(t+1)}\end{array}\right\} \Rightarrow \vec{U}_j^{(t)} + \vec{I}^{(t)}\vec{Z}_{sys}^{(t+1)} = \vec{U}_j^{(t+1)} + \vec{I}^{(t+1)}\vec{Z}_{sys}^{(t+1)} \tag{3.29}$$

With $\vec{E}_{th}$ eliminated, the equation can be solved for $\vec{Z}_{sys}^{(t+1)}$:

$$\vec{Z}_{sys}^{(t+1)} = \frac{\vec{U}_j^{(t)} - \vec{U}_j^{(t+1)}}{\vec{I}^{(t+1)} - \vec{I}^{(t)}} = -\frac{\Delta\vec{U}_j^{(t+1)}}{\Delta\vec{I}^{(t+1)}} \tag{3.30}$$

From Equation (3.30) it is evident that the two sets of measurements of voltage and current must have different values of $\vec{U}_j$ and $\vec{I}$. To ensure that the two sets are different, the time window between the measurements can be increased, but the larger the time window, the less valid the assumption of a constant Thévenin equivalent becomes.

Since the assumption of a constant Thévenin equivalent is never completely valid due to, for example, variations in loads elsewhere in the system, the resulting Thévenin impedance will include some noise and requires filtering.

The load impedance can be calculated directly from the measurements of voltage and current:

$$\vec{Z}_{load}^{(t)} = \frac{\vec{U}_j^{(t)}}{\vec{I}^{(t)}} \tag{3.31}$$

Inserting (3.30) and (3.31) into (3.27) gives an expression to directly determine the ISI using the above method:

$$\mathrm{ISI}^{(t+1)} = \frac{I^{(t+1)}\Delta U_j^{(t+1)}}{U_j^{(t+1)}\Delta I^{(t+1)}} \tag{3.32}$$

3.7 Short-Circuit Capacity Index – $\mathrm{VSI_{SCC}}$

The *short-circuit capacity index* $\mathrm{VSI_{SCC}}$ [16] estimates the voltage stability of the system by comparing the *actual* short circuit capacity to the *minimum* short circuit capacity that can reliably supply the load.

Both short-circuit values are calculated from an estimated Thévenin equivalent, described in the previous section. First, the actual short circuit capacity, SCC_p, is calculated:

$$\mathrm{SCC}_p = \frac{E_{th}}{X_{th}} \tag{3.33}$$

By assuming that the load (S_L) corresponds to the maximum power transfer level, the minimum short circuit capacity can be calculated using Equation (2.8), which assumes conditions as they are at the maximum power transfer level. Using $X = X_{th}$, $E = E_{th}$ and $P_{L\,max} = S_L \cos\phi$ in Equation (2.8) gives:

$$S_L \cos^2\phi = \frac{E_{th}^2}{2X_{th}}(1 - \sin\phi) \tag{3.34}$$

Inserting the expression for the short circuit capacity, $\frac{E_{th}}{X_{th}} = \mathrm{SCC}_{min}$, the minimum short circuit capacity for the actual load level can be found as:

$$\mathrm{SCC}_{min} = \frac{2S_L(1 + \sin\phi)}{E_{th}} \tag{3.35}$$

If the two short-circuit capacities are equal, the previous assumption is correct and the system is at the maximum power transfer level. $\mathrm{VSI_{SCC}}$ is thus defined as the ratio of the two expressions:

$$\mathrm{VSI}_{SCC} = \frac{\mathrm{SCC}_{min}}{\mathrm{SCC}_p} = \frac{2S_L X_{th}(1 + \sin\phi)}{E_{th}^2} \tag{3.36}$$

3.8 Discussion

All studied indicators assume that the point of instability corresponds to the maximum power transfer level, i.e. the tip of the nose curve, which they then try to detect. The actual point of instability is, however, normally somewhere slightly below the maximum loadability point on the PV curve, depending on the load characteristic [4].

3.8.1 FVSI and L_{mn}

The similarity of the two indicators FVSI and L_{mn} can be illustrated by inserting $\delta = 0$ in the L_{mn} equation (3.11):

$$L_{mn}\Big|_{\delta=0} = \frac{4X_{ij}Q_j}{U_i^2 \sin^2(\theta)} = \frac{4Z_{ij}Q_j}{U_i^2 X_{ij}} = \text{FVSI} \tag{3.37}$$

As seen from the above equation, the only difference between L_{mn} and FVSI is that L_{mn} accounts for the voltage angle difference which FVSI assumes to be zero, and that is also the advantage of FVSI over L_{mn}. FVSI only requires measurements of magnitudes, while L_{mn} requires synchronised phasor measurements at both ends of the line, since the calculation includes the voltage angle difference between the buses.

The main problem is that both FVSI and L_{mn} are based on the assumption that the voltage instability occurs across the line they are being calculated for. This is often not the case, especially in radial sections of a network such as the one illustrated in Figure 3.4, where these indicators might perform poorly.

For example, in case of a voltage collapse between buses 1 and 4 in the figure, the indices will provide false results when calculated both between buses 1 and 4 and between buses 3 and 4. In the former case, the indices may indicate voltage collapse too early due to the loads on the intermediate buses, while in the latter case it might not indicate any voltage collapse at all.

3.8.2 SDI

The advantage of the SDI is that it only requires local phasor measurements. This means that the indicator is able to include the effect that the rest of the system has on the voltage stability at the measured bus with no additional measurements, unlike e.g. FVSI, L_{mn} and TPSI.

Due to the calculations involving delta-values (i.e. the difference between consecutive measurements), the S-difference indicator can be noisy and may require filtering.

3.8.3 ISI

Since not all buses have a clearly defined "load", the challenge of the ISI in meshed grids is to determine how the Thévenin-equivalent should be estimated, and this can be a source of erroneous results.

The impedance stability index is very similar to the SDI as they are both calculated from measurements of delta-values, and the similarity can be illustrated by inserting Equations (3.30) and (3.31) into (3.26):

$$\mathrm{SDI} = 1 + \frac{\left|\vec{I}_{ji}^{(t)*}\Delta\vec{U}_{j}^{(t+1)}\right|}{\left|\vec{U}_{j}^{(t)}\Delta\vec{I}_{ji}^{(t+1)*}\right|}\cos\theta = 1 + \frac{\left|\vec{Z}_{sys}^{(t+1)}\right|}{\left|\vec{Z}_{load}^{(t)}\right|}\cos\theta \approx 1 + |\mathrm{ISI}|\cos\theta \quad (3.38)$$

As the equation illustrates, the main difference between the two indicators is that the SDI accounts for the angle between the two terms and might therefore give slightly different results than ISI.

3.8.4 $\mathrm{VSI_{SCC}}$

$\mathrm{VSI_{SCC}}$ requires an estimate of the system's Thévenin equivalent, and has the same disadvantages as the ISI, namely the problem of determining an accurate equivalent model of the system.

Since an equivalent of the system needs to be obtained, one might argue that this indicator is overly complex, and utilising the equivalent parameters directly, such as in ISI, is more appropriate.

3.8.5 TPSI

TPSI requires synchronised phasor measurements at all buses within an area or throughout the system to give good results. The required amount of measurements can be reduced by using a state estimator, which provides estimated values of the voltage phasors throughout the system.

As the TPSI algorithm is outlined in [11], it is designed to be applied to a system as a whole and calculate the index for all load buses simultaneously. A suggested modification is to reverse the path-finding part of the

algorithm, starting at a given bus and searching for paths with increasing voltages / voltage angles. These paths will end at the same buses as the original algorithm starts at, and can simply be reversed so that the rest of the TPSI algorithm can be applied. This will allow TPSI to be calculated for any bus.

The main obstacle of TPSI is that it may require a large amount of calculations compared to the other indicators discussed here, due to the possibly high number of transmission paths leading to the considered buses. Additionally, transformers with off-nominal tap ratios or phase-shifts can confuse the path-finding algorithm if that is not accounted for.

3.9 Indicator Implementation Details

All of the studied indicators have been implemented in MATLAB for further use in the case studies, and this section briefly describes the implementation of each indicator.

SDI

SDI has been implemented as described in references [12] and [13], with two exceptions:

- Instead of disregarding measurements where ΔI is smaller than the threshold, the delta values are accumulated until the sum of ΔI becomes larger than the threshold. This was done in order to calculate the SDI value more accurately in periods where the variation in the current is low.
- If the line is producing reactive power, SDI can not be calculated and the output is set to 2.0 so that the condition can be detected.

ISI and VSI_{SCC}

ISI and VSI_{SCC} have been implemented according to the equations in the respective sections of this chapter. Estimation of the Thévenin equivalent used

by both indicators was done based on the equations in Section 3.6, but using a cumulative sum filtering method as described in reference [21, sec. 3.2.4].

Unless otherwise specified, the Thévenin-equivalent used in the calculations of the indicators ISI and VSI_{SCC} is estimated based on the direction of the active power flow of a single branch.

TPSI

The path-finding algorithm of TPSI was replaced by the more efficient method suggested in Section 3.8.

FVSI and L_{mn}

FVSI and L_{mn} were implemented according to the equations described in sections 3.2 and 3.3.

4 Mitigating Voltage Collapse

This chapter discusses various mitigation strategies for avoiding voltage collapse that can be utilised by a system integrity protection scheme.

4.1 Background

When the system is close to voltage instability, actions are required to relieve the situation and mitigate the possible oncoming voltage collapse. Actions to mitigate a voltage collapse must either reduce the reactive power consumption, increase the available reactive power or decrease the system impedance in order to maintain steady voltages. Reducing the active power load is also an option since it will reduce the (mostly reactive) transmission losses. The following sections will discuss a few possible actions.

As mentioned briefly in Chapter 2.3, voltage instability can be either a short-term or a long-term phenomenon, depending on the type of load. In the case of a short-term instability, the time period until the system collapses is only a few seconds, while in the case of a long-term instability, the time period is in the order of minutes [4]. If the stability indicators described in Chapter 3 are used to determine when to initiate mitigating actions, the time delay from a mitigation strategy is initiated until it is at full effect should be as short as possible since the indicators do not give any information about the time until a collapse.

4.2 Load Shedding

Load shedding is a conventional approach to mitigate an oncoming voltage collapse, and it is very effective since it will reduce both the active and the reactive power load. However, the main objective of the power system is to provide electricity to the load, so load shedding should be regarded as a last resort.

4.3 Switching of Reactive Compensation Devices

Switching of reactive compensation devices is also a very effective option. Shunt reactors can be disconnected to reduce the reactive load, shunt capacitors can be connected to increase the available reactive power and static var compensators (SVCs) can be enabled.

These are measures that should be recognised during operation planning, but unforeseen contingencies can occur and mistakes can be made so these measures should also be considered as mitigation actions to prevent voltage instability.

4.4 Altering Generator Active Power Production

Altering the active power generation on generators can be done to increase the amount of available reactive power. Increasing the active power generation near the critical region of the power system will reduce reactive transmission losses, while decreasing the active power production will increase the reactive power capability of the generators. These two options are described in detail below.

Both options are unconventional mitigation actions, and the effect of these measures is tested in the case studies in Chapter 7.

4.4.1 Decreasing Active Power Production

Decreasing the active power output of a generator will increase its reactive power capability. This is illustrated in Figure 4.1, which shows the conceptual trajectory of the generator's operating point during such a maneuver. When the active power generation is decreased (vertical blue line, labeled 1), the generator's reactive power capability increases (horizontal blue line, labeled 2).

The actual trajectory in the PQ-plane will follow the curved, blue line labeled 3 in the figure. When an OEL is active, the field current is held constant at its maximum long-term value, so that when the active power output

is decreased, the operating point follows the maximum reactive power limit curve.

The effectiveness of this method depends heavily on the situation. Decreasing the active power generation in an area that is close to voltage collapse has the potential to worsen the situation since it can result in an increased import of active power to the region, increasing the reactive transmission losses and thus reducing the effect of the measure.

This mitigation action will only have an effect on generators where the overexcitation limiter is active. If the limiter is not active, the generator is either not at the reactive capability limit, or the excitation system is utilising the thermal overload capability of the field winding to produce as much reactive power as required regardless of the field current limit.

4.4.2 Increasing Active Power Generation

Increasing the active power generation within an area that is close to voltage instability can be almost as effective as shedding load. The amount of active power being transferred to the critical area will be reduced, reducing the

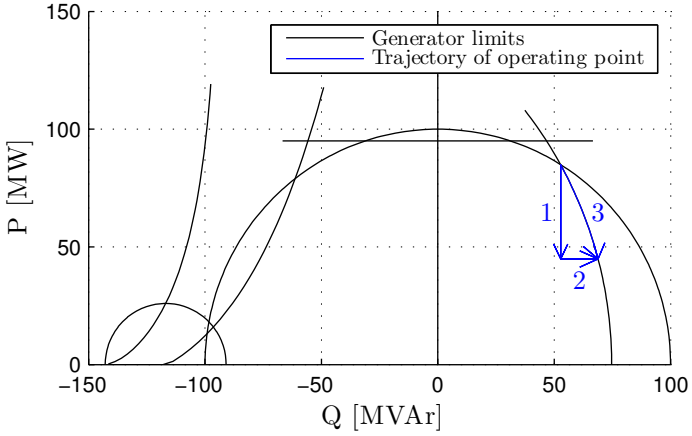

Figure 4.1: Effect of decreasing active power generation on a generator's reactive power capability. 1. decreased active power, 2. increased reactive power capability, 3. trajectory of operating point.

reactive power losses and thus improving the voltage stability.

The power increase can be done on generators that are already online, but not at their maximum active power output limit, or on offline generators that can be brought online in a short amount of time (seconds).

Following the opposite direction of the trajectory in Figure 4.1, one can see that increasing the active power output can result in a decrease in the reactive output if the over-exciation limiter is active. Additionally, if the limiter is not active before the increase, the increase can result in the OEL being activated, reducing the reactive power output.

This approach assumes that the generators are able to increase their active power generation and that they can do so in a short amount of time, which may not always be the case.

4.4.3 Combining Both Methods

A combination of both methods described above can be a more optimal solution, depending on the situation at hand. The active power output can be reduced on generators operating close to their maximum, while it can be increased on generators with a low active power output to get a more optimal use of the capabilities of all generators.

4.5 Increasing Voltage Set Points of Voltage Controlling Equipment

Increasing the voltage set points of voltage controlling equipment is another unconventional mitigating action. The set point increase will cause the voltage regulating units to increase their reactive power output in order to increase the voltage. This adds more reactive power to the system, and the increased voltages will reduce transmission losses and cause shunt capacitors to produce more reactive power.

Additionally, the reactive power capability of synchronous generators is affected by an increased terminal voltage, as shown in Figure 4.2. In the

case shown in the figure, the maximum reactive power limit (arrow 1) barely changes, but the armature current limit (arrow 2) is increased noticeably, allowing more reactive power output near the maximum active power limit.

The disadvantage of this method is that the increased reactive power output from synchronous generators can cause overloading of the field winding, which, after a time delay, will activate the overexcitation limiter and reduce or eliminate the effect of increasing the AVR set point.

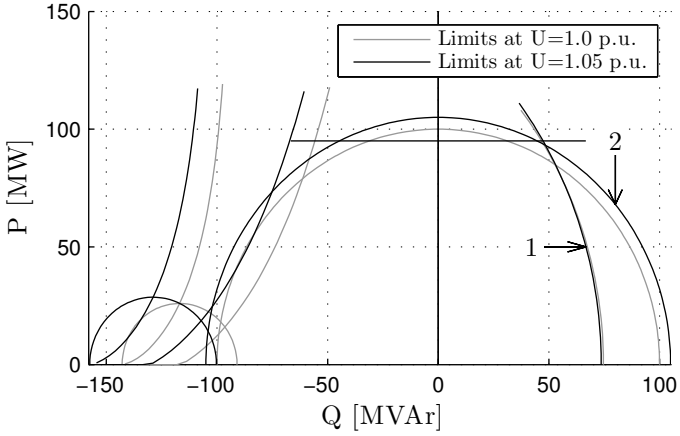

Figure 4.2: Effect of increasing generator terminal voltage on the reactive power capability of a synchronous generator. 1. Maximum reactive power capability, 2. armature current limit.

5 Description of Proposed System Integrity Protection Scheme

As mentioned in Chapter 4, the voltage stability indicators do not give any information about the time until the voltage collapses, and the time period can be in the order of a few seconds to several minutes. Due to the possibly short time-periods involved, the system operator may not be able to respond quickly enough to prevent a voltage collapse.

A solution to this is to hand over the responsibility to a system integrity protection scheme (SIPS). A SIPS will be able to respond automatically and immediately, and perform the required actions in a timely manner. The system should choose among the available mitigation strategies based on the severity of the system state and try to avoid load shedding as far as possible.

This chapter describes a SIPS that is based on an algorithm that attempts to mitigate voltage instability by using information from voltage stability indicators. The SIPS can additionally use information from overexcitation limiters (OELs) on generators in the system.

5.1 Overview

The basics of the proposed mitigation algorithm is illustrated in Figure 5.1, where one or more indicators are used to assess the system state. Two levels of severity are used, *alarm* and *critical*, where the alarm level is less severe than the critical level.

At the alarm level, the system is close to instability, and the algorithm will try to relieve the situation by applying mitigation actions that do not involve shedding of load, referred to as *alternative* actions or strategies. Should the distance to voltage instability continue to decrease, the indicator(s) will reach

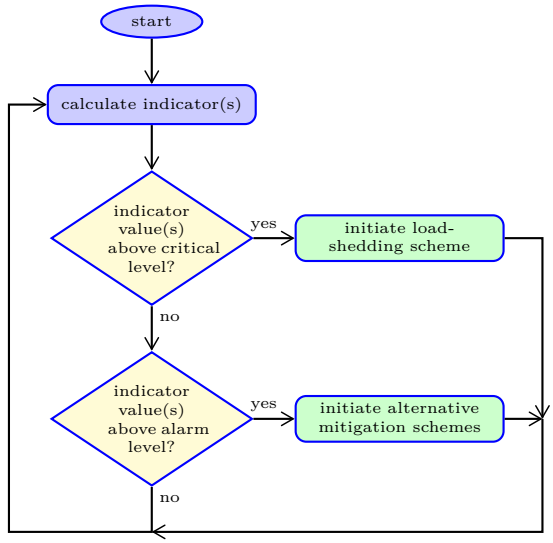

Figure 5.1: Flowchart illustrating the basics of the proposed mitigation algorithm.

the critical level. At the critical level, the algorithm starts to shed load until the distance to voltage stability returns to an acceptable level.

The SIPS can, in addition to this algorithm, use activation signals from OELs as an input. Activation of an OEL in a system or an area that is close to voltage instability will reduce the reactive power capability of that generator and push the system further towards instability. Depending on the size of the generator and on the proximity of the generator to the voltage-critical area, OEL activation may cause immediate voltage collapse.

A suggested use of the OEL signals is to initiate immediate load shedding in case of OEL activation while the system is in the alarm state. Alternatively, the signals can be used to trigger one of the mitigation actions described in Section 4.4 – increasing or decreasing the active power generation. Activation of the OEL indicates that the generator is highly affected by the stressed situation, and thus the same generator should be able to relieve the situation.

A third use of the OEL signals is to initiate other mitigation actions in the

vicinity of the activated OEL, since the signal indicates that there is a deficit of reactive power in that area.

5.2 Pre-Commissioning Considerations

Selection of indicator(s)

Detailed analysis must be done before the algorithm is commissioned in a power system, in order to determine which indicators give the best results in the given area(s).

Determining critical and alarm levels

When appropriate indicators have been selected, critical and alarm levels must be determined. The critical level should be chosen so that, given a short-term voltage instability, there is enough time for the load-shedding signal to have an effect before the voltage collapses.

The alarm level is less severe than the critical level, and should be chosen so that the margin to the critical level is large enough for the alternative mitigation actions to have an effect. The margin should not be too large, to prevent the algorithm from attempting to mitigate voltage instability under normal operating conditions.

5.3 Operational Details

In operation, the algorithm continuously monitors the system state via voltage stability indicators and initiates mitigating actions if the indicators exceed predefined thresholds.

5.3.1 Selection of Mitigation Actions

If the system enters the alarm state, the algorithm must decide which mitigation actions to apply in the area where the system is closest to instability. This can be done by continuously monitoring the state of reactive compensation

equipment and keeping a list of online generators that are available for voltage and governor set point adjustments.

The following list of mitigation actions can be defined, sorted by their assumed effectiveness as described in Chapter 4:

1. Load shedding
2. Switching of reactive compensation devices
3. Increasing voltage set points of voltage controlling equipment
4. Increasing generator active power generation
5. Decreasing generator active power generation

Load shedding should only be initiated if the system enters the critical state, since the purpose of the alarm state is to try to prevent load shedding.

5.3.2 Selection of Buses for Mitigation Actions

For the mitigation actions listed above, it is important to determine which generators, SVCs, loads, etc. that have the largest influence on the voltage in the critical area.

As mentioned earlier in this chapter, the activation signal from OELs can be used to determine which generators are influenced by the voltage instability, and thus which generators can be used to improve the situation. Sometimes these signals may not be available, and an alternative is then to use the information available in the impedance matrix of the system, assuming that it is available from e.g. the system control centre. In the following derivation, the effect a generator on bus j has on the voltage at the critical bus i is considered.

The off-diagonal impedance matrix element Z_{ij} is defined as:

$$\vec{Z}_{ij} = \frac{\Delta\vec{U}_i}{\Delta\vec{I}_j} \tag{5.1}$$

Rearranging and considering ΔI_j as a current injection from the generator, the vectorial change in the voltage on the load bus can be expressed as:

$$\Delta\vec{U}_i = \Delta\vec{I}_j\vec{Z}_{ij} \tag{5.2}$$

To determine the influence of $\Delta\vec{U}_i$ on the voltage *magnitude* at the load bus, which is what is of interest from a voltage stability perspective, further considerations are required:

$$\begin{aligned}\Delta U_i &= |\vec{U}_i + \Delta\vec{U}_i| - |\vec{U}_i| \\ &= |\vec{U}_i + \Delta\vec{I}_j\vec{Z}_{ij}| - |\vec{U}_i|\end{aligned} \tag{5.3}$$

For simple assessments where voltage vectors are unknown, Equation (5.2) can be used, and for more accurate assessments, Equation (5.3) should be used.

If additional information such as the U/I_Q-slopes of AVRs is available, it can be utilised to make a better estimate of which generators to perform actions on. Using the same procedure as above, but now considering a change in the load at bus i, $\Delta\vec{I}_i$, the effect of the load change on the generator bus voltage can be expressed as:

$$\Delta\vec{U}_j = \Delta\vec{I}_i\vec{Z}_{ji} \tag{5.4}$$

Since AVRs only sense the magnitude of the voltages, the change in the magnitude of the generator bus voltage can be expressed by applying the same consideration as in Equation (5.3):

$$\begin{aligned}\Delta U_j &= |\vec{U}_j + \Delta\vec{U}_j| - |\vec{U}_j| \\ &= |\vec{U}_j + \Delta\vec{I}_i\vec{Z}_{ji}| - |\vec{U}_j|\end{aligned} \tag{5.5}$$

The change in voltage on the generator bus will cause the AVR to respond according to the droop of the U/I_Q characteristic, denoted $\tan\alpha$ [6, p.99]:

$$\begin{aligned}\Delta I_j &= -\frac{\Delta U_j}{\tan\alpha} \\ &= -\frac{|(\vec{U}_j + \Delta\vec{I}_i\vec{Z}_{ji})| - |\vec{U}_j|}{\tan\alpha}\end{aligned} \tag{5.6}$$

Equation (5.6) expresses the relationship between a change in the load and the resulting reactive power output from the generator. If the relationship is strong, i.e. ΔI_j is large, it is reasonable to assume that the generator is equally able to affect the voltage on the load bus. Since the droop of the U/I_Q characteristic is included, the equation will favour the most sensitive generators, i.e. the generators that are most likely to attempt to counteract voltage set point adjustments at other, nearby generators.

Both of the above methods are simplified and do not account for the effect of voltage controlling equipment at other buses, but they should provide a reasonable indication of which buses that are suitable to initiate mitigation actions at.

These methods can also be used to detect where it would be most efficient to shed load by replacing the generator bus (j) with other load buses.

6 Case Study: Two-bus system

In this chapter, case studies in a simple two-bus system are presented. The system was constructed to study the behaviour of the voltage stability indicators under ideal conditions, and to verify the implementation of the indicators. It consists of an infinite bus supplying an SVC-compensated load through a single line, as shown in Figure 6.1.

The load is modelled as a constant-impedance load with a power factor of 0.95. It is initially shunt-compensated so that the load-side voltage is 1.0 p.u. The per-unit power reference is 100 MVA and the per-unit voltage reference is 132 kV.

To study the indicators, the load was increased gradually, keeping the power factor constant, until the voltage collapsed or the simulation stopped converging. In the first simulation (Case 1), the SVC was offline, and in the second simulation (Case 2), the SVC was online and controlling the voltage on the load bus. The capacity of the SVC is very large (1 Gvar).

These two scenarios were designed to emulate the extremes of two conditions that may occur in a real system, i.e. controlled and uncontrolled load-bus voltages.

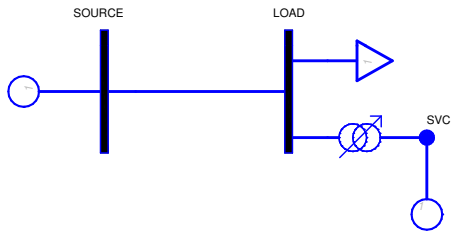

Figure 6.1: Single-line diagram of the two-bus system.

6.1 Simulation Results

6.1.1 Case 1: Uncontrolled Load Bus Voltage

The results from Case 1 are shown in Figure 6.2. The PV-curve in Figure 6.2a illustrates the course of events clearly. Initially, the load bus voltage is 1.0 p.u. and the load power is 0.2 p.u. As the load power increases, the load voltage drops. When the load power reaches 1.84 p.u. at $t = 61$, the maximum power transfer level is reached, and the power consumed by the load decreases as the load impedance continues to decrease until the voltage reaches zero, at which point the simulation stops.

The indicators are plotted in Figure 6.2b. As seen, all indicators, except FVSI and L_{mn}, reach their critical values at the maximum power transfer level.

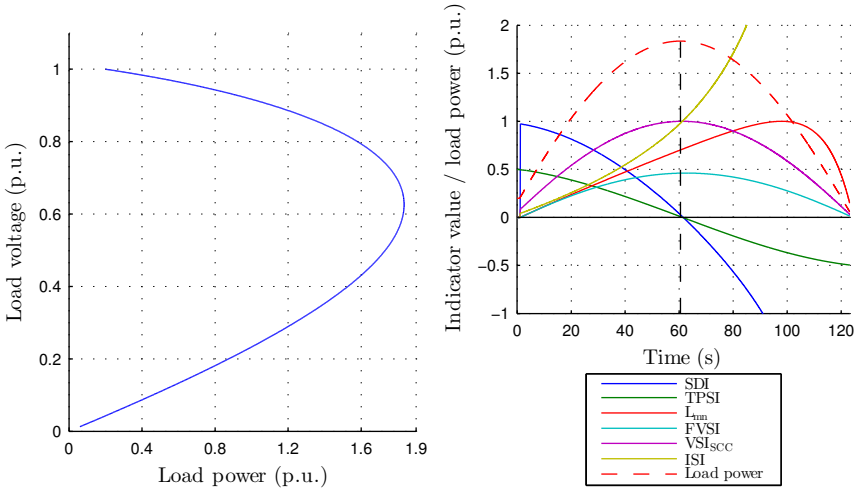

(a) PV-curve (b) Indicators

Figure 6.2: Simulation results, Case 1 in the two-bus system. Vertical dashed line indicates the maximum power transfer level.

6.1.2 Case 2: SVC Controlling Load Bus Voltage

The results from Case 2 are shown in Figure 6.3. The PV-curve in Figure 6.3a illustrates the effect of the SVC compared to Case 1. The curve is nearly a straight line compared to the case without the SVC, with only a slight drop at higher power levels due to the droop of the SVC's AVR.

The simulation stops converging shortly after the observed "tip" of the PV-curve, at which point the SVC reaches its reactive power limit and both voltage and load power drops rapidly. The maximum power transfer level in this case corresponds to a load power of 4.89 p.u. at $t = 99$ s.

The indicators, shown in Figure 6.3b, give a slightly different response than in Case 1. FVSI and L_{mn} both fail, SDI and ISI detect the observed tip of the nose curve, while TPSI and VSI_{SCC} reach their critical values a bit earlier. The reasons for the differing results are discussed below.

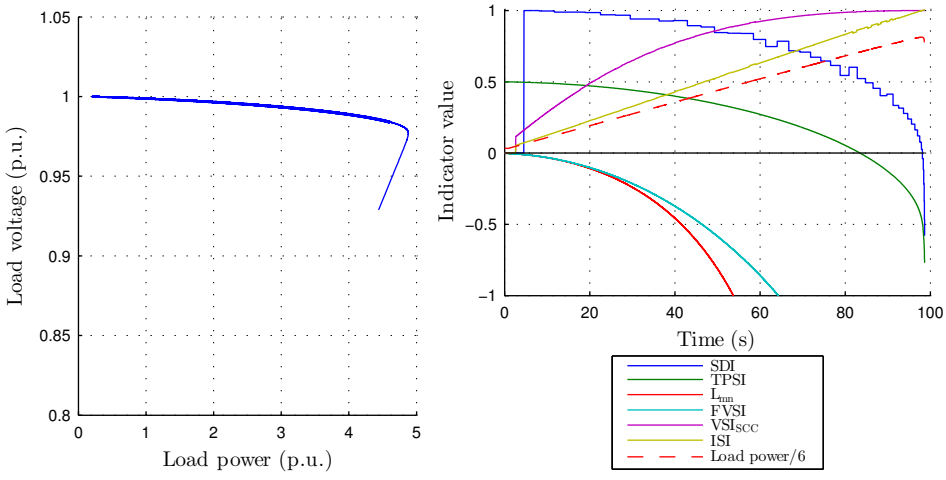

(a) PV-curve (b) Indicators

Figure 6.3: Simulation results, Case 2 in the two-bus system.

6.2 Discussion

6.2.1 Indicator Performance

SDI and ISI correctly detect the maximum power transfer level in both cases and continue to give "worse" values as the maximum transfer level is passed, which is the expected response of a good indicator.

TPSI detects the maximum loading point correctly in Case 1, but in Case 2 it indicates voltage instability before the actual instability point. Studying the results further, it can be seen that when TPSI becomes zero in Case 2, the voltage angle difference between the two buses is 60°, as shown in Figure 6.4. Inserting $\delta = 60°$ and $U_1 = U_2 = 1.0$ in the two-bus TPSI equation, (3.16), it corresponds to the zero response. This indicates that the system passes the tip of a PV-curve. The theoretical PV curves of the system, shown in Figure 6.5, confirm that the system indeed operates on the lower half of the PV curves towards the end of the simulation.

If the voltage on the load bus had been unregulated, TPSI would correctly indicate the point of instability, but the SVC stabilises the system by increasing the injection of reactive power as the load increases. This permits operation on the lower half of the PV curve, but it is not a recommended operating scenario since the stability of the situation depends heavily on the SVC's ability to stabilise the system during disturbances. Should the SVC reach its limit under such conditions, a collapse is imminent. Based on this reasoning, it can be argued that TPSI (and VSI_{SCC}) are the only indicators giving correct results in Case 2.

VSI_{SCC} is very close to its critical value at the same time as TPSI reaches zero in Case 2, indicating that it is well-suited to detect the maximum power transfer level. However, the indicator exhibits an inherent problem in Case 1, where the indicator value decreases after passing the maximum power transfer level. This behaviour is caused by the decreasing power consumed by the load, which causes a decrease in S_L in Equation (3.36), and thus a decrease in the indicator value.

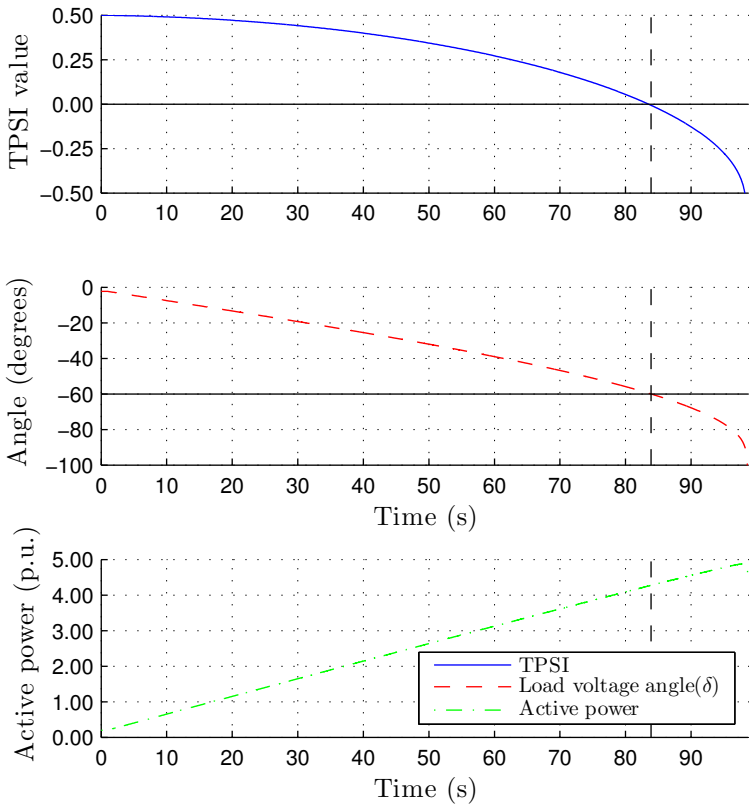

Figure 6.4: TPSI value, voltage angle and active power for case 2 in the two-bus system. Vertical dashed line indicates time of TPSI = 0.

FVSI and L_{mn} fail to indicate voltage instability in both cases. The reason for this is that both indicators are based only on the equation for received reactive power at the line end, and neither the load bus voltage nor the load power is considered. From equations (3.7) and (3.11), one can see that both indicators are proportional to the received reactive power at the load bus, and that appears to be what is causing issues. In the studied cases, the only variable in Equation (3.7) is the reactive power received at the load bus. Equation (3.11) also includes the angle difference and the power factor of the load, which is why it reaches the critical value in Case 1.

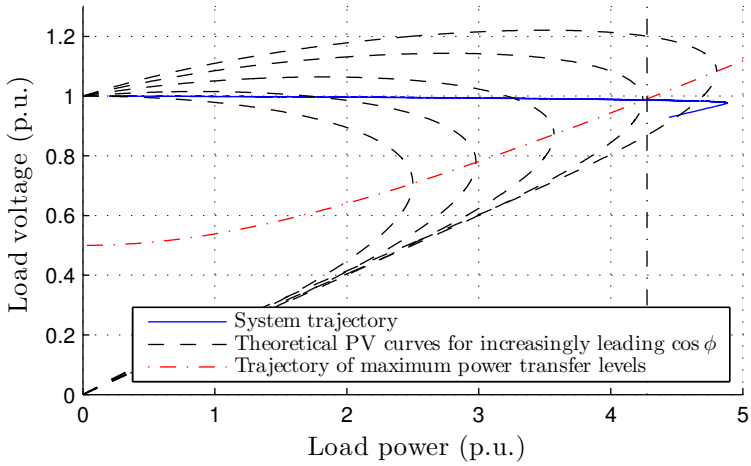

Figure 6.5: PV-plot for Case 2 in the two-bus system, including theoretical PV curves. Dash-dotted vertical line indicates point of TPSI=0.

In Case 2 both FVSI and L_{mn} give negative values since the SVC causes reactive power to flow from the load bus towards the infinite bus to accommodate the reactive losses in the line. Equally, if the load had consumed no or very little reactive power and there was no SVC to support the load-side voltage, both indicators would have a value close to zero since they are both proportional to the received reactive power.

6.2.2 Indicator Linearity

In Figure 6.6, indicator values are plotted versus load power for both cases. This is done to illustrate how well the indicators are able to indicate the distance to instability.

In Case 1, VSI_{SCC} is the most linear indicator, increasing in a straight line from the starting point up to its critical value. However, as mentioned above, the indicator value returns to zero following the same path, after passing the maximum power transfer level. This implies that the indicator is only able to indicate the *distance* from the maximum power transfer level, and not which half of the PV curve the system is at (stable upper half or unstable lower half).

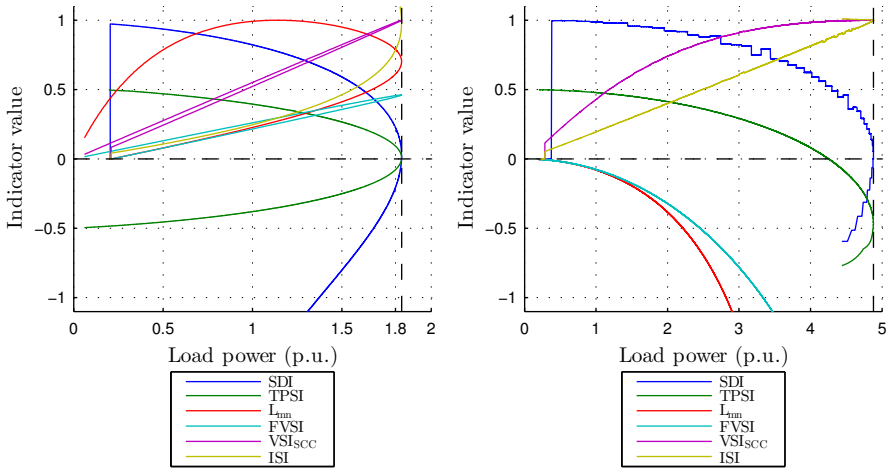

(a) Case 1 (b) Case 2

Figure 6.6: Indicator values vs. load power for the two-bus system. Dashed vertical lines indicate maximum load power.

ISI and SDI approach their critical values in a more curved manner and rapidly become more critical as the load approaches the critical level in Case 1. In Case 2, however, ISI is completely linear while SDI is similar to Case 1, probably due to the angle-term in SDI, as shown in Equation (3.38). TPSI behaves equally in both cases, having a similar shape as SDI, and continues to worsen as the critical point is passed.

The curved behaviour of these indicators when approaching the maximum power transfer level indicates that when selecting a critical value for the indicators, there must be a reasonable margin to account for the rapid change in the indicator value close to the maximum power transfer level.

L_{mn} and FVSI are not discussed here since they do not provide any useful information in either of the cases.

7 Case Study: IEEE Reliability Test System

In this chapter, a case study of the IEEE Reliability Test System (IEEE RTS) is described. The behaviour of the voltage stability indicators are studied for two contingencies that lead to voltage collapse, and possible mitigation actions and the proposed SIPS are tested.

The 1996 IEEE Reliability Test System is a power system model developed by the IEEE Application of Probability Methods Subcommittee. The model consists of three identical, interconnected areas and was originally designed for power system reliability evaluation studies. Each area is divided into two voltage levels, 230 kV and 138 kV. An overview of the system is given in Figure 7.1, and a detailed single-line diagram of one area is shown in Figure 7.2.

7.1 Model Description and Assumptions

In this study, an extended model of the IEEE RTS has been used. The model is developed by Ph.D. candidate Emil Hillberg and includes more detailed dynamic models of the generators, as described in [22]. Additionally, overexcitation limiter models were added to all generators in order to limit their reactive power capability, and a simplified, generic load restoration model was used to model load restoration dynamics. It is assumed that measurements required for calculations of all voltage stability indices are available. The per-unit power reference is 100 MVA, and voltage references are indicated in figures 7.1 and 7.2.

7.1.1 Overexcitation Limiters

The overexcitation limiter model that has been used in this study is the *MAXEX2* model from the standard PSS/E model library [23]. The block diagram is shown in Figure 7.3. MAXEX2 is a simplified generic OEL model with a piecewise

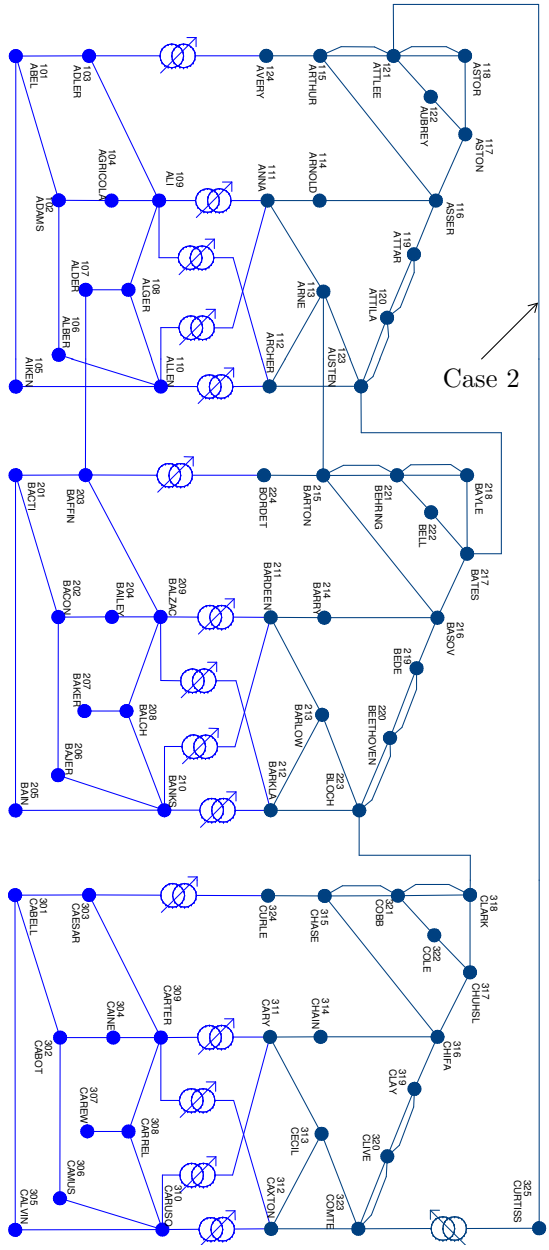

Figure 7.1: Single-line diagram of the three-area IEEE Reliability Test System, area A (left), area B (middle) and area C (right). Dark blue buses: 230 kV, light blue buses: 138 kV.

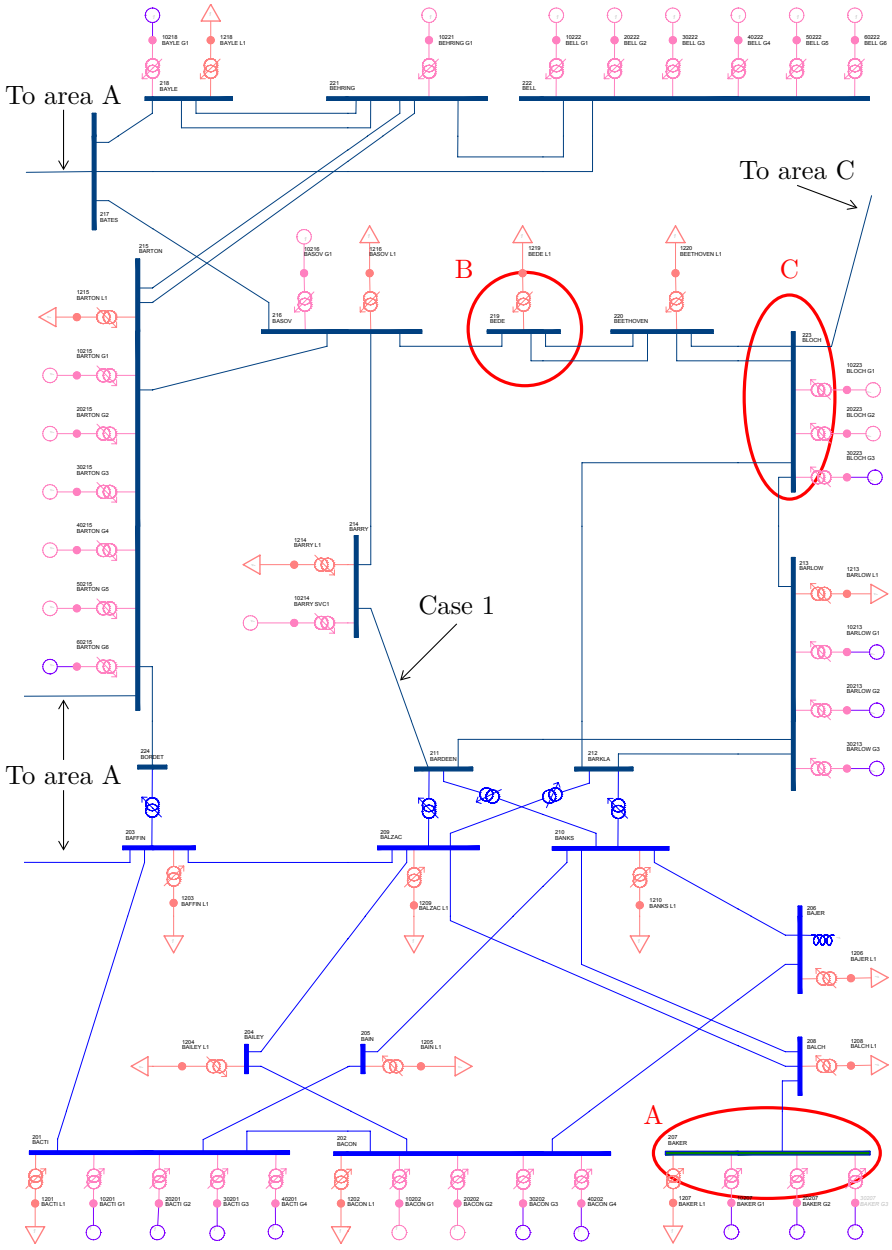

Figure 7.2: Single-line diagram of one area (area B) of the IEEE Reliability Test System, area interconnections not included. Dark blue buses: 230 kV, light blue buses: 138 kV. Red circles indicate buses to be studied below.

linear inverse time delay characteristic and is designed to be used as a summed limiter, i.e. the OEL model limits the field current by reducing the voltage set point of the AVR.

Reference [24] does not define any maximum field current limits or nominal generator power factors for the IEEE RTS model. Instead, maximum active and reactive power outputs are specified. Therefore, the field current limits were assumed to correspond to the field current required to operate the generators at the specified maximum power outputs at 1.0 p.u. terminal voltage.

The time delay for the OELs was chosen by assuming that the thermal capability of the field winding corresponds to the requirement in IEEE C50.13-2005, *IEEE Standard for Cylindrical-Rotor 50 Hz and 60 Hz Synchronous Generators* [25]. It was further assumed that the limiter characteristic has been coordinated with an overexcitation protection relay, by providing a margin between the thermal capability and the OEL limit, as shown in Figure 7.4.

7.1.2 Load Modelling

Since no load classification is defined for the IEEE RTS system, the polynomial ZIP load model was employed, which consists of three components: constant impedance, constant current and constant power. The parameters are given in Table 7.1.

Load restoration mechanisms were modelled using the generic load restoration model class EXTL from the standard PSS/E model library [23]. The EXTL-class models adjust the load represented by the ZIP model in order to

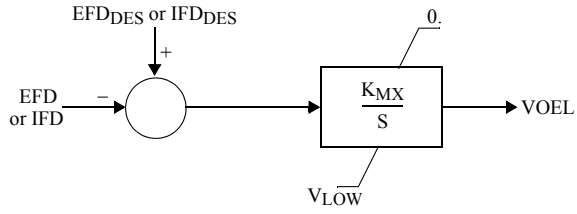

Figure 7.3: Block diagram of overexcitation limiter model MAXEX2 (time delay function not included), from [23].

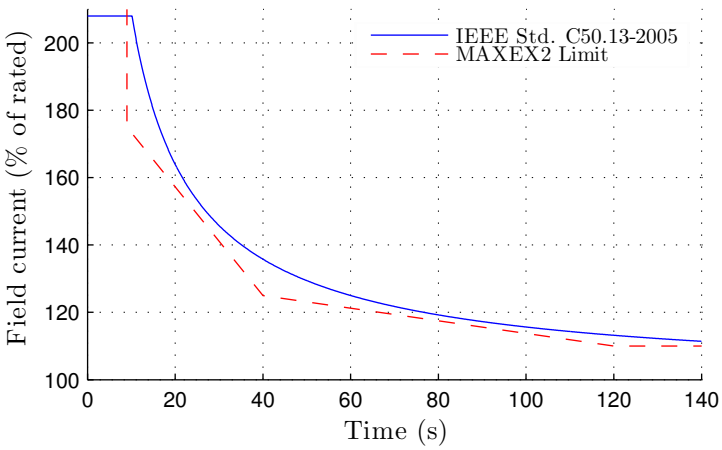

Figure 7.4: OEL time delay used in the IEEE RTS studies.

Table 7.1: ZIP load model data used in IEEE RTS model simulations.

	Active power	Reactive power
Fraction of constant impedance (Z)	0.6	1.0
Fraction of constant current (I)	0.4	0
Fraction of constant power (P)	0.0	0

restore the load to the initial power level after a voltage change. The block diagram is shown in Figure 7.5, and a typical load restoration response by this model is shown in Figure 7.6.

The EXTL models were given a relatively high time-constant, in order to model the typical response of thermostat controlled loads. In a real system there will be a more complex composition of both fast and slow load restoration mechanisms, but the chosen load model is adequate to simulate the effect of a voltage collapse, and may also illustrate the involved mechanisms more clearly due to the slower progression of the collapse.

Detailed model data can be found in Appendix B.

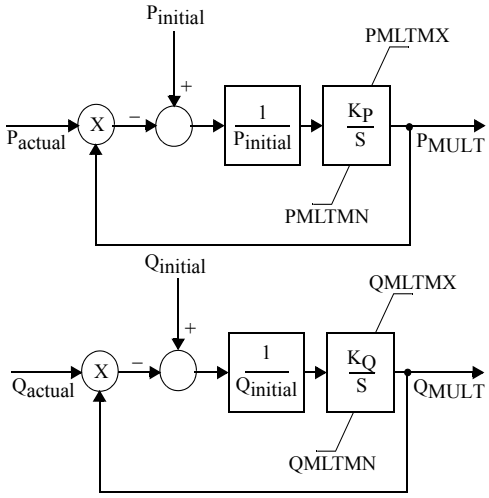

Figure 7.5: Block diagram for EXTL-class load restoration model, from [23].

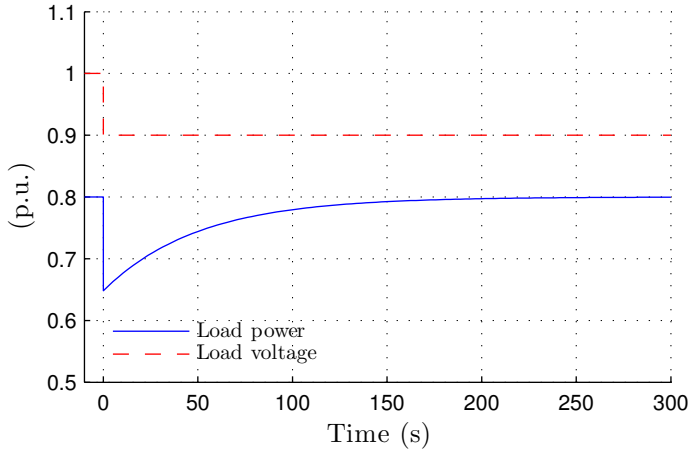

Figure 7.6: Response of EXTL-class load restoration models to a 10% voltage drop, assuming a constant-impedance load.

7.2 Operating Scenario

The power flow of the studied scenario is summarised in Table 7.2. Areas A and C have a surplus of active power, while area B has a total deficit of approximately 870 MW. Due to the large deficit, area B is the area that is considered most likely to experience voltage instability. The generators in the system play an important role in maintaining voltage stability, so a list of offline generators is provided in Table 7.3.

7.3 Contingency Analysis

Based on the operating scenario described above, a contingency analysis has been performed to identify failures which may lead to voltage instability. The contingencies have been selected based on the highest loaded inter-area tie-lines and on the lines and transformers supplying the highly loaded 138 kV subarea in area B. To limit the analysis, mainly N-1 contingencies have been considered. Since the matter of interest is voltage stability, no faults were simulated before tripping components in order to avoid other types of instability or disturbances that may occur.

The results are listed in Table 7.4, and of the studied contingencies, two were found to lead to voltage instability and three brought the system very close to instability. The results from the two voltage-unstable cases, outage of the line between buses 214 and 211 and of the line between buses 121 and 325, referred to as Case 1 and Case 2, respectively, are examined in detail below.

Table 7.2: Power flow summary, IEEE RTS operating scenario.

	Area A	Area B	Area C	Total
Generation [MW]	1715.3	934.0	2189.0	4838.3
Load [MW]	1459.0	1713.7	1468.9	4531.6
Export to A [MW]	—	-405.1	211.8	-193.3
Export to B [MW]	405.1	—	469.0	874.1
Export to C [MW]	-211.8	-469.0	—	680.8

Table 7.3: Offline generators, IEEE RTS operating scenario.

Bus no.	Offline/total no. of generators	Rated active power [MW]
Area A		
101	4/4	20/20/76/76
102	2/4	76/76
107	3/3	100/100/100
113	2/3	197/197
118	1/1	400
Area B		
201	4/4	20/20/76/76
202	2/4	76/76
207	3/3	100/100/100
213	3/3	197/197
215	1/6	155
218	1/1	400
223	1/3	350
Area C		
301	4/4	20/20/76/76
302	2/4	76/76
307	3/3	100/100/100
318	1/1	400

7.4 Simulation Results, Case 1: Outage of Line 214-211

Figure 7.7 shows the voltages at all buses in the system during a simulation of disconnection of the line between buses 214 and 211. At time $t = 1.0$ second, the line is tripped. As a consequence, the voltages in area B drop significantly, and due to load restoration, the voltages keep declining. At $t = 59$ s, the overexcitation limiters on both generators at bus 202 are activated, followed by activation of OELs at buses 223 ($t = 160$ s) and 221 ($t = 313$ s). Finally, at $t = 334$ s, the simulation stops converging, at which point the lowest bus voltage is only 0.33 p.u.

Below, the results at three buses are examined in detail; buses 207, 219 and 223, which are indicated by red circles in the single-line diagram in Figure 7.2. These buses were selected in order to analyse the performance of the voltage

Table 7.4: Contingencies simulated in IEEE RTS model.

Component	Result
Lines	
217-222	Stable
216-217	Stable
209-208	Marginally voltage stable, close to instability on bus 207
210-208	Marginally voltage stable, close to instability on bus 207
212-223	Stable
213-223	Stable, but low voltages on buses 207, 208
318-223	Angle instability
213-212	Stable
224-215	Stable
123-217	Stable
121-325	Voltage unstable after 540 seconds
214-211	Voltage unstable after 330 seconds
Cables	
206-210 + Reactor	Marginally voltage stable, close to instability on bus 207
201-202	Stable
Transformers	
211-209	Stable
211-210	Stable
212-209	Stable
212-210	Stable
Generators and SVCs	
One at bus 202	Stable
Both at bus 202	Stable
SVC at bus 214	Stable, low voltages on buses 207, 208

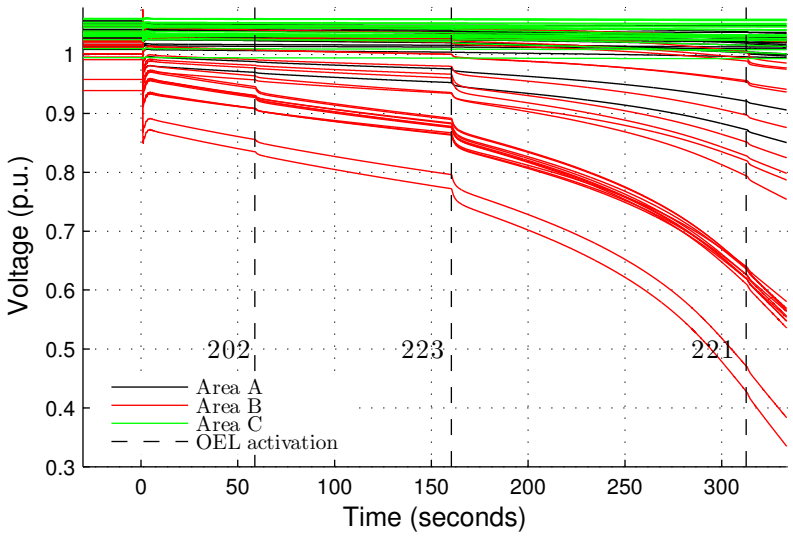

Figure 7.7: Case 1: Bus voltages after disconnection of line between buses 214 and 211, IEEE RTS. Activation of OELs at buses 202, 223 and 221 indicated.

stability indicators in different parts of a meshed power system. In the following analysis, bus 207 is referred to as A, bus 219 as B and bus 223 as C.

Bus 207 is at the end of a radial section with all its generators offline, bus 219 is a load bus in a meshed region with online generation units nearby, and on bus 223, a generator bus, the power flow on an inter-area tie-line is studied.

In the PV plots for the studied buses and lines, the load current and apparent load power are also included in order to properly identify whether the system is on the lower half of the PV curve. Under certain conditions, the trajectory in the PV plane can resemble the lower half of a PV curve while the transmission is still stable. Such conditions can be identified by considering the *current-voltage* curve (IV curve) along with the PV and SV (apparent power – voltage) curves.

A characteristic of voltage instability is that an increased load current causes a reduced load power. By including the current and apparent power in the PV-plot, one can easily see whether the current increases as the power

decreases.

7.4.1 Case 1A: Bus 207

The two buses with the lowest voltages in Figure 7.7 are buses 207 and 208. The low voltages indicate that the buses are close to voltage instability, and in the PV-plot for bus 207, Figure 7.8a, it is clearly shown that the bus voltage ends up on the lower half of the PV-curve after activation of the OELs at bus 223 ($t = 160$ s). Load restoration caused by the decreased voltage causes both a further decreasing bus voltage and a reduction in consumed power, and the instability is confirmed by the increasing current.

The voltage stability indicators for bus 207 are shown in figures 7.8b and 7.8c. Indicators ISI, SDI and VSI_{SCC} reach their critical values shortly after the OELs at bus 223 are activated. VSI_{SCC} is, however, close to the critical value the entire time after the line trip, and decreases after passing the maximum loading point, which is as expected based on the results from the two-bus system.

SDI returns to indicate a stable system towards the end of the simulation, which probably relates to the declining increase in the current seen in the rightmost part of the PV plot.

The figure also illustrates the noise in both SDI and the Thévenin estimation. After the line trip, the values of SDI, ISI and VSI_{SCC} oscillate for a while before stabilising at a reasonable value, and after each OEL activation these indicators show large spikes into the unstable region.

TPSI reaches the critical value approximately 104 seconds after the OEL activation at bus 223, at $t = 264$ seconds, and L_{mn} and FVSI are never even close to the critical value and are therefore excluded from the figure.

7.4.2 Case 1B: Bus 219

On bus 219, the power flows of all connected branches have been examined for voltage instability. The results are shown in figures 7.9, 7.10 and 7.11. At this

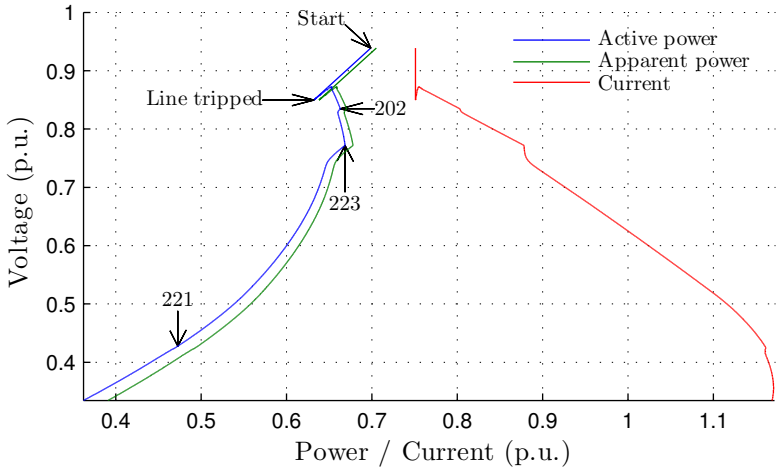

(a) PV-plot, numbered arrows indicate OEL activation.

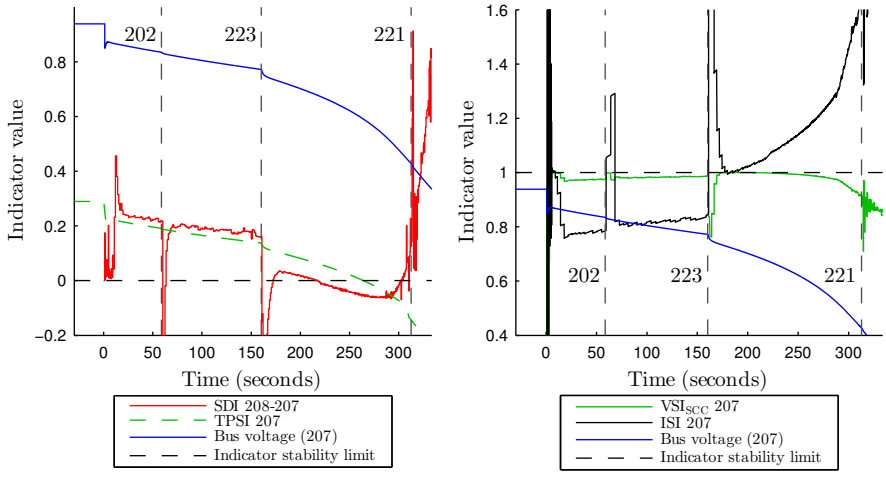

(b) Indicators whose critical value is 0 (c) Indicators whose critical value is 1

Figure 7.8: Case 1A: PV curve and indicators for bus 207. Dashed vertical lines indicate activation of OELs in the area.

bus, the voltage is not a good indication of voltage instability as it does not decrease as much as on bus 207.

Branch 219-1219

The PV-curve for the power flow towards the load on bus 219 is shown in Figure 7.9a. The figure clearly shows that the tip of the nose curve is passed at approximately $t = 202.9$ s due to load restoration following the voltage drop caused by activation of the OELs at bus 223. Instability is confirmed by the monotonously increasing current and decreasing apparent power.

The indicators for this branch are shown in figures 7.9b and 7.9c. Similar to the results from bus 207, ISI, SDI and $\mathrm{VSI_{SCC}}$ reach their critical values approximately when the system passes the tip of the nose curve, and $\mathrm{VSI_{SCC}}$ is very close to the critical value the entire time and decreases as the maximum loading point is passed. FVSI and $\mathrm{L_{mn}}$ do not detect the instability at all and are therefore excluded from the plot.

The cause of the notches seen in the SDI curve in Figure 7.9b at times (approximately) $t = 50$, $t = 120$ and $t = 200 - 300$ has not been identified, but may be related to nonlinear events within the models that are used.

TPSI, being a bus-based indicator, is for completeness only included in Figure 7.9b. Similar to FVSI and $\mathrm{L_{mn}}$, TPSI does not detect the instability. The step-decrease in the value seen around $t = 280$ s is a result of the voltage angle at bus 219 decreasing below the angle at bus 220. This also causes the direction of the active power flow between buses 219 and 220 to change shortly after, as shown in Figure 7.11a. The new angle difference enables the path-finding algorithm of TPSI to find new, less stable paths into area C.

Branch 219-216

Figure 7.10a illustrates the PV-curve of the power flow on the line from bus 216 to bus 219. The shape of the PV-curve strongly resembles the lower half of a nose curve, and the current increases with decreased active power. However, the transmission is not unstable since the apparent power continues to increase

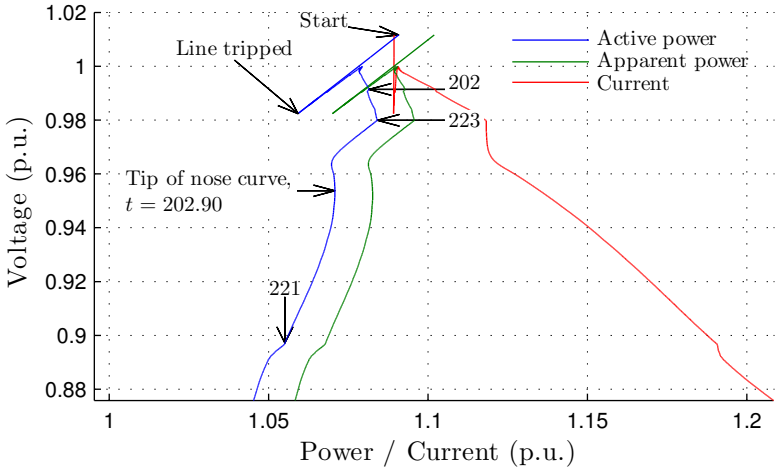

(a) PV-plot, numbered arrows indicate OEL activation.

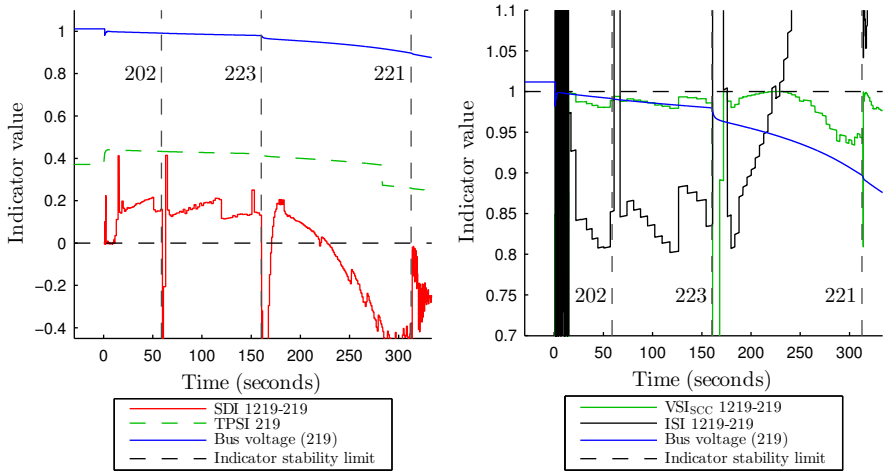

(b) Indicators whose critical value is 0 (c) Indicators whose critical value is 1

Figure 7.9: Case 1B: PV curve and indicators for power flow in transformer 219-1219. Dashed vertical lines indicate activation of OELs in the area.

with the increasing current, indicating that the load further "downstream" is decreasing.

The voltage stability indicators, plotted in figures 7.10b and 7.10c, all indicate that the line is far from instability. The only difference is that as the apparent power continues to increase after activation of the OELs on bus 223, SDI indicates that the stability is improving, while ISI and especially VSI_{SCC} indicate that the transmission is getting closer to instability. The reason for this has not been identified, but it is probably related to the angle-term in SDI.

The values of FVSI and L_{mn} increase due to the increasing reactive power received at bus 219. However, based on the poor results of these indicators at the other studied buses and lines, and also in the two-bus system, the value of the information from these indicators is questionable.

Branch 219-220

The PV-plot for the sum of the power flow on the lines from bus 219 to 220 is shown in Figure 7.11a. This plot is nearly identical to the plot for the line between buses 219-216 (Figure 7.10a), but shifted to the left by approximately 1.0 p.u.

Comparing the indicators for these lines, shown in Figure 7.11b, to the indicators for the 219-216-line, the results are very different. ISI and VSI_{SCC} both have values close to zero, and only ISI increases while VSI_{SCC} remains relatively constant. However, at this distance from the critical value, it may be related to the linearity of the indicators. SDI is not included in the results since the lines are producing more reactive power than they are consuming, invalidating the SDI calculations (ref. [12, 13]). FVSI and L_{mn} are, as usually, not of any use here since the reactive power flowing towards the bus is negative.

7.4.3 Case 1C: Bus 223

At bus 223, the stability of the power flow on the tie-line from bus 318 in area C is examined. The received active and apparent power is plotted versus the voltage on bus 223 in Figure 7.12a. Here, the transfer on the line appears to

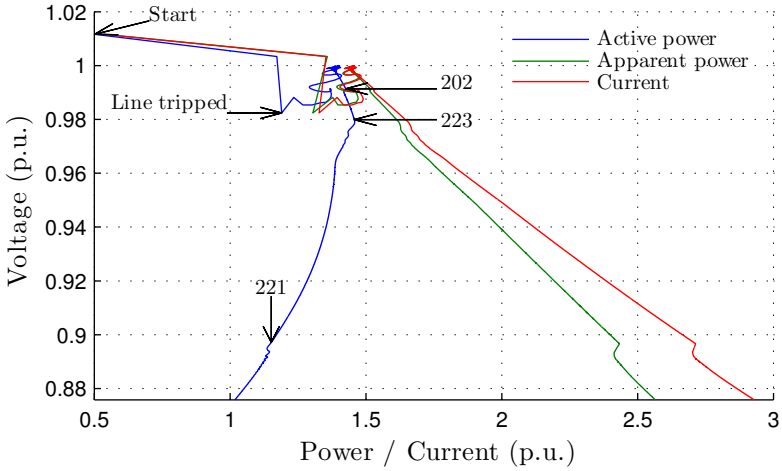

(a) PV-plot, numbered arrows indicate OEL activation.

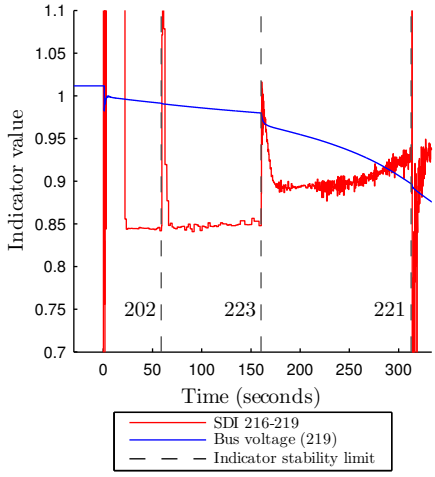

(b) Indicators whose critical value is 0

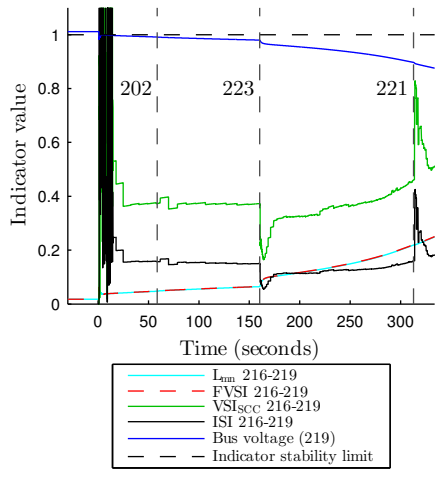

(c) Indicators whose critical value is 1

Figure 7.10: Case 1B: PV curve and indicators for power flow in line 216-219. Dashed vertical lines indicate activation of OELs in the area.

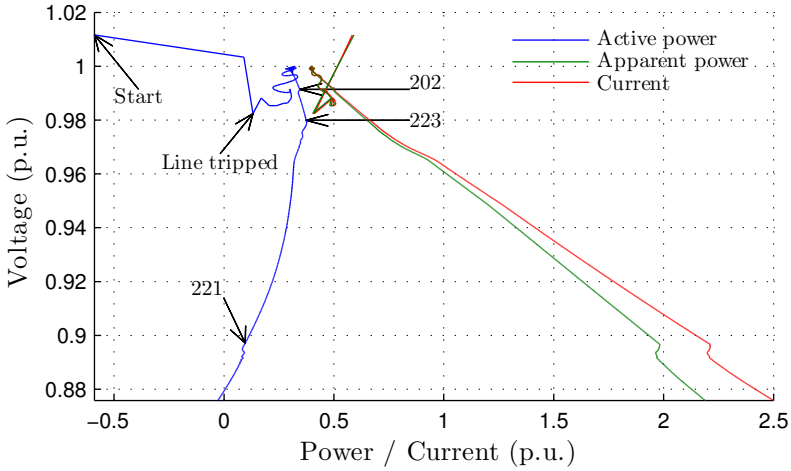

(a) PV-plot, numbered arrows indicate OEL activation.

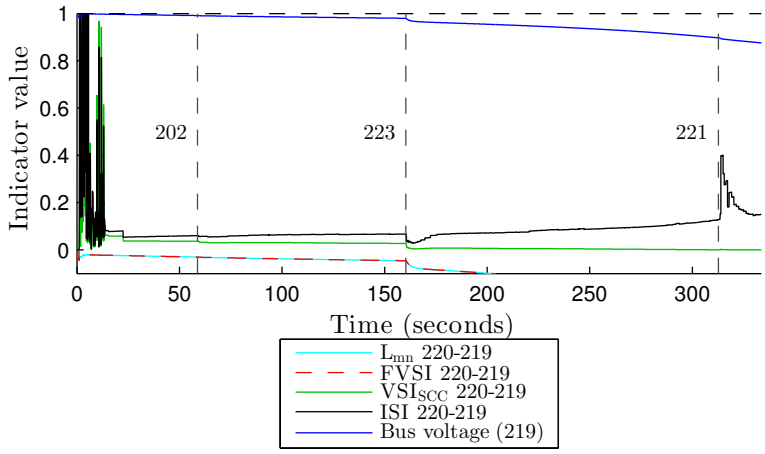

(b) Indicators whose critical value is 1

Figure 7.11: Case 1B: PV curve and indicators for power flow in lines 219-220. Dashed vertical lines indicate activation of OELs in the area.

become unstable shortly after activation of the OELs on bus 223. However, after a while, the current starts decreasing again, indicating that the transfer stabilises.

The indicators for the transmission on the inter-area tie-line are shown in figures 7.12b and 7.12c. After activation of the OELs at this bus, the decreasing power in the receiving end of the tie-line causes SDI to indicate that the stability of the transmission is improving, whereas TPSI, which uses information from the entire system, indicates that the stability at the bus is degrading.

Also ISI and VSI_{SCC} move in the opposite direction of SDI and indicate that the stability is degrading as the received power (and current) decreases. The gap between the ISI and VSI_{SCC} values is caused by the difference in the linearity of the indicators, as was shown in the two-bus study in Section 6.2.2.

In this case, it is difficult to tell which of the line-based indicators are giving the correct distance to the maximum loading point. ISI and VSI_{SCC} are based on the same estimated Thévenin equivalent, so it is natural that they give similar results (i.e. decreasing distance).

7.5 Simulation Results, Case 2: Outage of Line 121-325

In this section, the results from a simulation of an outage of the inter-area tieline between buses 121 (area A) and 325 (area C), are studied briefly.

Figure 7.13 shows the voltages at all buses during this contingency. At $t = 1.0$ the line is tripped, which causes the voltages in areas A and B to drop. The power flow from area C to area A on the disconnected line was 212 MVA, which after disconnection must be transferred to area A via area B, increasing the load on the inter-area tieline between areas B and C from 470 MVA to 716 MVA. 716 MVA is above the short-term thermal overload rating of the line (625 MVA), however, in the interest of studying the resulting voltage instability, this is ignored.

After the line has been tripped and the resulting oscillations have stopped, the voltages appear to be relatively steady until the OELs at bus 223 are activated at $t = 82$ s, causing the voltages in area B to drop further and start

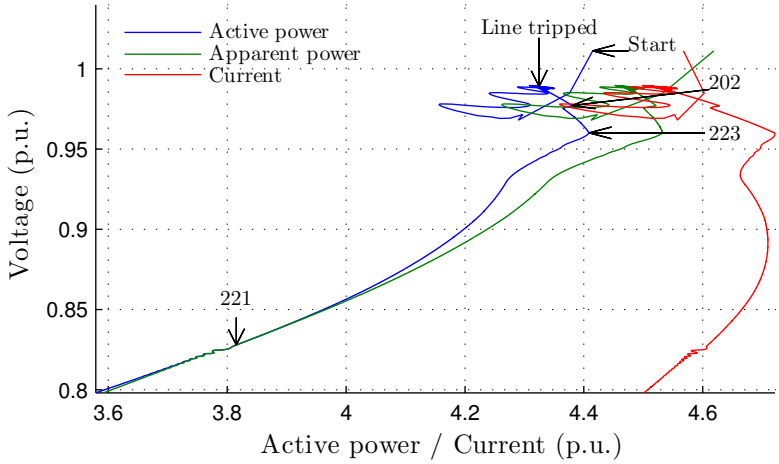

(a) PV-plot, numbered arrows indicate OEL activation.

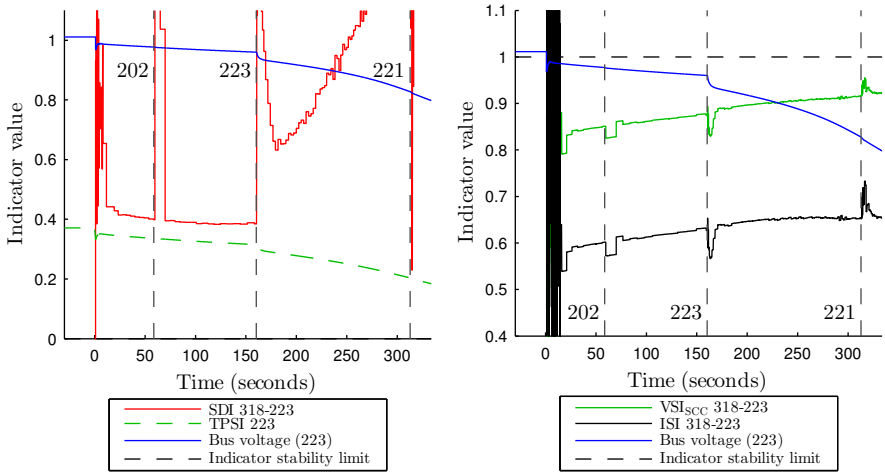

(b) Indicators whose critical value is 0 (c) Indicators whose critical value is 1

Figure 7.12: Case 1C: PV curve and indicators for the power flow in line 223-318. Dashed vertical lines indicate activation of OELs in the area.

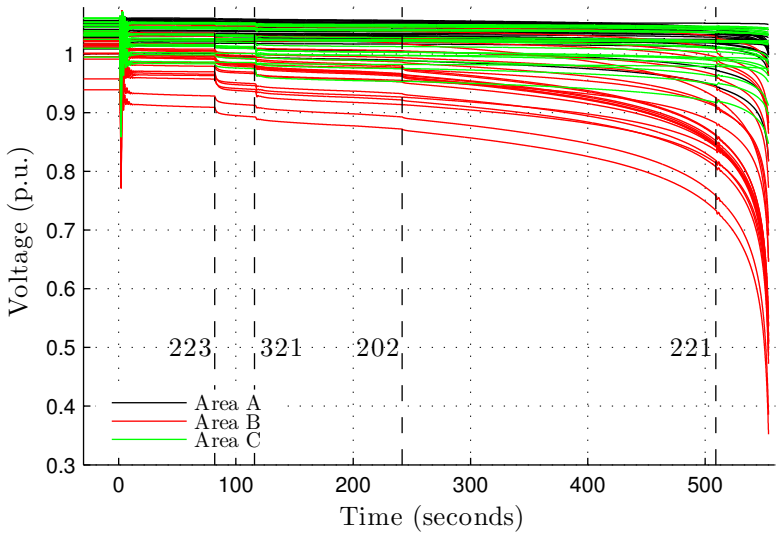

Figure 7.13: Case 2: Bus voltages after disconnection of line between buses 121 and 325, IEEE RTS. Activation of OELs at buses 223, 321, 202 and 221 indicated.

sagging. Shortly after, at $t = 116$ s, the OEL at bus 321 is activated. The voltages continue to sag, and at $t = 242$ s, the OELs at bus 202 are activated, accelerating the rate of the voltage decline in area B. Around $t = 500$ s, the voltages in area B start to drop significantly. At $t = 509$ s, the OEL at bus 221 is activated, and shortly after, at $t = 554$ s, the simulation stops converging, at which point the voltages are collapsing.

Compared to Case 1, Case 2 results in a voltage instability in the entire area B due to an unstable transmission from area C, while Case 1 only caused the voltage to collapse in parts of area B.

7.5.1 Case 2C: Bus 223

At bus 223, the stability of the transmission from bus 318 in area C is examined. The PV plot shown in Figure 7.14a clearly illustrates the instability that occurs. Due to the oscillations from $t = 1.0$ s to approximately $t = 7.2$ s, this time period is not included in the PV plot.

After activation of the OELs at bus 223, the transmission appears to become unstable, as both the active and the apparent power decrease while the current increases. However, when the OEL at bus 321 is activated, the transmission again appears to stabilise as both active and apparent power increase with increasing current, until the OELs at bus 202 are activated and the current increases while the received power decreases. Activation of the OEL at bus 221 does not influence the course of events much.

As seen in figures 7.14b and 7.14c, all indicators indicate that the system is stable after the line trip. When the first OEL is activated, all indicators except TPSI indicate instability. VSI_{SCC} is assumed to be beyond its stability limit as its value is declining throughout the rest of the simulation. SDI seems to creep back into the stable region shortly before the OEL at bus 321 is activated, corresponding to the considerations of the PV plot. After activation of the OEL at bus 321, SDI and ISI continue to indicate instability, and after approximately 380 seconds, even TPSI detects the instability.

FVSI and L_{mn} are excluded since they do not provide any useful information.

7.5.2 Case 2A and B: Buses 207 and 219

At bus 207, the power flow from bus 208 is studied (i.e. to the load at bus 207), and at bus 219 the power flow to the load bus (1219) is examined. The results are shown in figures 7.15 and 7.16, and are very similar. In the PV plots (figures 7.15a and 7.16a), both buses are stable and seem to return to the initial power level after the line trip, and also after activation of OELs at buses 223 and 321 they remain stable and return to the same power level. It is not until activation of the OEL at bus 202 that both buses become unstable as the power decreases while the current increases.

The indicators at these buses, shown in figures 7.15b, 7.15c, 7.16b and 7.16c, also give very similar results. SDI indicates that both buses are stable and that the stability is degrading as time progresses towards activation of the OELs at bus 202. However, in neither of the cases SDI goes below the critical value (except for the noise), it just stays very close to it for the rest of the simulation.

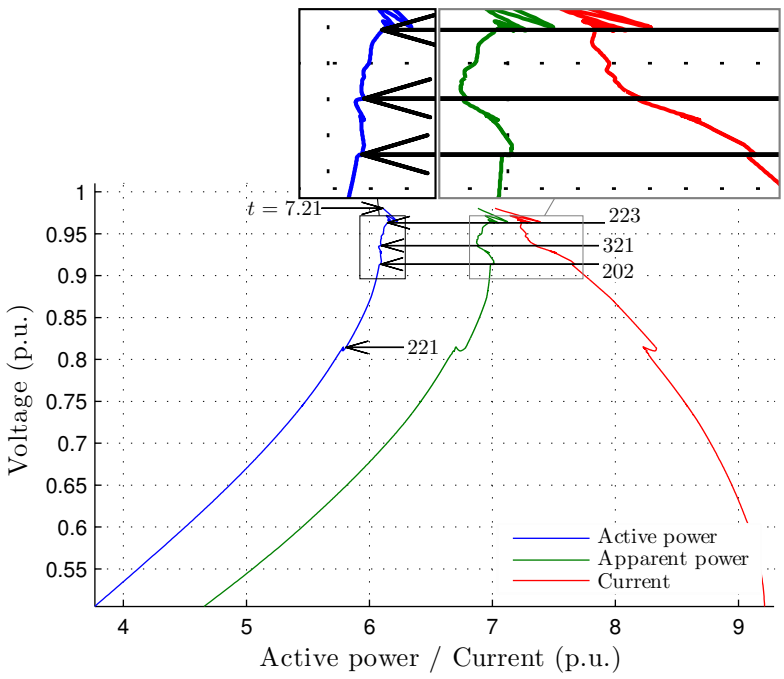

(a) PV-plot, numbered arrows indicate OEL activation.

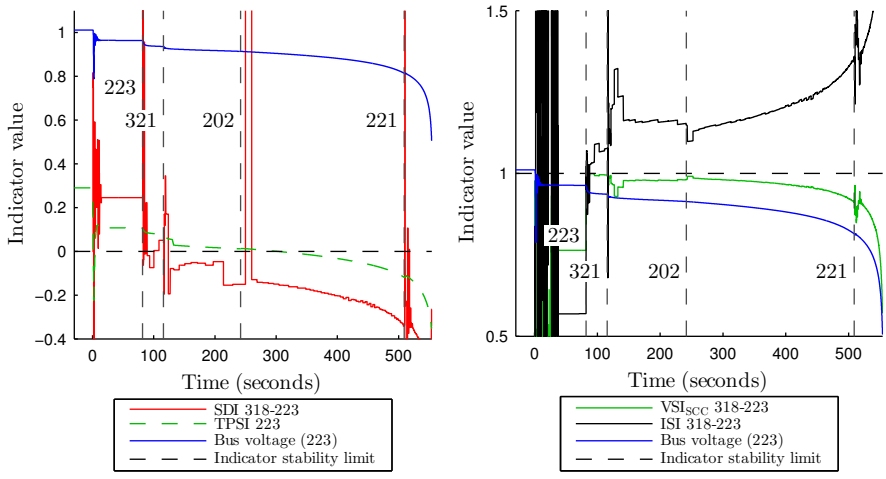

(b) Indicators whose critical value is 0 (c) Indicators whose critical value is 1

Figure 7.14: Case 2C: PV curve and indicators for line 223-318. Dashed vertical lines indicate activation of OELs in the area.

At bus 207, SDI increases towards the end of the simulation, corresponding to the point where the voltage decreases rapidly. A similar trend can be seen in the last few seconds at bus 219 too, and is similar to the situation in Figure 7.8b (Case 1A), where the increase in the current is declining.

ISI shows similar results as SDI, but actually passes its critical value at approximately $t = 430$ seconds at both buses. At bus 219, activation of the OELs at bus 202 causes a step in the ISI output, unlike SDI which is nearly unaffected. At the end of the simulation, ISI does not return to a stable value like SDI, but instead increases further into the unstable region.

VSI_{SCC} seems to perform better than SDI and ISI. At both buses, it detects instability immediately after activation of the OEL at bus 202, and stays close to the instability level throughout the rest of the simulation.

TPSI correctly detects the instability at bus 207 as it reaches its critical value shortly after activation of the OELs at bus 202. At bus 219, TPSI is slightly more inaccurate and reaches the critical value at approximately $t = 430$ seconds, simultaneously as ISI reaches the critical value.

7.6 Discussion

7.6.1 Indicators

The indicators that are based on local measurements, ISI, SDI and VSI_{SCC}, appear to be the most accurate indicators when it comes to detecting the maximum power transfer level and instability. A common factor of all three indicators is that they are based on measurements of delta-values, i.e. the difference between consecutive measurements, which makes them prone to noise, as can be seen from the plots of the indicators.

Another disadvantage of these indicators is that abrupt changes in the system state, in this case disconnection of a line or activation of OELs, result in large spikes in the indicator values. The observed spikes correspond to the notches in the PV-curves as the system transitions from one state to another, and is a result of the indicators being defined for steady-state conditions, while

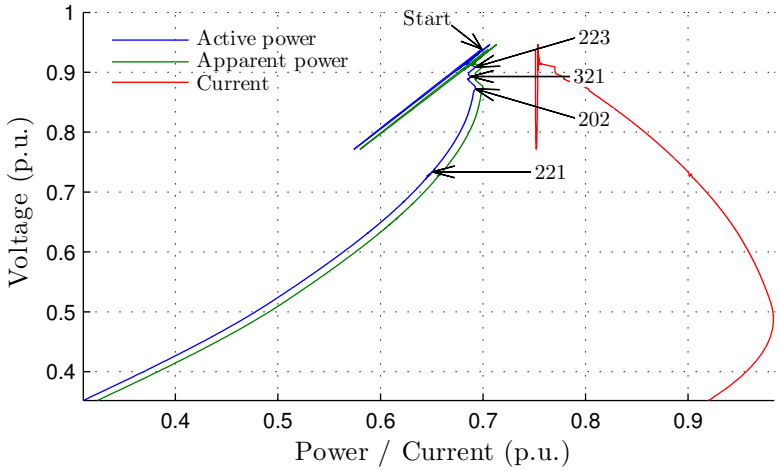

(a) PV-plot, numbered arrows indicate OEL activation.

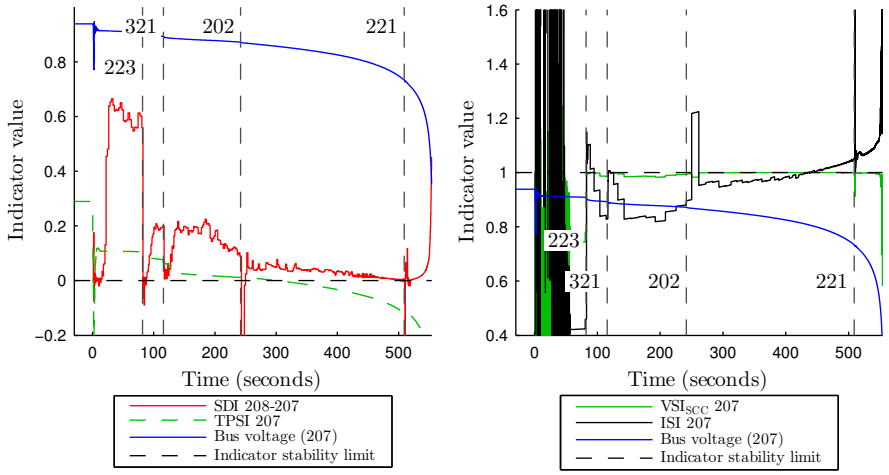

(b) Indicators whose critical value is 0 (c) Indicators whose critical value is 1

Figure 7.15: Case 2A: PV curves and indicators for bus 207. Dashed vertical lines indicate activation of OELs in the area.

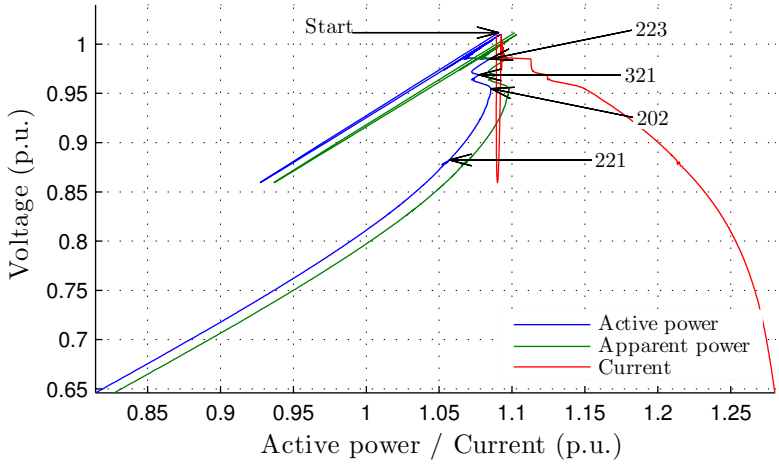

(a) PV-plot, numbered arrows indicate OEL activation.

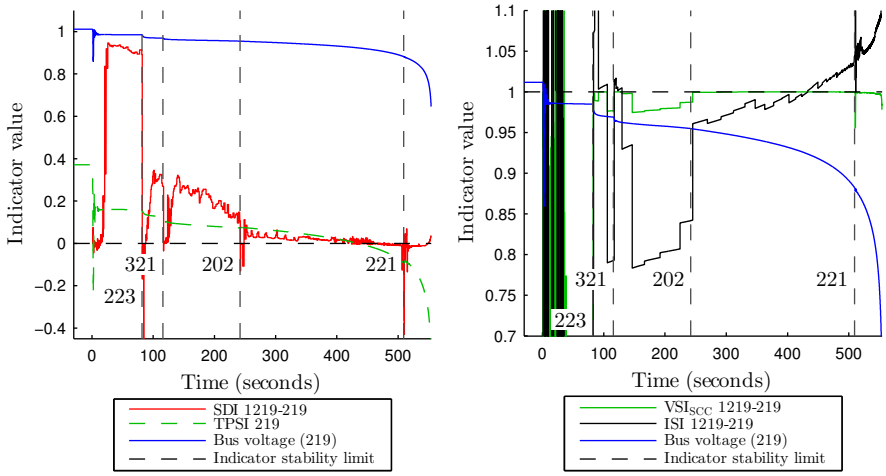

(b) Indicators whose critical value is 0 (c) Indicators whose critical value is 1

Figure 7.16: Case 2B: PV curves and indicators for transformer 219-1219. Dashed vertical lines indicate activation of OELs in the area.

the transition between two stable operating points is a transient event.

An important observation for these three indicators is that the power flow of all branches connected to a bus must be considered, as illustrated at bus 219, where the indicators only indicate instability when calculated for the power flowing towards the load at the bus. Additionally, the results from the two cases show that to properly detect voltage instability, all lines in the system should be considered, not just the lines supplying load buses.

When studying Case 2, indicators ISI and SDI for the load buses did not immediately reach their critical values when the system became unstable. A reason for this can be that the instability is caused by the transfer on the line between areas B and C, and not directly at the load buses as in Case 1.

FVSI and L_{mn} perform poorly at all buses that are examined, which corresponds to the results from the two-bus system.

TPSI shows varying results at the studied buses. At bus 207, it detected the instability after both contingencies, but did not reach the critical value until a while after passing the maximum loading point in Case 2. With a correctly chosen threshold it might be usable at this bus.

At bus 219 in Case 1, TPSI fails to detect the instability that was observed when studying the load at that bus, and even indicated an improved state after the line trip. The step change in TPSI at bus 219 in Case 1B when the angle at bus 219 became lower than the angle at bus 220 illustrates a problem with TPSI. It indicates that the concept of transmission paths that is used in TPSI is not correct. The authors of the article describing TPSI [11] noted that they had not yet found a theoretical basis for this concept. Ideally the path finding algorithm should consider every source in the system and the effect each source has on the total power flow, i.e. similar to the superposition principle, although this might be challenging to do in real-time.

Based on the results, TPSI seems not to be a good indicator due to the dependence on the direction of power flows. Thus the performance depends on the operating scenario, and the reliability of the indicator is questionable.

7.6.2 Validity of Results

As stated in Section 7.1.2, the load restoration model that has been used is very simplified, which can be seen from the slowly degrading voltages in both of the studied cases, especially in Case 1. Additionally, the ZIP model is only valid until a certain voltage level [4], at which point the load characteristics will change, depending on the type of load. However, as the general voltage instability phenomenon is the focus of the study, the exact behaviour of the load characteristics is of less importance.

The low voltages and high currents that are observed in both collapse scenarios are characteristic of a well-progressed voltage instability. In a real system, protective relays such as overcurrent relays, distance protection relays and undervoltage load shedding relays would have acted and altered the course of events significantly. The purpose of this study is to investigate whether voltage stability indicators are able to identify voltage instabilities caused by contingencies, so the lack of protective relays does not influence the final conclusions.

7.7 Mitigation Actions

In this section, simulations of the various mitigation actions described in Chapter 4 are studied. The tests are done based on Case 1, i.e. outage of the line between buses 214 and 211.

Mitigation actions are tested one by one in order to be able to study the effect of each individual action. However, one action alone may not be enough to avoid a voltage collapse, so the effect of each action is measured by considering the impact it has on the time to the critical event that was identified in the base-case simulation, in this case activation of the OELs at bus 223. The proposed mitigation algorithm from Chapter 5 is also simulated.

7.7.1 Determination of Triggering Mechanism

As described in Chapter 5, mitigation actions can be triggered either by indicator values or activation of OELs. Below, indicator thresholds and candidate OEL signals are discussed based on the simulation results from the previous section.

Indicators

Indicators FVSI, L_{mn} and TPSI are considered unusable for initiating mitigation actions. FVSI and L_{mn} failed even for the simplest cases in the two-bus system, and the performance of TPSI has been shown to depend heavily upon the direction of power flows, and thus also on the contingency and operating scenario at hand, and is therefore deemed unreliable.

Bus 207 is one of the first buses to become unstable in Case 1, and for the given operating scenario it is considered to be representative of the voltage stability of the 138 kV subsystem in area B, so only the indicators for this bus are considered. All three remaining indicators, ISI, SDI and VSI_{SCC}, give reasonable results at bus 207. VSI_{SCC} is, however, very close to its critical value the entire time, and SDI is a bit slower than ISI to reach the critical value, so ISI has been selected as the best indicator for this bus. 0.8 is chosen as the alarm level since this would have initiated mitigation actions at appropriate times following both contingencies studied above. The indicator does not reach its critical value during the apparent instability in Case 2 (Figure 7.15c), so the value of the indicator after activation of the OELs at bus 202 in Case 2 (0.95) is used to determine the critical level. A margin of 0.03 is used so that the critical value becomes 0.92. The margins are relatively small, but are appropriate for the tests that are to be performed here.

OEL activation signals

For Case 1, activation of the overexcitation limiters at bus 223 seems to be the critical event that accelerates the degradation of the voltages in area B under both contingencies. This can be seen from the PV plots for the studied buses (see e.g. figures 7.8a, 7.9a and 7.12a), where activation of the OELs at bus 223 has a large impact on the trajectory of the system. Similarly, activation of the OELs at bus 202 accelerated the decreasing voltages in Case 2 (see Figure 7.13).

Activation of these OELs are therefore considered early warning signals for a pending voltage instability. When an OEL is activated, it implies that there is a lack of reactive power in the region and thus that the situation may be stressed.

7.7.2 Ranking of Buses for Applying Mitigation Strategies

To determine which generators and other equipment to use in the mitigation strategies that are to be tested, the method described in Section 5.3.2 (Equation (5.3)) has been applied for buses 202 and 207, where bus 202 corresponds to the bus where the first OEL is activated, and bus 207 is the bus that is assumed to be the weakest bus in the studied scenario. A capacitive current injection ($\Delta\vec{I}_j$) of 1.0 p.u. was used for all considered buses. The impedance matrix was obtained by exporting and inverting the admittance matrix for the studied scenario from PSS/E, and includes load and generator impedances.

The results are listed in Table 7.5, where only the buses with equipment suitable for mitigation actions are included. As seen, the reactor on bus 206 has the largest impact on both buses, followed by buses 202 and 223. Looking at the single-line diagram in Figure 7.2, the results seem reasonable based on the given network configuration and the apparent electrical distance between the considered buses.

7.7.3 Results

The results from simulations of each mitigation action are summarised in Table 7.6 and discussed briefly below. For the simulations of single mitigation actions, activation of the OELs at bus 202 was used as the triggering signal

Table 7.5: Ranking of buses for applying mitigation strategies, calculated for buses 202 and 207 in the IEEE RTS model after outage of line 211-214.

Bus j	ΔU_{202}	ΔU_{207}	Type of equipment
206	0.0934	0.0744	Shunt reactor
202	—	0.0697	Generators
223	0.0556	0.0470	Generators
216	0.0475	0.0368	Generators
215	0.0472	0.0361	Generators
214	0.0462	0.0356	SVC
221	0.0460	0.0350	Generators
222	0.0459	0.0350	Generators
218	0.0452	0.0344	Generators

with an assumed delay of 200 ms, except for mitigation actions involving adjustments of governor set points, where a delay of ten seconds is used to account for various delays in the turbine control system.

For the simulation that tests the proposed mitigation algorithm, the ISI value at bus 207 is used to initiate mitigation actions since the level of severity must be measured, and continuous monitoring of the stability of the system is required, as per the algorithm described in Chapter 5. Threshold values described in the previous section are used.

Table 7.6: Summary of effect of mitigation actions, ordered by effectiveness.

#	Mitigation action	Time of OEL activation (s)			Diverge
		Bus 202	Bus 223	Bus 221	time (s)
1	Disconnecting shunt reactor at bus 206	59	—	—	∞
9	Load shedding, 50 % at bus 207	59	—	—	∞
8	Increasing AVR set points at buses 214, 215 and 216	59	280	—	527
7	Increasing AVR set points at bus 216	59	219	—	434
5	Increasing governor set points at buses 202 and 216	59	216	—	409
2	Increasing governor set points at bus 202	59	176	341	347
4	Increasing governor set points at buses 202, 223 and 216	59	162	—	355
–	*No action (base case)*	*59*	*160*	*313*	*334*
3	Increasing governor set points at buses 202 and 223	59	155	—	316
6	Decreasing governor set points at bus 202 by 7.5 MW	59	151	—	284

Switching of shunt-compensation devices

The reactor at bus 206 is the only fixed shunt compensation device in area B, and has therefore been used to test this mitigation strategy, action number 1 in Table 7.6. As shown in Table 7.5, bus 206 is also the bus that is calculated to have the largest influence on the voltage at both buses 202 and 207. The combination of a good location and a relatively high rating (100 Mvar) makes this mitigation strategy able to completely mitigate the collapse and stabilise the system.

Switching of shunt components of this size can lead to high bus voltages in the system, which is a risk of this mitigation action. In the studied case, however, that is not an issue. The highest steady-state bus voltage in area B after disconnection is 1.056, which is acceptable when considering the severity of the situation.

Increasing governor set point

Quick ramping of active power is only possible with certain types of power plants, e.g. hydro and gas powered plants. Most of the power plants in the IEEE RTS are thermal plants with very strict limitations on the ramping rate, and there is only one hydro power plant in each area, at buses 122, 222 and 322.

In the studied scenario, bus 222 is in the lower end of the ranking list in Table 7.5, so using this generator will not give representative results for the mitigation action. For testing purposes, the ramping rates of the generators have been ignored (assuming e.g. a hydropower-based system), and based on Table 7.5, four tests were performed. First, the active power was increased only at bus 202, then at buses 202 and 223, at buses 202, 223 and 216, and finally at buses 202 and 216. The total power output was increased by 12 MW at bus 202, 74 MW at bus 223 and 92 MW at bus 216 for all studied cases.

The results show that when increasing the active power output only at bus 202, mitigation action number 2, the time to the critical event increases by 16 seconds. When also increasing the active power output at bus 223 (action

number 3), the time to the critical event decreases by five seconds, since the increased power output requires a higher field current, accelerating the time to activation of the OELs at these generators.

When the power is increased also at bus 216, mitigation action number 4, the time to the critical event increases, but only by two seconds, indicating that this mitigation action is heavily dependent upon the location of the generators.

The final combination, increasing the power output at buses 202 and 216 (action number 5), gives the best results, increasing the time to the critical event by 56 seconds.

Decreasing governor set point

There are only two generators online in the 138 kV subsystem in area B, both at bus 202, so these were used to examine the effect of decreasing the governor set points (mitigation action number 6). The results show that for the studied case, decreasing the governor set point worsen the situation. The active power output was reduced by approximately 7.5 MW at each generator, which resulted in a total increase in the reactive output of only 3.5 Mvar. Several levels of reduction in the active power generation were simulated, and the results are plotted in Figure 7.17. As shown, the time to the critical event (activation of the OELs at bus 223) decreases with increasing reduction in the active power output, making this a bad mitigation strategy.

Increasing AVR set point

Due to the lack of online generators in area B, testing of this mitigation strategy is challenging, especially since the OELs at bus 202 are activated before any mitigating actions are initiated. Using Table 7.5, the next alternative is the generator at bus 223. However, at this bus the voltage set point is already relatively high, at 1.05 p.u., which has been assumed to be the upper limit for voltage set points.

The mitigation strategy was therefore tested by increasing the voltage set point at bus 216 (which is the next in the list) to 1.05 p.u. However, increasing

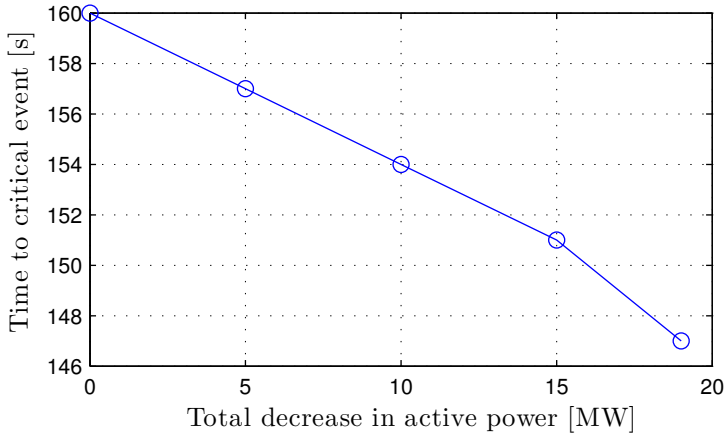

Figure 7.17: Effect of decreasing governor set points at bus 202 on time to the critical event.

the voltage reference solely at bus 216 will reduce the reactive power output from other nearby voltage controlling equipment, reducing the presumed effect of increasing the voltage set point. Another test was therefore performed where the voltage set points at buses 214, 215 and 216 was increased to 1.05 p.u.

Increasing the voltage set point at bus 216 (mitigation action number 7) delayed the activation of the OELs at bus 223 by two minutes and the simulation diverged 100 seconds later than the base case. Increasing the voltage set point at buses 214, 215 and 216 (mitigation action number 8) further delayed activation of the OELs at bus 223 by approximately one minute.

These results indicate that increasing the set point of AVRs near the voltage-critical region does improve the voltage stability. However, the mitigation strategy could not be applied at optimal locations since there were no suitable generators available within the 138 kV region, reducing the effect of the strategy.

Load shedding

Shedding 50 % of the load at bus 207 (approximately 36 MW, or 2.1 % of the total load in area B), which is the assumed weakest bus, completely mitigates

the voltage collapse, illustrating the effectiveness of this mitigation strategy (mitigation action number 9).

Test of proposed SIPS

The results from the test of the SIPS proposed in Chapter 5 are shown in Figure 7.18. Only the mitigation algorithm of the SIPS has been used in this simulation, OEL signals were not utilised. Mitigation actions are delayed by ten seconds in order to avoid initiating mitigation actions during the spikes in the indicator value that are observed during transient events. The algorithm is using Table 7.5 and the list of mitigation actions in Section 5.3.1 to determine which mitigation actions to initiate. It is assumed that the generator at bus 223 is at its maximum AVR set point limit, and the shunt reactor at bus 206 is not used to mitigate the instability since this would stabilise the system immediately, and the SIPS will not be tested properly.

The first mitigation action is initiated at $t = 70$ s. The algorithm starts out gently and increases the AVR set point at bus 216 to 1.05. This improves the situation for slightly more than a minute, after which the indicator value reaches the alarm level once again at $t = 141$ s. This time, the AVR set point is increased to 1.05 at buses 215 and 214. The "sensitivities" for the remaining buses, in Table 7.5, are assumed to be too low to initiate mitigation actions.

90 seconds later, at $t = 233$ s, shortly after activation of the OEL at bus 223, the indicator value is far above the critical level and load shedding is initiated. Load is shed at bus 207 in steps of 7 MW (10 % of the initial load) with a delay of 10 seconds between each step until the indicator value goes below the critical level. A total of 14 MW is shed at this stage.

The indicator value decreases rapidly after the initial load shedding, but becomes critical 50 seconds later, at $t = 276$ s, which initiates shedding of 7 MW additional load.

After the final load shedding, the system appears to be stable. The voltage increases due to the load restoration model, which now reduces the load as a result of the increased voltage following the load shedding. The indicator value

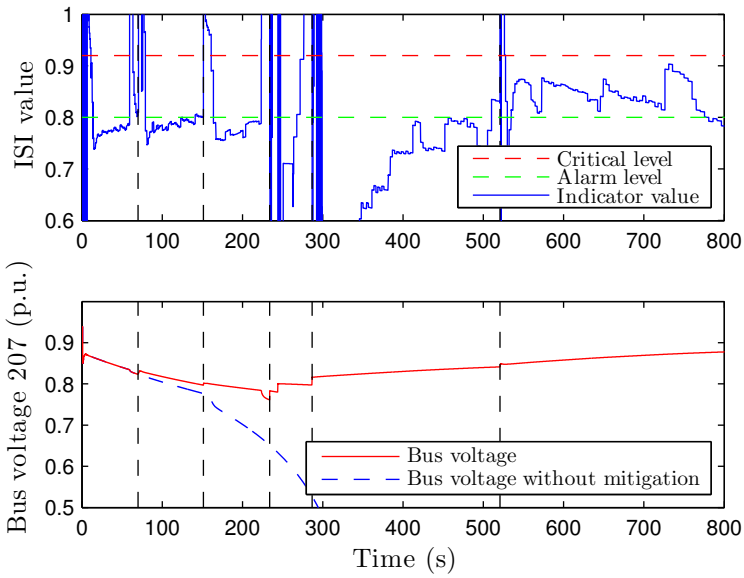

Figure 7.18: IEEE RTS: Results from test of proposed mitigation algorithm during outage of line 214-211. Vertical lines indicate initiated mitigation actions.

is, however, increasing, and at $t = 510$ s the alarm level threshold is reached. Since all AVR set points have been adjusted, the algorithm attempts the next mitigation action in the list, which increases the active power generation at bus 202.

The effect of the last mitigation action causes the indicator value to stop increasing, but it is still above the alarm level. Due to the low effect of increasing the active power generation at buses with a low value in Table 7.5, no further mitigation actions are attempted. The indicator value is gradually decreasing, and at $t = 780$ s the system leaves the alarm level.

After exhausting all available mitigation strategies, the algorithm is finally able to stabilise the system. The effect of the mitigation actions is also shown in the voltage plot in Figure 7.18, where the voltage on bus 207 is plotted with and without mitigation actions. Note that the voltage on the bus is very low, at only approximately 0.8 p.u. at the lowest point.

The cause of the notches seen in the indicator value during the last 500 seconds of the simulation has not been identified. They appear to be the result of discrete events such as tap changer action, but neither tap changers nor other discrete components have been modelled. One theory is that they are caused by non-linearities in the implementation of the EXTL load restoration model, as a slight change can be seen in the rate of increase of the measured load impedance at each notch in the indicator value (the change is too small to be clearly displayed in a plot).

Another theory is that the notches are a result of floating point precision problems. In PSS/E, the voltage angles are referred to an arbitrary 50 Hz reference voltage. When changes in load and generation occur, such as in this simulation, the frequency will change, and the voltage angles begin to drift. This can be a problem, especially in simulations of long time periods, such as here, since the voltage angles will lose precision as they drift from zero. The Thévenin impedance estimation method employed here is using very little filtering, and is as such sensitive to this kind of noise.

7.7.4 Discussion

Mitigation strategies

For the studied case, the assumed effectiveness of the considered mitigation actions (in Section 5.3.1) corresponds very well to the results in Table 7.6. Switching of shunt compensation devices and load shedding turned out to completely mitigate the instability. Increasing AVR set points was also very effective, delaying the time to the critical event by up to two minutes, even at less-than-ideal buses.

The effect of altering the active power generation showed varying results. When the active power output at bus 223 was increased, it worsened the situation since the increased generation caused the OEL at this critical bus to activate sooner. Increasing the active power output at other buses, however, resulted in an increase in the time to the critical event. Decreasing the active power output only worsened the situation, even though more reactive power became available due to the increased transmission losses.

The success of the latter two mitigation strategies thus appears to depend on proper selection of generators. More advanced rescheduling strategies might yield better results, using for example area generation control systems to shift active power generation closer to the critical area.

Not all mitigation strategies could be tested within the critical area (i.e. in the 138 kV subarea), but this should be considered normal since voltage instability is a result of a lack of reactive or (indirectly) active power.

Proposed mitigation algorithm

The simulation of the proposed mitigation algorithm illustrated that by selecting proper mitigation actions, the algorithm is able to avoid a voltage collapse. Although load shedding was required, the amount of load that was shed (21 MW) was lower than when load shedding was used as the only mitigation action, where 36 MW load had to be shed to stabilise the system.

During the simulation of the mitigation algorithm, the voltages at bus 207 were quite low, approximately 0.8 p.u. at the lowest point. However, the low voltage is not an issue in itself as long as it remains stable at that level. Although not included directly in the simulation, the load transformers are assumed to have onload tap changers that increase the voltage at the load buses so that the voltage remains within the required limits. The increased load-side voltage will cause an increase in the load, which is assumed to be accounted for by the load restoration model.

The main problem with the indicator that was used in this simulation is that the value is noisy, and there are large spikes in the indicator value when abrupt changes occur in the system. In the simulation this was accounted for by adding a relatively long delay (ten seconds) before initiating mitigation actions. A real power system is likely to have instability mechanisms that are much faster than the load restoration model used in this study, and proper filtering of the indicator output will be required. The largest spikes may not be possible to completely remove by filtering, and a better indicator may be required.

8 Case Study: Hammerfest/Skaidi in Northern Norway

A goal of this project is to test the proposed mitigation algorithm in a model of a real power system. Statnett SF has kindly provided a model of the Norwegian power system for this purpose. The model represents the transmission system in Norway and also contains simplified equivalents of subtransmission grids. It consists of 2301 buses, 615 generators, 2751 lines and 1962 transformers, and the neighbouring power systems (Finland and Sweden) are modelled by loads representing the import or export for the given situation. Two critical contingencies have been identified where the system experiences voltage collapse, and various mitigation actions are considered and tested.

Due to restrictions on the data from the supplied model, only information that is publicly available is presented here.

8.1 Model Description and Assumptions

The Hammerfest/Skaidi region in Finnmark in Northern Norway has been selected for the studies, as this is a region that has been experiencing voltage stability problems, and relatively large increases in load are planned in the region within the next few years [26]. An overview of the transmission system in Finnmark is shown in Figure 8.1, and the surrounding transmission system is illustrated in Figure 8.2. In addition to the indicated hydropower plants in the first figure, there are two wind-power stations and several smaller hydropower units scattered around the region.

In the Hammerfest/Skaidi region, the largest consumer of power is Hammerfest LNG, an export facility for liquefied natural gas (LNG), located at Melkøya, a small island north of the city of Hammerfest. The LNG plant has five gas turbines with a total capacity of approximately 250 MW which keeps

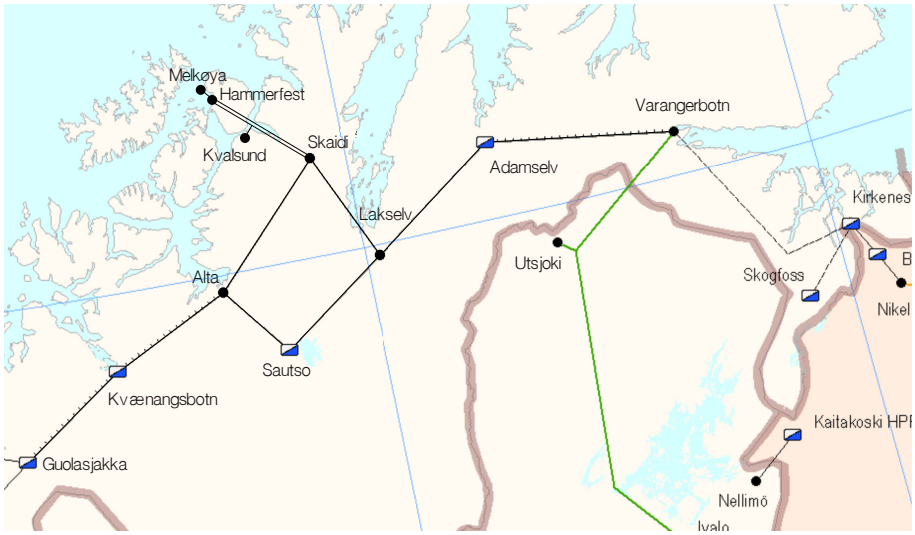

Figure 8.1: Overview of the transmission system in Finnmark, based on [27]. Blue and white squares indicate hydropower plants.

the plant self-supplied with electric power [28]. The plant is also grid connected to ensure a reliable supply in case of contingencies.

In the following studies the two wind-power plants mentioned above are assumed to be offline, since wind power is intermittent and the system should be able to operate without them. In addition, an intricate control system that keeps the Melkøya-plant's reactive power exchange with the grid to a minimum has not been modelled.

The base operating scenario is a high load case provided by Statnett SF, which models a typical cold winter day. Many of the hydropower plants in Northern Norway are run-of-the-river plants with little or no storage capacity, and since precipitation comes as snow and most rivers are frozen during the winter, these plants are producing little to no power in this scenario.

8.1.1 Overexcitation limiters

In the model supplied by Statnett, many of the excitation system models did not include an overexcitation limiter. The MAXEX2 model from the PSS/E

Figure 8.2: Overview of the transmission system in Norway, Sweden and Finland, from [27]. The region of study is indicated by the red circle.

model library [23] was therefore applied to all generators in Finnmark and to the generators that are electrically closest westwards in the system. The field current limit was set to the field current required to operate the generators at maximum rated power output at the nominal power factor with a terminal voltage of 1.0 p.u. Nominal power factors were assumed to be 0.85, as per the requirement in the Statnett grid code (FIKS) [29]. The generators at Melkøya have a nominal power factor of 0.8 [26]. The time delay characteristic that was used for the studies in the IEEE RTS model is used here too, see Section 7.1.1 for details.

The model from Statnett includes equivalent models of machines that are at lower voltage levels than included in the model. These machines are assumed to not be able to provide any reactive power to the transmission system. The field current on these machines is therefore limited to the current required to operate the machine at unity power factor at 1.0 p.u. terminal voltage. There is no time delay related to this limit.

8.1.2 Load modelling

The loads in Hammerfest and at Melkøya are modelled using a CLOD-type load model from the PSS/E model library [23]. The CLOD models represent a load consisting of induction motors, lighting, transformers and other types of load, as shown in Figure 8.3. CLOD represents induction motors with dynamic models using typical values.

The loads in Hammerfest were modelled based on the share of industrial and residential loads provided by [26]. The industrial loads are assumed to consist mainly of "large induction motors", and residential loads are represented by the rightmost block in Figure 8.3 with $K_P = 1$.

The main consumers of load at Melkøya are two variable speed drives for cooling compressor motors (80 % of the total load). The rest of the load is assumed to consist of large induction motors (approximately 10 % of the load) and other loads with a constant-current voltage characteristic ($K_P = 1.0$).

The remaining loads in Finnmark are represented by a ZIP load model with

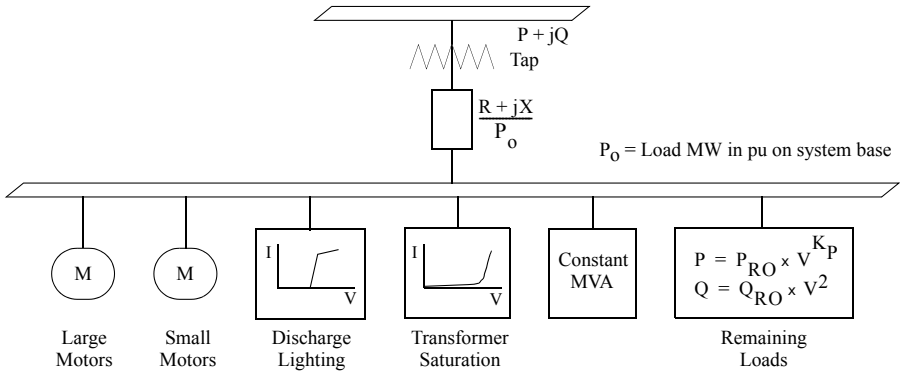

Figure 8.3: CLOD model load representation, from [23].

load restoration modelled by an EXTL model. The data for both models are equal to the data used in the IEEE RTS studies, see Section 7.1.2 for details.

8.2 Case 1: Trip of Two Generators at Melkøya

8.2.1 Operating Scenario

In the studied scenario, it is assumed that one of the gas turbines at the Melkøya plant is offline due to maintenance. The total load in Finnmark is approximately 500 MW (Melkøya plant included), of which 150 MW is imported from other regions. The power flow from Skaidi to Hammerfest is approximately 60 MW, of which 15 MW supplies the load at Melkøya.

In the following simulation, two additional generators are tripped at Melkøya, the first at $t = 70$ s and the second one minute later, at $t = 130$ s.

8.2.2 Simulation Results

The bus voltages during this contingency are shown in Figure 8.4. The barely visible low-frequency oscillations are caused by sinusoidal load variations that were introduced at a few nearby buses to allow delta-value based indicators to be calculated. In a real system, there will always be variations in the voltage and current, and the oscillations are an attempt to emulate these variations.

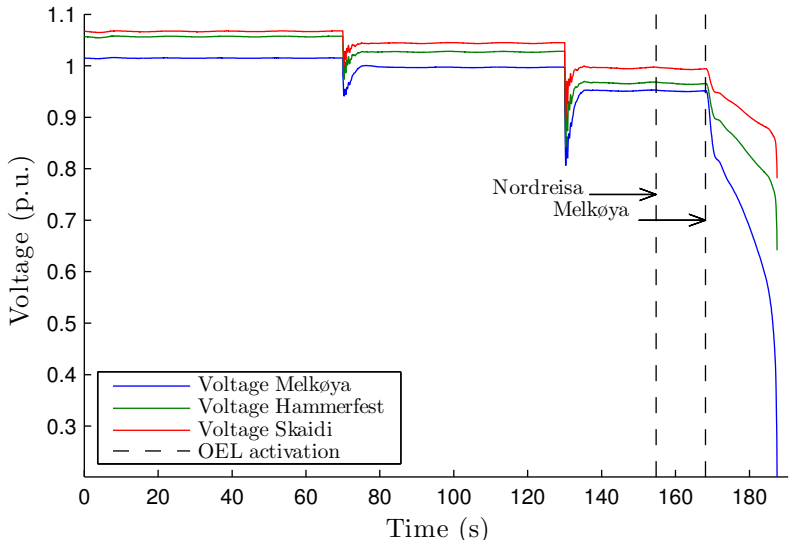

Figure 8.4: Case 1: Bus voltages. Dashed vertical lines indicate activation of OELs.

The effect of tripping the generators is clearly shown in the figure, and at $t = 168$ s, the OELs at the remaining generators at Melkøya are activated. This causes the voltage at Melkøya to drop significantly due to the large amount of constant power load, and the simulation stops converging at $t = 187$ s, at which point the lowest bus voltage is only 0.2 p.u.

The active power imported to the Melkøya plant increases by approximately 50 MW for each generator that is tripped, so that the total import after tripping the second generator is approximately 110 MW, which is below the limit for the overload protection relay on the plant's grid connection as shown in Figure 8.5.

The OEL that is activated first is at the Nordreisa bus, west of Kvænangsbotn in Figure 8.1. This is a result of the increased power flow from the rest of the system caused by the outage of generators at the LNG plant.

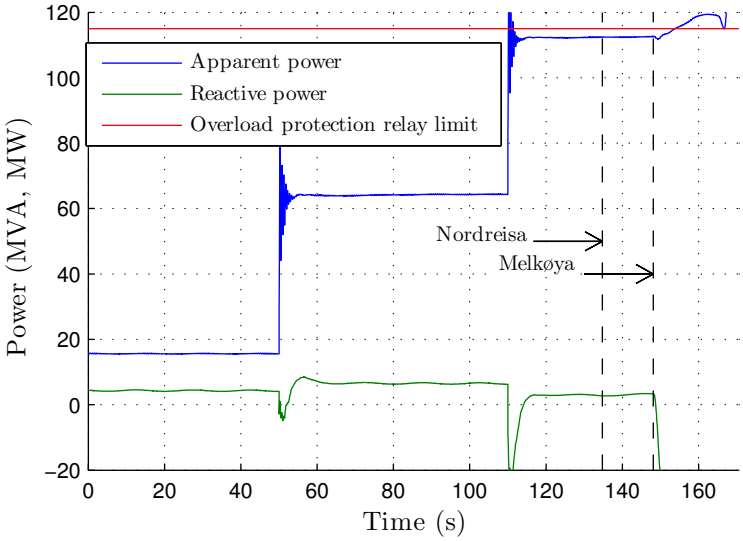

Figure 8.5: Case 1: Powerflow between Melkøya LNG and the Hammerfest bus. Positive direction of reactive power flow is towards the Hammerfest bus, active power is flowing towards LNG plant. Dashed vertical lines indicate activation of OELs.

Indicators

Hammerfest The PV-plot and indicators for the load in Hammerfest (LNG plant not included) are shown in Figure 8.6. From the PV-plot, it can be seen that the system appears to move along the lower half of a PV curve as the generators are tripped. For each generator that is tripped at Melkøya, the load at the Hammerfest bus ends up at an operating point (indicated by arrows) where the voltage is lower, the load power is reduced and the current increased. The CLOD-type load model's steady state characteristic is not constant power, which makes stable operation on the lower half of the PV curve possible. The spiral shapes in the plot are a result of the system oscillating before settling at stable operating points.

When the OELs at Melkøya are activated, the system clearly becomes voltage unstable and moves rapidly downwards in the PV plane, and the current increases while the load power decreases.

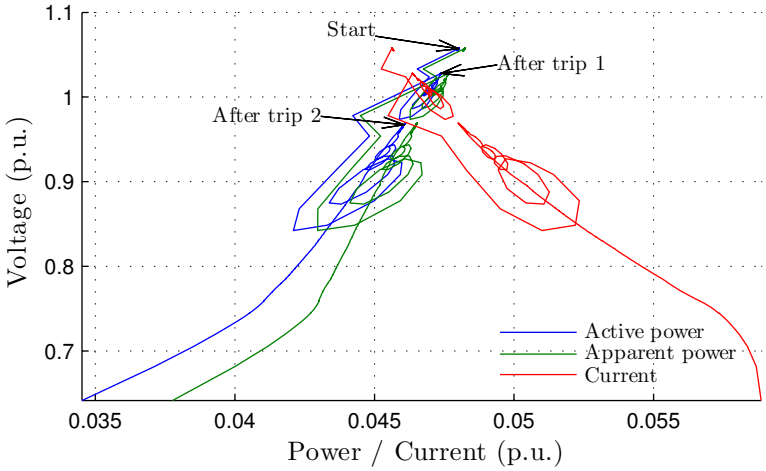

(a) PV-plot

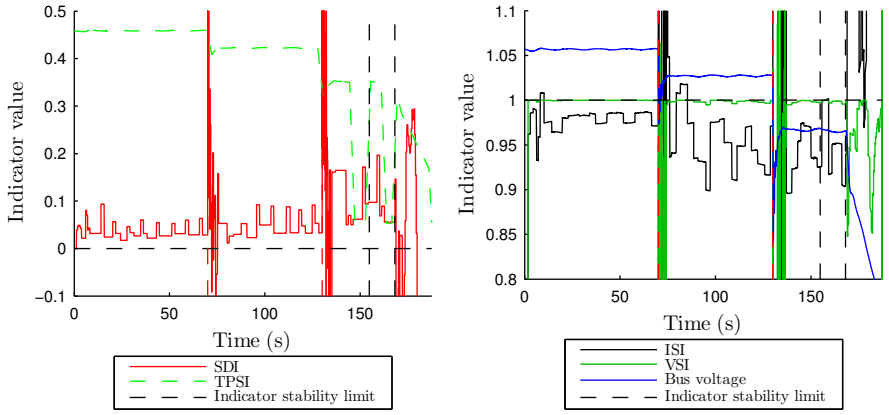

(b) Indicators whose critical value is 0 (c) Indicators whose critical value is 1

Figure 8.6: Case 1: Hammerfest: PV curve and indicators for load in Hammerfest. Dashed vertical lines indicate activation of OELs.

All indicators except TPSI indicate that the system is close to instability throughout the entire simulation. VSI_{SCC} is at the critical level the entire time, while ISI reaches the critical value when the OELs at Melkøya are activated. These results are very similar to the results from Case 2 in the RTS model, where the indicator values at the load buses are close to the stability limits throughout the entire simulation.

The reason for VSI_{SCC} being close to the stability limit throughout the entire simulation is probably due to its characteristics close to the stability limit on voltage controlled buses. It can be assumed that before the OELs are activated at Melkøya, the generators are, to a certain extent, controlling the bus voltage in Hammerfest, making this situation similar to Case 2 in the two-bus model (Section 6.1.2). Here, VSI_{SCC} has a curved shape similar to the first 90° of a sine wave, so that it reaches the critical value too early.

Lines from Skaidi to Hammerfest The PV-plot and indicators for the power flow on the lines from Skaidi to Hammerfest are shown in Figure 8.7, measured at the Hammerfest bus. In contrast to the previous PV-plot, the trajectory of stable operating points for the transmission on the lines to Hammerfest appears to be moving along the stable region of a PV curve.

The indicator values for these lines are more sensible than the indicators for the load, and the effect of tripping generators is shown as the indicator values move closer to the stability limit for each generator that is tripped. The indicators also seem to become more sensitive to the load variations. In the first minute of the simulation, the load variations are barely noticeable in ISI and VSI_{SCC}, but after tripping the first generator, these indicators seem to oscillate more.

SDI is generally very noisy in this case, and the simple filtering technique that is used is not adequate. The general trend in the indicator value is still visible, and SDI appears to indicate a longer distance to voltage instability than ISI and VSI_{SCC}.

None of the indicators for the lines to Hammerfest (except VSI_{SCC}, which might be too pessimistic, as mentioned above) reach their critical value until

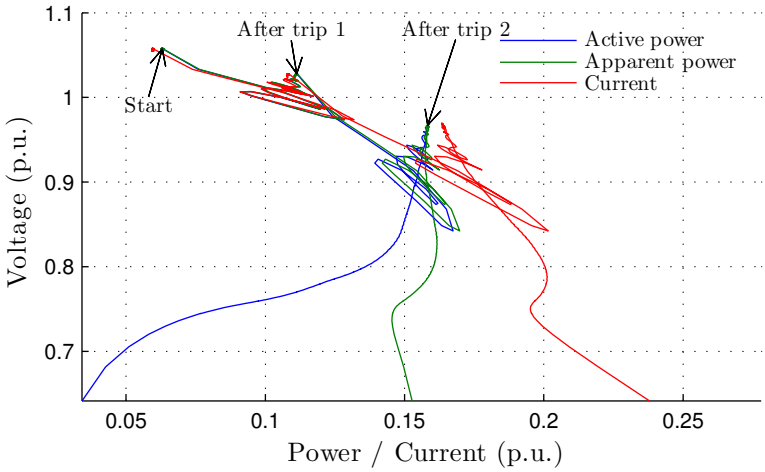

(a) PV-plot

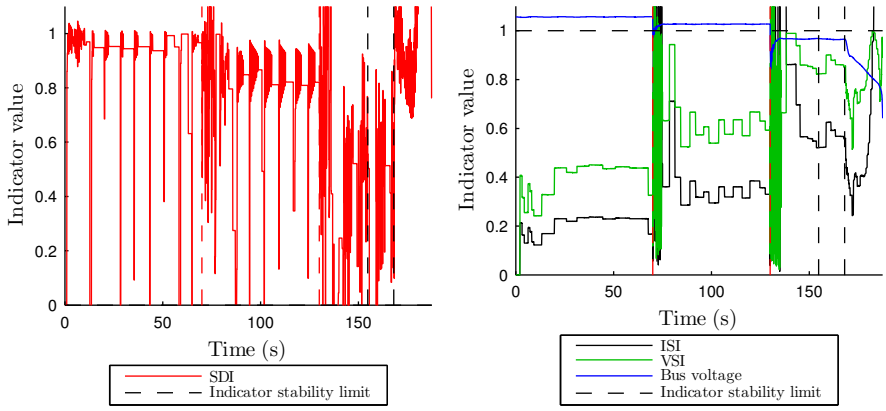

(b) Indicators whose critical value is 0 (c) Indicators whose critical value is 1

Figure 8.7: Case 1: Hammerfest-Skaidi: PV curve and indicators for lines between Hammerfest and Skaidi. Dashed vertical lines indicate activation of OELs.

the last few seconds of the simulation, when the voltage is collapsing. This is because activation of the OELs at Melkøya is such a significant event that it pushes the system way beyond the stability limit. The available reactive power is reduced by approximately 30 Mvar in an already weak area.

The indicators shown in this section are the ones that give the best results for indicating the voltage instability in the region. Other notable findings are that the indicators for the line between Sautso and Lakselv are relatively close to their stability limits (i.e. similar to Figure 8.7).

Mitigation actions

In this case, the situation becomes very severe with little, if any, warning from the indicators, and few mitigation actions are available. Most of the power plants in the nearby region are run-of-the-river plants with little active power regulation capability, and those that can be regulated are already at their maximum output. All shunt compensation equipment is switched correctly, leaving only two possible mitigation actions, load shedding and increasing AVR setpoints. Rankings of buses for mitigation actions has been calculated using Equation (5.3), and the results are listed in Table 8.1. As expected for this relatively simple network layout, the nearest buses are the most effective ones to initiate mitigation actions at.

Simulations have been done where the voltage setpoint was increased at buses Kvalsund, Adamselv, Sautso and Kvænangsbotn ten seconds after tripping the third generator at Melkøya (i.e. when $\mathrm{VSI_{SCC}}$ reaches 0.8 in Fig-

Table 8.1: Ranking of buses for applying mitigation strategies, calculated for the Hammerfest bus.

Bus j	$\Delta U_{Hammerfest}$	Type of equipment
Kvalsund	0.0585	Generators
Adamselv	0.0572	Generators
Sautso	0.0589	Generators
Kvænangsbotn	0.0390	Generators
Guolas	0.0351	Generators

ure 8.7c), but this was not enough to mitigate the collapse, the OEL activation was just delayed by approximately 20 seconds.

Considering that this scenario is a typical cold winter day where one would want to avoid shedding residential loads, the only remaining mitigation actions are to either disconnect the LNG plant and let it run islanded, or to shed enough of the load at the plant to save the power system. This has not been simulated, since it is obvious that disconnecting the cause of the problem will stabilise the system.

8.3 Case 2: Trip of one Generator at Melkøya with Outage of the Line Between Alta and Skaidi

8.3.1 Operating Scenario

This case is similar to Case 1. It is assumed that one of the gas turbines at the Melkøya plant is offline due to maintenance, and the loads are unchanged. One of the generators in Adamselv power plant is offline (25 MW of a total of 50 MW), and the line between Alta and Skaidi is out of service.

This might be an unusual operating scenario, but outages of lines can occur and in a liberalised power market the producers are free to decide their own schedules, so one can not assume that all generators are available at all times. The generator in Adamselv can be assumed to be offline due to for example maintenance, faults or low water reservoir levels.

Below, the result of tripping one more generator at the Melkøya plant is examined.

8.3.2 Simulation Results

The bus voltages during this contingency are shown in Figure 8.8. Since the line between Alta and Skaidi is offline, the line between Sautso and Lakselv, which was identified as a weak line in the previous case, is even more loaded now than in Case 1. As a result, the voltages in the region east of this line drop significantly when the generator at Melkøya is tripped at $t = 40$ s. Shortly after,

the OELs at buses Nordreisa, Kvalsund and even Varangerbotn are activated, after which the voltages begin to sag as a result of the EXTL load model attempting to restore the load in the region. At $t = 173$ s, the OEL at the Sautso bus are activated causing the voltages to decrease further, followed by activation of the OEL at the Adamselv bus, and finally, at $t = 248$ s, the OELs at Melkøya are activated, causing the voltage to collapse rapidly.

The power flow from the Melkøya plant to the Hammerfest bus is shown in Figure 8.9. Compared to Case 1, the reactive power flow from the plant is in this case more significant, and the results are therefore less representative of the real system.

Indicators

Lines from Skaidi to Hammerfest The PV plot and indicators for the lines from Skaidi to Hammerfest (at the Hammerfest bus) is shown in Figure 8.10. In the PV plot, the system appears to be stable until the OELs at

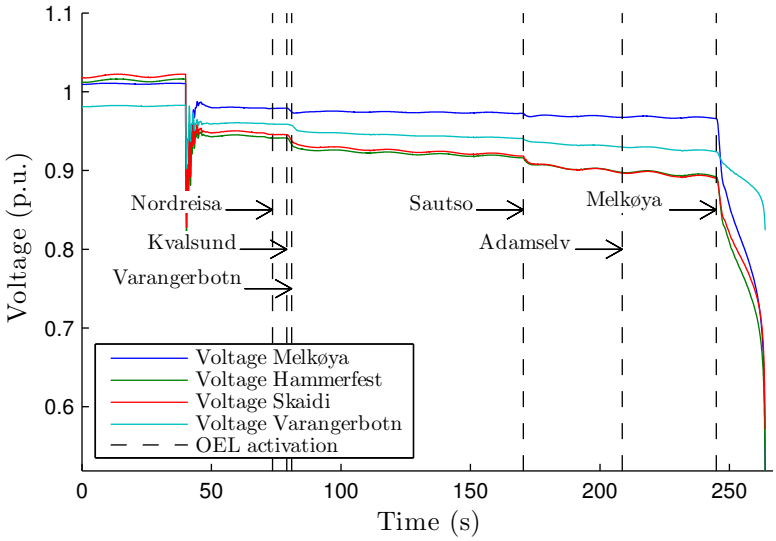

Figure 8.8: Case 2: Bus voltages. Dashed vertical lines indicate activation of OELs.

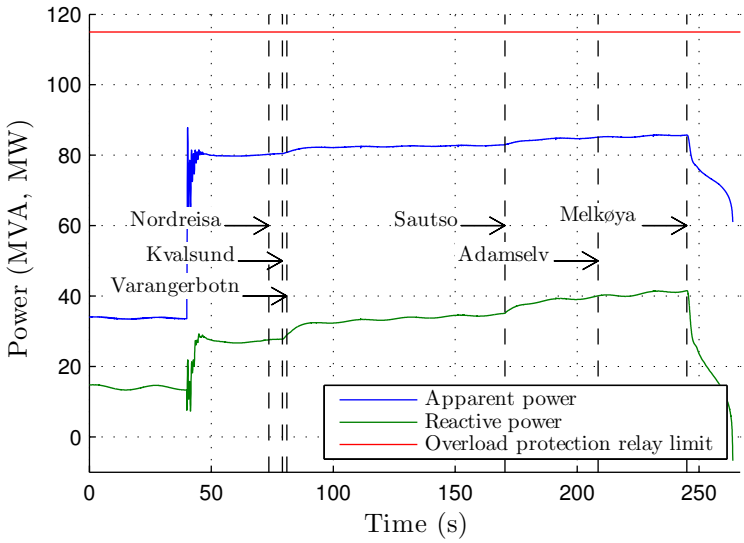

Figure 8.9: Case 2: Powerflow between Melkøya LNG and the Hammerfest bus. Positive direction of reactive power flow is towards the Hammerfest bus, active power is flowing towards LNG plant. Dashed vertical lines indicate activation of OELs.

Melkøya are activated, at which point the power starts decreasing while the current increases. Indicators VSI_{SCC}, ISI and TPSI confirm this, and also indicate that the stability of the system is gradually degrading. They are all within their stable regions until the OELs at Melkøya are activated. SDI, although noisy, indicates that the system is unstable throughout the entire simulation, and that it is stabilising when the OELs at Melkøya are activated, i.e. completely opposite of the other indicators.

The indicators for the load in Hammerfest behave equally as in Case 1 and are therefore not repeated here.

Line from Sautso to Lakselv Results for the line between buses Sautso and Lakselv, that was identified as weak in the previous case, is shown in Figure 8.11. From the PV plot it is clearly visible that the transmission on this line is weak. After tripping the generator on Melkøya, the voltage on the

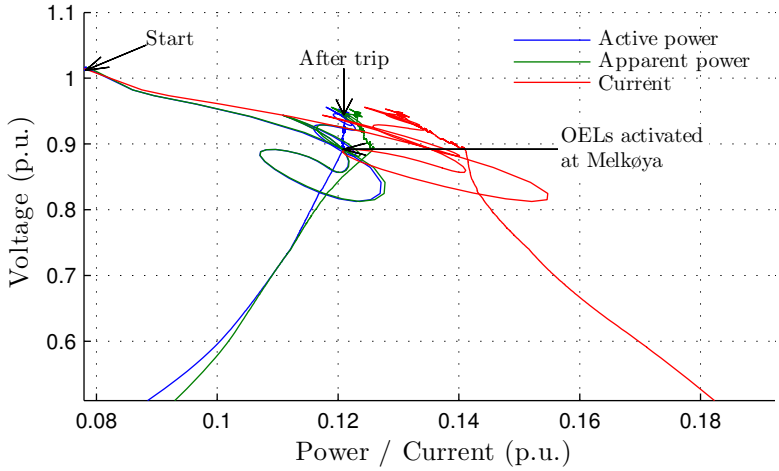

(a) PV-plot

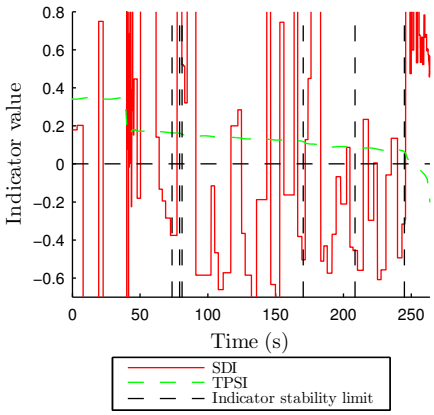

(b) Indicators whose critical value is 0

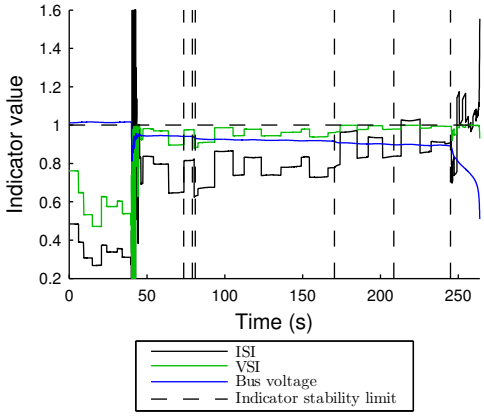

(c) Indicators whose critical value is 1

Figure 8.10: Case 2: Hammerfest-Skaidi: PV curve and indicators for lines between Hammerfest and Skaidi, measured at the Hammerfest bus. Dashed vertical lines indicate activation of OELs.

Lakselv bus drops to 0.85 p.u. as the transmission on the line increases, but then recovers due to AVRs at nearby generators. The transmission appears to be stable the entire time.

The indicators confirm that the system is stable, but after tripping the generator at Melkøya, all four indicators are very close to their stability limits. When the OELs at the Sautso bus are activated, the distance to instability decreases even more. However, when the OELs at Melkøya are activated, SDI and TPSI indicate that the transmission stabilises while ISI indicates that the system is unstable.

Mitigation actions

In this scenario, there are even fewer mitigation actions available than in Case 1. All OELs in the nearby region are activated at some point during the simulation, making the only possible mitigation actions switching of a reactor at the Varangerbotn bus and load shedding. In the following, it is assumed that the mitigation algorithm is using input from OELs to trigger switching of reactive compensation equipment.

Since it is desirable to not shed load during cold winter days, only switching of the 40 Mvar reactor at the Varangerbotn bus was tested. It is assumed that the representation of the generator at the Varangerbotn bus corresponds relatively well to the real situation, so that the OEL signal can be utilised to trigger disconnection of the reactor. This was tested in another simulation of Case 2, and the resulting bus voltages are shown in Figure 8.12.

As the figure illustrates, the bus voltages appear to stabilise after disconnecting the reactor at $t = 80$ s, and no OEL timers are active towards the end of the simulation. The oscillations in the voltages are caused by the load variations that were introduced to allow indicator values to be calculated. The voltages at buses Hammerfest and Skaidi are still low, and the indicators for the Sautso-Lakselv and Skaidi-Hammerfest lines are very close to their stability limits, indicating that the system is still close to instability and very vulnerable to further disturbances.

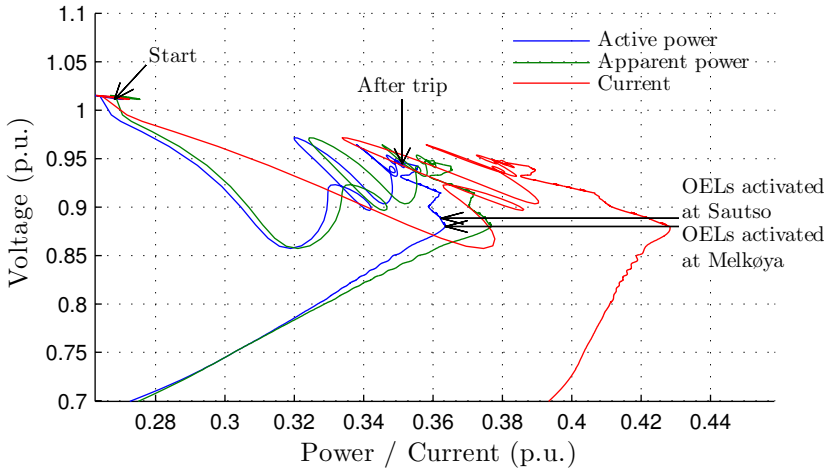

(a) PV-plot

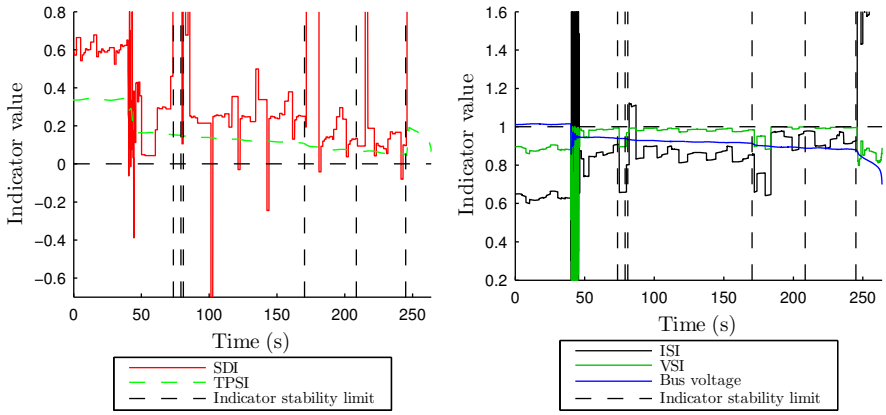

(b) Indicators whose critical value is 0 (c) Indicators whose critical value is 1

Figure 8.11: Case 2: Sautso-Lakselv: PV curve and indicators for the line between Sautso and Lakselv, measured at the Lakselv bus. Dashed vertical lines indicate activation of OELs.

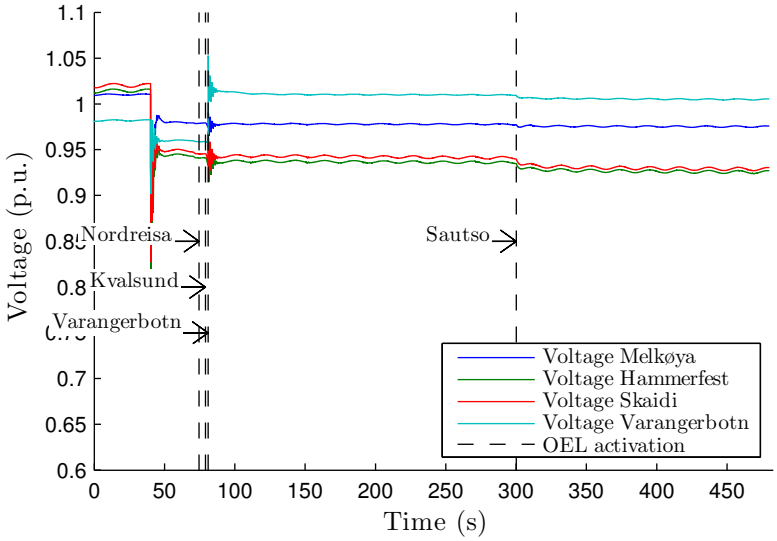

Figure 8.12: Case 2, including disconnection of reactor: Bus voltages. Dashed vertical lines indicate activation of OELs.

8.4 Discussion

8.4.1 Indicators

In Case 1 the indicators were not able to detect the instability before it was too late, since activation of the OELs at Melkøya results in a large step in the distance to voltage instability at the Hammerfest bus. In Case 2, the indicators were closer to their stability limit throughout the entire simulation since the disconnected line made the system significantly weaker. This illustrates that the indicators can reliably assess the situation of the network, but they can not foresee the future.

The problem of detecting that it is necessary to initiate mitigation actions thus remains, especially for Case 1. The indicator values never reach levels that are far enough from what can be considered normal operating values to justify load shedding, so other means must be used to detect the oncoming situation. One proposed solution is to extract the OEL timer activation signal from the generators at Melkøya, and, if possible, field current or field voltage

measurements. These signals can then be used to indicate that the OELs will soon be activated, and possibly also the time remaining until activation, which can further be used to initiate a "nice" load shedding in the LNG plant, or to start up offline generators if possible.

8.4.2 Mitigation Actions and Proposed Mitigation Algorithm

The region that has been studied here (the Hammerfest area) is relatively small compared to the unstable 138 kV region in the IEEE RTS case studies, implying that there are fewer mitigation actions available. The effectiveness of the proposed mitigation algorithm is therefore reduced. The purpose of the mitigation algorithm is to avoid load shedding, but since there are very few available measures to do so, the algorithm fails in Case 1. In Case 2, switching of a reactor relatively far from the critical region is able to mitigate the collapse, but this action was initiated based on OEL input and not indicator values directly.

The mitigation action for Case 2 was successful since the significant drop in the voltages after tripping the generator caused load restoration not only in the Hammerfest area, but in the entire Finnmark region. Disconnecting the shunt reactor restored the easternmost voltages, and thus reduced load restoration and also the load on the weak Sautso-Lakselv line.

8.4.3 Validity of Results

The dynamic model that was provided by Statnett SF is not suitable for the type of simulations that has been done here. All of the generators at lower voltage levels were modelled as being able to control the voltage on the transmission-level bus they are connected to, with essentially no limitations on the reactive power capability when compared to the limits in the power flow model. In this study, the power factor for these units was limited to approximately 1.0, but it might have been better to model the units as negative loads, as that would better reflect the effect of these generators on the transmission system bus voltage.

Tap changers were not modelled due to the time limitations of this study. When considering Case 1, where the load at the Hammerfest bus appeared to be moving along the lower half of the PV curve, tap changers would probably make the scenario unstable sooner since they would have attempted to increase the load-side voltage and thus to restore the load.

The OEL models that were implemented for this study are very simplified, and the field current limits that were used are based on several assumptions. There are a vast number of different limiter types and limiter characteristics, not all limiters may be tuned according to the requirements in FIKS [29], and the field current limit of the generators may not correspond to the IEEE C50.13-2005 standard. However, the error should not be too large, since the assumptions are well-reasoned.

The accuracy of the model of what is assumed to be Nedre Porsa Kraftverk at the Kvalsund bus is questionable. In the provided model, the machine is connected directly to the Kvalsund bus in Figure 8.1 via a transformer, while it is assumed that in reality it is connected to the Kvalsund bus via several transformers and a subtransmission system, all of which will affect the generator's ability to supply reactive power to Hammerfest and Skaidi and the ability to control the voltage on the Kvalsund bus directly.

Another source of inaccuracies in the results is the lack of modelling of the reactive power control system at the Melkøya plant. In Case 1, the reactive power from Melkøya is close to zero throughout the entire simulation, and there is at most an export of 6 Mvar to the Hammerfest bus, which is assumed to be negligible. In Case 2, the reactive power export from Melkøya is more significant, up to approximately 40 Mvar. Had the reactive power control system been modelled, it would have reduced the reactive power export, and the voltage would probably have collapsed sooner, either at the Hammerfest bus or at the Lakselv bus, due to the lack of reactive power.

The lack of representation of the transmission systems in the neighbouring countries probably affects the results to some extent too. In Case 2, where an OEL was activated at the Varangerbotn bus, the reactive power import from Finland would most likely have increased due to the reduced voltage at

the Varangerbotn bus, possibly stabilising the system or at least relieving the situation. Tripping of the generators at Melkøya would possibly also lead to an increased import from the neighbouring countries. In the studied model, much of the active power that must be imported following the generator trips is imported from far south in the Norwegian system, which contributes to deteriorating the voltage stability in the northern regions of the model.

9 Discussion

This chapter gives a summarising discussion of the findings of all case studies in the previous chapters.

9.1 Voltage Stability Indicators

Of the six studied indicators, the three that were based on local measurements, SDI, ISI and VSI_{SCC}, appeared to work best under all conditions. ISI and VSI_{SCC} correctly detected instability in all cases where the voltage collapsed, but VSI_{SCC} appeared to reach its critical value before any of the other indicators, indicating that it might be a bit pessimistic. This was also shown in Case 2 in the two-bus study, where the VSI_{SCC} curve has the shape of the first 90° of a sine wave.

The results from the two-bus study also showed that VSI_{SCC} is only able to detect the distance to the tip of the PV curve, i.e. the distance to the maximum power transfer level, but not whether the system is on the stable or unstable half of the PV curve. Therefore, if VSI_{SCC} is to be used to detect voltage instability, it has to be combined with another indicator that is able to detect whether the system is stable or not, such as SDI or ISI.

Although the indicators SDI and ISI are very similar, SDI showed varying results in the simulations. After passing the instability point, it would often return to indicate a stable system as the collapse progressed, while ISI consistently detected the instability correctly.

The main problem with the above mentioned indicators, ISI, SDI and VSI_{SCC}, is that they are all based on calculations on consecutive measurements and are using a steady-state criteria, which causes them to show false results during transient events. The indicators that are based on wide-area measurements, FVSI, L_{mn} and TPSI, do not show this behaviour. However, they are not as good at indicating instability as the other indicators. FVSI

and L_{mn} failed even under ideal conditions in the two-bus system, and TPSI shows so varying results that it cannot be trusted to reliably give good results in a meshed system.

The results from the case studies show that all lines, or at least the most critical lines, in the system must be monitored for instability. The indicators will only indicate instability for the line(s) where the instability occurs.

9.2 Performance of Proposed SIPS

The simulations in the larger system models showed that in the areas where voltage instability is a problem, there are few available mitigation actions, which is as expected. In the IEEE RTS model, the mitigation algorithm was tested for Case 1, and succeeded, but it exhausted all available mitigation actions before finally stabilising the system. In the model of the Norwegian power system, there were not enough available actions to mitigate the collapse in Case 1 without shedding load, and in Case 2 the collapse was avoided by disconnecting a shunt reactor relatively far from from the critical region.

An important result from the simulations is that the proposed mitigation algorithm works better when slower instability mechanisms are present, or when the system is gradually approaching instability, as in the cases studied in the IEEE RTS model. In the model of the Norwegian power system, the instability mechanisms are very fast in both of the studied cases, and the event that triggers the voltage instability is very severe, leading to an immediate collapse and leaving no time for mitigating actions. In such cases, additional signals from OELs can be used to warn about those severe events, and to trigger load shedding when the critical OELs are activated.

OEL signals were shown to be usable to initiate certain mitigation actions. In the simulations they give an indication of where the problem is located (i.e. where there is a lack of reactive power), and can be used to initiate mitigating actions to supply more reactive power in the vicinity of the activated OEL. In the Hammerfest-case, signals from the OELs at the Melkøya-plant can be used to initiate emergency load shedding since this is a critical event for the stability

of the Hammerfest area, and OEL signals also proved useful to mitigate the collapse in Case 2.

Depending on the MVA-rating of the generator, different mitigating actions can be initiated. OELs on small generators are normally activated sooner, and should thus be used to initiate mitigating actions that do not result in load shedding. OEL activation signals from larger generators are usually more critical, since the reduced amount of reactive power can be much larger, as in the case of the generators at Melkøya.

A combination of both OEL signals and indicators seems to be the best solution. The discrete nature of OEL activation signals gives a clear indication of a lack of reactive power, and thus of problematic regions. The indicators show the distance to instability and thus give an assessment of the situation at all times.

From a practical point of view, automatic switching of equipment and adjustment of setpoints in the system can potentially worsen the situation or lead to extremely high or low voltages. If the proposed mitigation algorithm is to be used in a SIPS in a real system, detailed analyses must be performed to determine which mitigation actions the SIPS can initiate autonomously and which conditions that must be fulfilled before initiating these actions (e.g. voltage levels for switching of reactive compensation equipment). OEL signals that can be used in the SIPS must also be identified, and the system models that are used for these studies must be verified to ensure satisfactory performance of the SIPS.

10 Conclusion

Of the studied indicators, the ones that are based only on local measurements were shown to be the most reliable indicators. A combination of the indicators ISI and VSI_{SCC} will give a reasonable, slightly conservative measure of the voltage stability of the system, where VSI_{SCC} is used to estimate the distance to the maximum power transfer level and ISI determines whether the system is on the stable upper half of the PV curve or not. The problem with these indicators is that they often indicate instability during transient events

The suggested unconventional mitigation actions have been tested by simulations, and almost all of them had a positive impact on the voltage stability of the system. Increasing AVR set points was the most effective action, followed by increasing governor set points. Decreasing the governor set points to allow the generator to produce more reactive power did not provide the intended relief, instead the increased reactive transmission losses were greater than the gained reactive power production from the generator.

The proposed system integrity protection scheme is based on both signals from activation of overexcitation limiters and on calculation of voltage stability indicators, using the proposed mitigation algorithm. The mitigation algorithm appears to work well, as was shown in a simulation in the IEEE RTS model, but to avoid load shedding it requires an abundance of available mitigation actions. Due to this requirement, the algorithm is better suited for instabilities in larger areas where more mitigation actions normally are possible. This was also shown in the model of the Norwegian power system, where the mitigation algorithm is unable to prevent the collapse in one of the studied scenarios in the relatively small Hammerfest/Skaidi area without shedding load.

11 Further Work

There are several ways to continue the work of this thesis. Firstly, the implementation details of the proposed SIPS must be ironed out. Only the basic principles of the SIPS and the accompanying mitigation algorithm are described here, since the details will be specific for each system. If further studies are to be done in the model provided by Statnett, the models of the power plants near Hammerfest should be improved. The representation of Nedre Porsa Kraftverk near the Kvalsund bus is especially of importance, since it plays an important role in the voltage stability of the Hammerfest/Skaidi area.

For use in the real world, the effect of measurement errors and filtering should be examined, especially for the indicators relying on consecutive measurements (SDI, ISI and VSI_{SCC}). The indicators should also be tested with measured values from a real system to determine whether they can be used under the actual conditions in the system.

The number of indicators that were examined is limited, and several of the indicators were shown to be very similar to each other, such as SDI/ISI and L_{mn}/FVSI. More indicators should be identified and compared to those that were found in this study.

The mitigation strategies that are described and discussed here are relatively simple. More advanced strategies should be identified and examined further, such as area rescheduling of active power, where some of the active power generation is moved closer to the region that is identified as being close to voltage instability. This will reduce the import to the region, and thus also reduce the reactive power losses.

Another suggestion for further work is to examine the possibilities of improving the path-finding algorithm of TPSI to make the indicator more reliable in meshed systems.

The possibility of using voltage stability indicators for lines to determine

whether circuit contingencies will lead to voltage instability can also be explored. The idea is that when a line is disconnected from a bus, the power flow on this line will be transferred to other lines in the system, and if one of those lines is close to instability, the disconnection can make the system unstable.

References

[1] P. Kundur, *Power System Stability and Control*. McGraw-Hill Professional, January 1994.

[2] IEEE Task Force on Blackout Experience, Mitigation, and Role of New Technologies, "Blackout Experiences and Lessons, Best Practices for System Dynamic Performance, and the Role of New Technologies," IEEE, Tech. Rep. Special Publication 07TP190, July 2007.

[3] P. Kundur, J. Paserba, V. Ajjarapu, G. Andersson, A. Bose, C. Canizares, N. Hatziargyriou, D. Hill, A. Stankovic, C. Taylor, T. van Cutsem, and V. Vittal, "Definition and classification of power system stability, IEEE/CIGRE joint task force on stability terms and definitions," *IEEE Transactions on Power Systems*, vol. 19, no. 2, pp. 1387 – 1401, August 2004.

[4] T. van Cutsem and C. Vournas, *Voltage Stability of Electric Power Systems*. Springer, 1998.

[5] V. Ajjarapu and C. Christy, "The continuation power flow: a tool for steady state voltage stability analysis," *IEEE Transactions on Power Systems*, vol. 7, no. 1, pp. 416–423, feb 1992.

[6] J. Machowski, J. Bialek, and J. R. Bumby, *Power System Dynamics: Stability and Control*, 2nd ed. John Wiley and sons, Ltd, 2008.

[7] J. van Hecke, N. Hatziargyriou, and T. van Cutsem, "Indices predicting voltage collapse including dynamic phenomena," CIGRE publication, Tech. Rep., 1994, report of CIGRE working group 38.02.11, J. van Hecke (convenor).

[8] "Ockham's razor," Encyclopædia Britannica Online, 26 april 2012. [Online]. Available: http://www.britannica.com/EBchecked/topic/424706/Ockhams-razor

[9] I. Musirin and T. A. Rahman, "Novel fast voltage stability index (FVSI) for voltage stability analysis in power transmission system," in *Student Conference on Research and Development*, 2002, pp. 265 – 268.

[10] M. Moghavvemi and F. Omar, "Technique for contingency monitoring and voltage collapse prediction," *IEE Proceedings on Generation, Transmission and Distribution*, vol. 145, no. 6, pp. 634 – 640, nov 1998.

[11] F. Gubina and B. Strmčnik, "Voltage collapse proximity index determination using voltage phasors approach," *IEEE Transactions on Power Systems*, vol. 10, no. 2, pp. 788 –794, may 1995.

[12] G. Verbic and F. Gubina, "A novel concept for voltage collapse protection based on local phasors," in *IEEE/PES Transmission and Distribution Conference and Exhibition 2002: Asia Pacific.*, vol. 1, oct. 2002, pp. 124 – 129.

[13] ——, "A new concept of voltage-collapse protection based on local phasors," *IEEE Transactions on Power Delivery*, vol. 19, no. 2, pp. 576 – 581, april 2004.

[14] M. Begovic, B. Milosevic, and D. Novosel, "A novel method for voltage instability protection," in *Proceedings of the 35th Annual Hawaii International Conference on System Sciences, 2002.*, jan. 2002, pp. 802 – 811.

[15] K. Vu, M. Begovic, D. Novosel, and M. Saha, "Use of local measurements to estimate voltage-stability margin," in *20th International Conference on Power Industry Computer Applications*, may 1997, pp. 318 –323.

[16] L. Huang, J. Xu, Y. Sun, T. Cui, and F. Dai, "Online monitoring of wide-area voltage stability based on short circuit capacity," in *2011 Asia-Pacific Power and Energy Engineering Conference (APPEEC)*, march 2011, pp. 1–5.

[17] K. Vu, M. Begouic, and D. Novosel, "Grids get smart protection and control," *IEEE Computer Applications in Power*, vol. 10, no. 4, pp. 40 –44, oct 1997.

[18] D. Julian, R. Schulz, K. Vu, W. Quaintance, N. Bhatt, and D. Novosel, "Quantifying proximity to voltage collapse using the voltage instability predictor (VIP)," in *IEEE Power Engineering Society Summer Meeting*, 2000, pp. 931 –936.

[19] S.-J. Tsai and K.-H. Wong, "On-line estimation of thevenin equivalent with varying system states," in *2008 IEEE Power and Energy Society General Meeting - Conversion and Delivery of Electrical Energy in the 21st Century*, july 2008, pp. 1 –7.

[20] K. Ohtsuka, S. Yokokawa, H. Tanaka, and H. Doi, "An equivalent of multi-machine power systems and its identification for on-line application to decentralized stabilizers," *IEEE Transactions on Power Systems*, vol. 4, no. 2, pp. 687 –693, may 1989.

[21] L. Warland, "A Voltage Instability Predictor Using Local Area Measurements – VIP++," Ph.D. dissertation, Norwegian University of Science and Technology, Faculty of Electrical Engineering and Telecommunications, Department of Electric Power Systems, February 2002.

[22] E. Johansson, K. Uhlen, G. Kjølle, and T. Toftevaag, "Reliability Evaluation of Wide Area Monitoring Applications and Extreme Contingencies," in *17th Power Systems Computation Conference*, Stockholm, Sweden, August 2011.

[23] Siemens Energy Inc. and Siemens Power Technologies International, *PSS®E model library*, PSS®E 32.0.5 ed., October 2010.

[24] C. Grigg, P. Wong, P. Albrecht, R. Allan, M. Bhavaraju, R. Billinton, Q. Chen, C. Fong, S. Haddad, S. Kuruganty, W. Li, R. Mukerji, D. Patton, N. Rau, D. Reppen, A. Schneider, M. Shahidehpour, and C. Singh, "The IEEE Reliability Test System - 1996. A report prepared by the Reliability Test System Task Force of the Application of Probability Methods Subcommittee," *IEEE Transactions on Power Systems*, vol. 14, no. 3, pp. 1010 –1020, aug 1999.

[25] "IEEE Standard for Cylindrical-Rotor 50 Hz and 60 Hz Synchronous Generators Rated 10 MVA and Above," *IEEE Std C50.13-2005*, 2006.

[26] J. Å. Walseth, Statnett SF, personal communication, 2012.

[27] ENTSO-E, "ENTSO-E Grid Map," 06 June 2012. [Online]. Available: https://www.entsoe.eu/index.php?id=77

[28] Det kongelige olje- og energidepartement, "Gasskraftprosjekter i Norge," nov 2005. [Online]. Available: http://www.regjeringen.no/Upload/OED/Faktaark/Gasskraftprosjekter_i_Norge.pdf

[29] Statnett SF, "Funksjonskrav i kraftsystemet," apr 2012. [Online]. Available: http://www.statnett.no/no/Kraftsystemet/Systemansvaret-FoS/styrende-dokumenter/

[30] J. Walker, "Operating characteristics of salient-pole machines," *Proceedings of the IEE - Part II: Power Engineering*, vol. 100, no. 73, pp. 13 –24, february 1953.

[31] R. Bruck and H. Messerle, "The capability of alternators," *Proceedings of the IEE - Part A: Power Engineering*, vol. 102, no. 5, pp. 611 –618, october 1955.

[32] K. Bonfert, *Betriebsverhalten der Synchronmaschine.* Springer-Verlag, 1962.

[33] T. Olsen, "Generatorers reaktive produksjon og deres betydning for spenningsstabiliteten i et elkraftsystem," Master's thesis, Norwegian University of Science and Technology, december 1999.

[34] Application of Probability Methods Subcommittee, "IEEE Reliability Test System," *IEEE Transactions on Power Apparatus and Systems*, vol. PAS-98, no. 6, pp. 2047 –2054, nov. 1979.

Appendices

Appendix A

Description of Synchronous Machine Capability Diagram

This appendix gives a brief introduction to the capability diagram of synchronous generators. The diagram is derived for a given voltage, U, saturation is not considered and resistances are assumed to be negligible. The quantities that are referred to in the following derivations are illustrated in Figure A.1. The content of this appendix is mainly based on [6, 30, 31, 32].

There are generally five constraints limiting the reactive capability of the

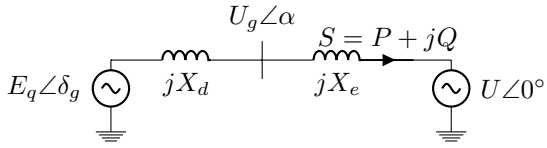

Figure A.1: Equivalent diagram of cylindrical rotor machine with external network

generator, and one active power limit.

1. armature current limit
2. maximum rotor field current limit
3. minimum rotor field current limit
4. steady-state rotor-angle stability limit
5. stator core end-region heating limit
6. maximum (and minimum) turbine power rating

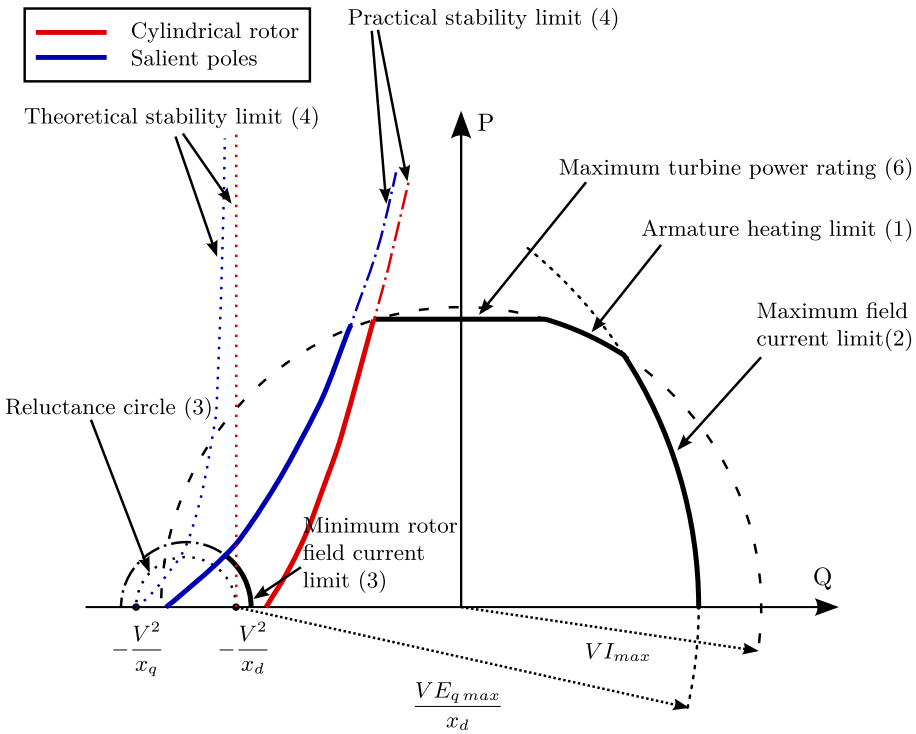

Figure A.2: Generator capability diagram, bold lines indicate the applicable limits.

A.1 Armature Current Limit

The first limit is given by the maximum armature current, I_{max}. For a given voltage U, this limit can be expressed as a power limit, $S_{max} = UI_{max}$, or in terms of P and Q, $P^2 + Q^2 = (UI_{max})^2$. This is a circle in the P-Q plane, and is illustrated by the dashed line in Figure A.2. This limit is equal for cylindrical-rotor and salient pole machines.

A.2 Maximum Rotor Field Current Limit

The second limit relates to the maximum long-term rotor field current limit. Here, the limit is only derived for cylindrical-rotor machines, but the difference for salient-pole machines is small at voltages close to the rated voltage [31].

In the synchronous machine, the rotor field current induces an air-gap electromotive force (emf), which can be represented in an equivalent diagram as a combination of the emf E_q and the magnetizing inductance X_d (for a detailed derivation, see [6, ch.3.3]).

By using the equivalent emf and magnetizing inductance, the field current limit can be transformed to the P-Q plane using the equations for active and reactive power for the cylindrical-rotor generator:

$$P = \frac{E_q U}{x_d} \sin \delta_g \quad \text{and} \quad Q = \frac{E_q U}{x_d} \cos \delta_g - \frac{U^2}{x_d} \tag{A.1}$$

δ_g is the power angle of the generator and x_d is the total d-axis synchronous reactance of the generator (the sum of the d-axis synchronous reactance and the external reactance between the generator terminals and the stiff voltage U, $x_d = X_d + X_e$).

Squaring both equations and using the identity $\sin^2 \delta_g + \cos^2 \delta_g = 1$ to eliminate δ_g from the equations yields:

$$P^2 + \left(Q + \frac{U^2}{x_d} \right)^2 = \left(\frac{E_q U}{x_d} \right)^2 \tag{A.2}$$

In the P-Q plane, equation (A.2) corresponds to a circle of radius $E_q U/x_d$, with the centre at $-U^2/x_d$ on the Q axis. With $E_q = E_{q\,max}$, the circle reflects the upper apparent power limit. In Figure A.2, this limit is illustrated by the black, dotted line.

A.3 Minimum Rotor Field Current Limit

The third limit relates to the minimum field current the excitation system is able to provide. The limit is only considered for salient-pole machines due to the additional reluctance power terms in the equation for active power for these machines, see equation (A.3).

$$P = \frac{E_q U}{x_d} \sin \delta_g + \frac{U^2}{2} \frac{x_d - x_q}{x_d x_q} \sin 2\delta_g \tag{A.3a}$$

$$Q = \frac{E_q U}{x_d} \cos \delta_g - \frac{U^2}{x_d} - U^2 \frac{x_d - x_q}{x_d x_q} \sin^2 \delta_g \tag{A.3b}$$

The reluctance power term makes the machine capable of producing active power at zero field current. The reluctance power can be determined by setting $E_q = 0$ in equation (A.3), and is illustrated by the dotted semi-circle at the negative half of the Q axis in Figure A.2.

Depending on the type of exciter, it may or may not be able to operate inside or close to the reluctance circle, so for certain exciters, Walker (1953) [30] suggests adding a 5 % margin to the reluctance circle to ensure stable operation of the exciter (dash-dotted semi-circle in the figure).

A.4 Steady-State Rotor Angle Stability Limit

The fourth limit is the rotor angle stability limit. This is the most complicated limit, as it depends on the external reactance (X_e) between the generator terminals and a stiff voltage (U), on the construction of the rotor and on the response time of the automatic voltage regulator (AVR) and the exciter.

A.4.1 Cylindrical Rotor

For a machine with a cylindrical rotor, the limit can be determined from equation (A.1) when $\frac{\partial P}{\partial \delta_g} = 0$, which gives $\delta_g = 90°$. This is the theoretical stability limit, and corresponds to a straight line in the P-Q plane at $Q = -U^2/x_d$.

In practice it is impossible to operate the machine at the theoretical stability limit. Walker (1953) [30] suggests adding a 10 % margin of active power to the theoretical limit. To determine this practical stability limit, for any point on the theoretical limit, the active power output should be reduced by 10 % (of the nominal rating) while keeping the field current constant. Both the theoretical and the practical limit for cylindrical-rotor generators are drawn in red in Figure A.2. The theoretical limit is dotted and the practical limit is dash-dotted.

A.4.2 Salient Pole Machine

The stability limit for salient pole machines becomes slightly more complicated due to the additional reluctance power terms in the equation for active power for these machines.

Based on equation (A.3a), the stability limit $\frac{\partial P}{\partial \delta_g} = 0$ now becomes [33]:

$$cos\delta_g = \frac{1}{4}\left(-\frac{E_q x_q}{U(x_d - x_q)} \pm \sqrt{\left(\frac{E_q x_q}{U(x_d - x_q)}\right)^2 + 8}\right) \tag{A.4}$$

By choosing a set of values for E_q, equation (A.4) gives the corresponding values of δ_g. The values of P and Q can then be calculated using equation (A.3), which gives a set of coordinates in the P-Q plane that correspond to the theoretical angle stability limit. Similarly as for the cylindrical rotor machine, a 10 % margin is used for the practical limit. Both limits are illustrated by the blue curves in Figure A.2.

A.4.3 Voltage Regulated Machine

In the above derivations it is assumed that the excitation level is constant, i.e. the effect of the AVR is not considered. If the machine is equipped with an AVR that is continuously acting (no deadband) and the AVR and the exciter have a fast response (relative to the rate of change of apparent power), it allows operating the machine at even larger power angles in steady-state.

With the above assumptions, the voltage at the generator terminals, U_g, can be considered constant in steady-state. The equation for the active power flow from the generator terminals to the stiff voltage U then becomes:

$$P_{U_g} = \frac{U_g U}{X_e} \sin \alpha \tag{A.5}$$

where X_e is the reactance between the generator terminals and the stiff voltage, and α is the voltage angle between the two voltages.

The stability criterion is now $\partial P_{U_g}/\partial \alpha = 0$, which gives $\alpha = 90°$. To determine the power angle of the generator referred to the stiff voltage, the voltage angle between the internal emf E_q and the terminal voltage U_g, hereby called δ_t, must be added to α.

Since resistances are neglected, the power output at the generator terminals is equal to the power output at the stiff voltage. By using the power flow equations at these two points, the angle δ_t can easily be determined. For simplicity, the cylindrical-rotor equation, (A.1), is used here:

$$P = \frac{E_q U_g}{X_d} \sin \delta_t = \frac{E_q U}{X_d + X_e} \sin \delta_g, \quad \text{where} \quad \delta_g = \alpha + \delta_t \tag{A.6}$$

Solving the equation for δ_t and using that, at the stability limit, $\alpha = 90°$, gives:

$$\tan \delta_{t\,max} = \frac{U}{U_g} \frac{X_d}{X_d + X_e} \tag{A.7}$$

The steady-state stability limit when considering the AVR thus becomes:

$$\delta_{g\,max,\,AVR} = 90^\circ + arctan\left(\frac{U}{U_g}\frac{X_d}{X_d + X_e}\right) \tag{A.8}$$

which is an angle that is larger than 90°.

Operation near this stability limit can only be achieved by slowly increasing the power angle. If the power angle changes too rapidly, the AVR's response could be too slow, and the stability limit for fixed excitation becomes the prevailing limit. The synchronous reactances of the generator will also change, approaching their transient values, and the transient stability limit must also be taken into consideration, since this can be lower than the regulated steady-state stability limit.

A.4.4 Transient Stability Limit

The stability limits explained in this appendix are valid for steady-state operation. The transient stability limit, which is greater than the steady-state limit (disregarding the AVR), is valid under transient conditions. The limit is calculated using transient values (x'_d, x'_q and E').

Figure A.3 illustrates all four stability limits for a 53 MVA salient pole machine in the P-Q plane. Note that the stability limit for machines with AVR is calculated from equation (A.8), which is based on the cylindrical-rotor equations and is therefore only an approximation. The transient stability limit is calculated using equation (A.4) with transient values (x'_d, x'_q and E').

A.5 Stator Core End-Region Heating Limit

Stator core end-region heating occurs during underexcited operation of the generator. The low field current during this operating condition causes an increase in the end-turn leakage flux compared to overexcited operation. The leakage flux enters and leaves the stator in a direction perpendicular to the laminations which causes eddy currents in the end-region and, as a result, heat is generated (for further details, see e.g. [1, p.194]). The heat generated increases with decreasing excitation and can become a problem, particularly in cylindrical-rotor machines.

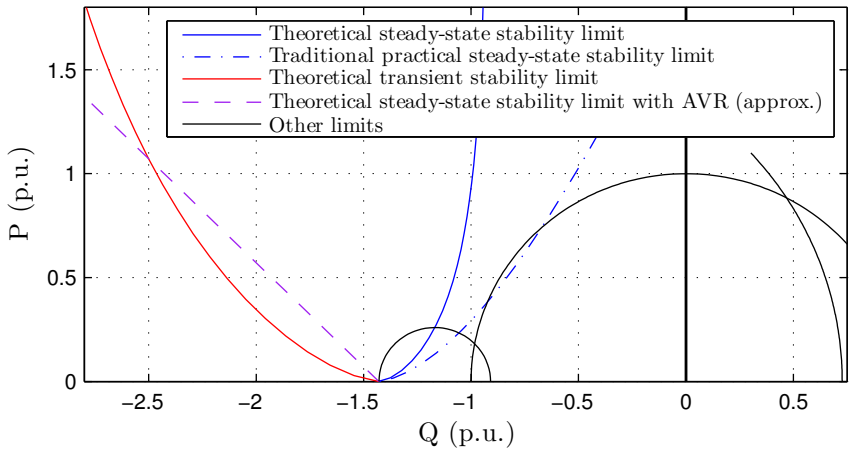

Figure A.3: Stability limits of a salient pole machine

The end-region heating limit is determined experimentally by the manufacturer, and is therefore difficult to include in the general capability diagram shown in Figure A.2. In many cases the limit is higher than the practical rotor angle stability limit, and for salient pole machines this limit is normally not a concern.

A.6 Maximum (and Minimum) Turbine Power Rating

In the P-Q plane the turbine power rating limits become two lines parallel to the Q-axis, one at $P = P_{max}$ and one at $P = P_{min}$.

Appendix B

Model data

B.1 Two-bus System

Infinite bus

The infinite bus was modelled using the GENCLS model, a classical generator model from the PSS/E model library. I.e. as a constant voltage behind a transient reactance. The inertia (H) and damping constant (D) were set to zero, which enables a special mode of the model in which the speed deviation and power angle are defined to be zero, making the model act as an infinite bus. The reactance of the model was given a value close to zero since the line models the reactance between the infinite bus and the load.

Load

The load is modelled as a constant-impedance load, with a small shunt capacitor bank to compensate the initial load level.

Table B.1: Shunt compensation and initial load model data

Parameter	Value
P_{load} (MW)	20.00
Q_{load} (Mvar)	6.57
Q_{shunt} (Mvar)	7.00

Line and transformer data

Table B.2: Line parameters, p.u. values referred to 100 MVA and 132 kV

Parameter	Value (p.u.)
R	0.0
X	0.2

Table B.3: SVC transformer parameters, p.u. values referred to 100 MVA and 132 kV

Parameter	Value
R (p.u.)	0.0000
X (p.u.)	0.0001
S_N (MVA)	100
U_1 (kV)	132
U_2 (kV)	18

SVC model data

The SVC was modelled using the CSVGN5 model from the PSS/E model library, which models a typical static var system including fast override and remote bus voltage control. The model does not separate the equipment to identify capacitor banks and reactors. The block diagram is shown in Figure B.1, and model parameters are given in Table B.4.

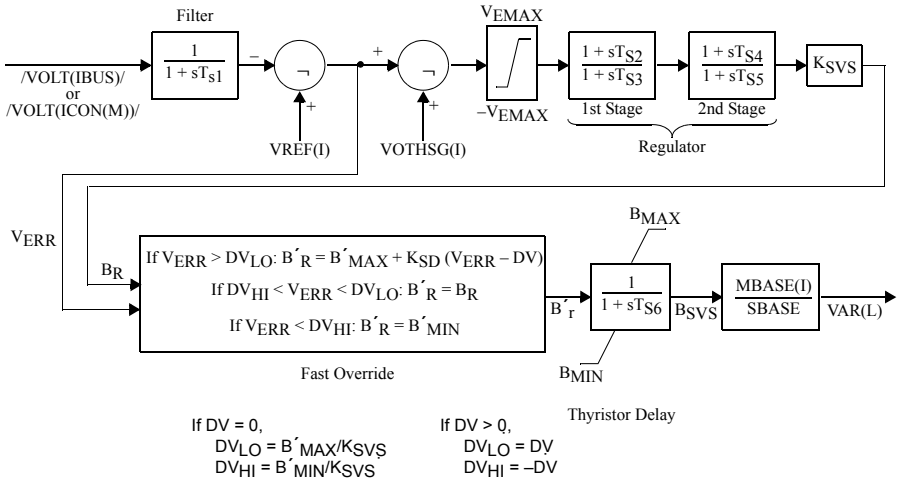

Figure B.1: CVSGN5 static var system model, from [23]

Table B.4: SVC model parameters, p.u. values referred to 200 MVA and 18 kV

Parameter	Value
T_{S1} (s)	0.00
T_{S2} (s)	0.00
T_{S3} (s)	0.66
T_{S4} (s)	0.00
T_{S5} (s)	0.00
T_{S6} (s)	0.03
$V_{\mathrm{E\,MAX}}$ (p.u.)	0.15
K_{SVS}	150.00
K_{SD}	0.00
B_{MAX} (p.u.)	5.00
B'_{MAX} (p.u.)	5.00
B_{MIN} (p.u.)	-5.00
B'_{MIN} (p.u.)	-5.00
DV	0.95

B.2 IEEE Reliability Test System

The IEEE Reliability Test System has been modelled as described in references [22, 24, 34]. In addition, overexcitation limiter models have been added to all generators.

Overexcitation limiter model data

Overexcitation limiters were modelled using the simplified generic MAXEX2 model from the PSS/E model library, which has a piecewise linear inverse time delay. The block diagram is shown in Figure B.2 (not including time delay circuit). The machine-specific model data is listed in Table B.5, and the time delay parameters, which are equal for all machines, are listed in Table B.6.

The field current limits are assumed to correspond to the the field current required to operate the generators at the specified maximum active and reactive power output.

The time delay was chosen by assuming that the thermal capability of the field winding corresponds to the requirement in the IEEE standard C50.13-2005, [25]. It was further assumed that the limiter characteristic has been coordinated with an overexcitation protection relay, adding a small margin between the thermal capability and the OEL limit.

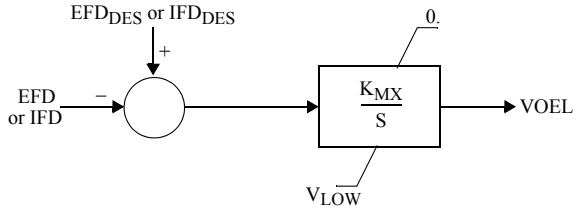

Figure B.2: MAXEX2 overexcitation limiter model, from [23]

Table B.5: Machine-specific OEL model parameters, IEEE RTS model

Unit type	EFD Rated	K_{MX}
U12	2.5085	0.80
U20	2.4587	0.80
U50	1.8091	0.80
U76	2.2484	0.80
U100	2.6435	0.80
U155	2.4118	0.80
U197	2.3528	0.80
U350	2.2858	0.80
U400	2.7016	0.80

Table B.6: Time delay parameters for OEL models, IEEE RTS model. P.u. values referred to *EFD Rated* of the specific machine

Parameter	Value
EFD_1 (p.u.)	1.10
EFD_2 (p.u.)	1.25
EFD_3 (p.u.)	1.75
$TIME_1$ (s)	120
$TIME_2$ (s)	40
$TIME_3$ (s)	9